

**DEVELOPMENT OF CARBONIC ANHYDRASE IX AND FOLATE
TARGETED SMALL MOLECULE DRUG CONJUGATES FOR THE
TREATMENT OF CANCER, SPINAL CORD INJURY AND
INFLAMMATORY DISEASES**

by
Spencer Gardeen

A Dissertation

*Submitted to the Faculty of Purdue University
In Partial Fulfillment of the Requirements for the degree of*

Doctor of Philosophy



Department of Chemistry
West Lafayette, Indiana
May 2021

THE PURDUE UNIVERSITY GRADUATE SCHOOL
STATEMENT OF COMMITTEE APPROVAL

Dr. Philip S. Low, Chair

Department of Chemistry

Dr. David Thompson

Department of Chemistry

Dr. Mingji Dai

Department of Chemistry

Dr. Chengde Mao

Department of Chemistry

Approved by:

Dr. Christine Hrycyna

I would like to dedicate this thesis to my parents, Scott and Doreen Gardeen. Thank you for never wavering in your support of my academic ambitions and for always being there for me.

ACKNOWLEDGMENTS

I would like to acknowledge Isaac Marks for his teachings and assistance in the carbonic anhydrase IX project. Seth Herr and Dr. Riyi Shi for their collaborative effort on the folate targeted acrolein scavenger's research. Dr. Low for his guiding wisdom over the years, along with his continued support in my academic career.

Development of a small molecule tubulysin B conjugate for the treatment of carbonic anhydrase IX Receptor Expressing Cancers. Reprinted (adapted) with permission from (Mol. Pharmaceutics 2018, 15, 6, 2289–2296). Copyright (2018) American Chemical Society.

Use of Carbonic Anhydrase IX Inhibitors for Selective Delivery of Attached Drugs to Solid Tumors. Reprinted/adapted by permission from [Springer Nature]: [Springer) [Carbonic Anhydrase as a Drug Target] by [Daumantas Matulis] [2019] (2019)

TABLE OF CONTENTS

LIST OF FIGURES	7
ABSTRACT.....	9
CHAPTER 1. DEVELOPMENT OF A SMALL MOLECULE TUBULYSIN B CONJUGATE FOR TREATMENT OF CARBONIC ANHYDRASE IX RECEPTOR EXPRESSING CANCERS	10
1.1 Abstract.....	10
1.2 Introduction	10
1.3 Materials and Methods	12
1.3.1 Materials.....	12
1.3.2 Synthesis CAIX Conjugates.....	12
1.3.3 Cell Culture and Animal Husbandry.....	14
1.3.4 Fluorescent microscopy of CAL-PEG2-FITC Conjugate (Compound 3).....	14
1.3.5 General Procedure for Determination of Binding Affinity of CAIX-FITC Conjugates	14
1.3.6 In Vitro Cytotoxicity Determination by 3H-Thymidine Uptake Assay	15
1.3.7 Evaluation of in Vivo Efficacy of Tubulyisin Conjugates in Tumor Xenografts	15
1.4 Results.....	16
1.4.1 Design and Synthesis of a CAIX-Targeted Drug Conjugate	16
1.4.2 In Vitro Binding to CAIX-Expressing Cells.....	18
1.4.3 Evaluation of the in Vivo Efficacy of Compound 6 in CAIX-Positive Cells.....	21
1.5 Discussion.....	25
1.6 References.....	26
1.7 Appendix A Supplemental Information	31
1.8 Appendix B Carbonic Anhydrase IX Book Chapter Review.....	49
CHAPTER 2. SYNTHESIS AND VALIDATION OF A FOLATE TARGETED ACROLEIN SCAVENGER	71
2.1 Abstract.....	71
2.2 Introduction	71
2.3 Materials and Methods	73

2.3.1	Animals and Diet:.....	73
2.3.2	Injury.....	73
2.3.3	Blood pressure.....	73
2.3.4	Perfusion:.....	74
2.3.5	Immunohistochemistry	74
2.3.6	Fluorescent and NIR Microscopy	74
2.3.7	Statistics.....	75
2.3.8	Synthesis of Folate Hydralazine	75
2.4	Results.....	76
2.4.1	Validation of Folate Targeting in Spinal Cord Injury <i>In Vivo</i>	76
2.4.2	Folate-Hydralazine Acrolein Scavenging Efficacy and Ablation of Toxicity	81
2.5	Discussion	85
2.6	Conclusion.....	86
2.7	References.....	86
2.8	Appendix A	88
CHAPTER 3. SYNTHESIS AND DEMONSTRATION OF FOLATE STEROID CONJUGATES		90
3.1	Abstract.....	90
3.2	Introduction	90
3.3	Materials and Methods	92
3.3.1	Synthesis of Folate Steroid Conjugates.....	92
3.3.2	Mechanistic Studies Using Peritonitis.....	96
3.4	Result	97
3.5	Discussion	109
3.6	Conclusion.....	110
3.7	References.....	111
3.8	Appendix A.....	114

LIST OF FIGURES

Figure 1.1 Binding of CAL-FITC (3) to SKRC-52 renal cell carcinoma cells. Twenty-five nanomolar CAL-PEG2-FITC was incubated with SKRC-52 cells for 1 h at 37 °C under normoxic conditions in the absence (A) or presence (B) of excess CAL to block available ligand binding sites. After washing, cells were analyzed for fluorescein fluorescence by confocal microscopy. (C,D) Analysis of the binding affinity of CAIX-FITC (conjugate 3) for A549 (lung carcinoma) (C) and HT29 (colorectal adenocarcinoma) (D) cells in the absence (triangles) and presence (circles) of 100-fold excess unconjugated inhibitor. Please note that data from different cell lines were shown in different panels to demonstrate the ability of CAL to target attached molecules to a diversity of cell lines..... 19

Figure 1.2 (A) In vitro cytotoxicity of compound 6 in unmodified (triangles) and CAIX-transfected (circles) HEK293 cells. Incorporation of 3H-thymidine was assayed in triplicate in cells treated for 2 h with different concentrations of compound 6. Error bars represent the standard deviation. (B) In vivo efficacy of compound 6 in nu/nu mice bearing HT29 xenografts (n = 5 in each group). Compound 6 was administered TIW at 1.25 µmol/kg in the presence (open circles) or absence (triangles) of 100-fold excess CAL containing no TubB (16). The competition and untreated groups were sacrificed when tumors exceeded 1500 mm³ as per the study's humane guidelines (day 16). (C) Whole body masses of mice treated in panel B. 23

Figure 2.1. Uptake and Quantification of Folate Near-Infrared Dye in Spinal Cord Injury. All animals received 40nmols of compound injected i.v. and after 24 hours were euthanized via perfusion. All arrows pointing to sliced sections of cord tissue. (A)Rostral cord sections (B) Epicenter/damaged cord (C) Surgery performed on rat, but no weight dropped on the spinal cord. (D) NIR dye with no folate targeting ligand of the epicenter. (E) MFI quantification of images A and B. Statistical significance represents a p-value <0.01..... 78

Figure 2.2 Confocal Microscopy Localization of F-NIR and Microglia/Macrophages in Injured Rat Spinal Cord. All animals received 40nmols of compound injected i.v. and after 24 hours were euthanized via perfusion. All arrows pointing to sliced sections of cord tissue (A) Sham (B) Rostral (C) Injury 79

Figure 2.3 Acrolein Staining and Quantification in Injured Rat Spinal Cords (A) Representative cord slices of immunohistochemical staining for acrolein for the respective experimental groups. (B) Quantification of representative images showing mean pixel intensity of acrolein staining. NS = not significant, * = p-value < 0.05, ** = p-value <0.01, *** = p-value <0.005. 82

Figure 2.4 Rat Spinal Cord Injury Blood Pressure Readings (A) Systolic and diastolic readings for rats day 4 (B) Systolic and diastolic readings for rats day 7. NS = not significant, * = p-value < 0.05, ** = p-value <0.01, *** = p-value <0.005, **** = p-value <0.001..... 84

Figure 3.1 M2 Polarization of Macrophages Exposed to Folate-HydroLink-Cys-Carba-Dex. 24HR-T-1; Cells incubated for 24hrs with Folate-HydroLink-Cys-Carba-Dex. 24-HR-C-1; Cells incubated for 24hrs with Folate-HydroLink-Cys-Carba-Dex and 100X concentration of folate-glucosamine as competition ligand. 100

Figure 3.2 Blocking Recruitment of Macrophages with Folate-PEG2-HydroLink-DimethylCys-Carba-Dex. Peritoneal macrophages were generated by IP injection of 3% thioglycolate into the peritoneal cavity of mice. 2 days later mice were treated with a single 10nmol injection of Folate-PEG2-HydroLink-DimethylCys-Carba-Dex. 2 days after treatment macrophages were isolated by peritoneal lavage, labeled with fluorescently conjugated antibody markers, and analyzed by flow cytometry. Experiment was performed in duplicate..... 104

Figure 3.3 Blocking Recruitment of Immune Cells with Folate-PEG12-Pyro-Dex. Peritoneal macrophages were generated by IP injection of 3% thioglycolate into the peritoneal cavity of a mouse. 2 days later mice were treated with a single 10nmol injection of Folate-PEG12-Pyro-Dex. 2 days after treatment macrophages were isolated by peritoneal lavage, labeled with fluorescently conjugated antibody markers, and analyzed by flow cytometry. Pilot experiment was performed with a single mouse. 108

ABSTRACT

In the field of drug development, a major issue constantly preventing translation to the clinic is drug toxicity. With so many drugs failing phase 1 clinical trials for this reason, solutions need to be developed to overcome this obstacle. The content of this thesis includes three separate and distinct projects that utilized small molecule drug conjugate technology to maintain desired efficacy and circumvent the toxicities associated with the well-known drugs tubulysin B, hydralazine, and dexamethasone.

CHAPTER 1. DEVELOPMENT OF A SMALL MOLECULE TUBULYSIN B CONJUGATE FOR TREATMENT OF CARBONIC ANHYDRASE IX RECEPTOR EXPRESSING CANCERS

Reprinted (adapted) with permission from (Mol. Pharmaceutics 2018, 15, 6, 2289–2296). Copyright (2018) American Chemical Society.

1.1 Abstract

Carbonic anhydrase IX (CAIX) is a membrane-spanning zinc metalloenzyme that catalyzes the reversible consumption of CO₂ and water to form H⁺ + HCO₃⁻. Many human cancers upregulate CAIX to help control the pH in their hypoxic microenvironments. The consequent overexpression of CAIX on malignant cells and low expression on normal tissues render CAIX a particularly attractive target for small molecule inhibitors, antibody–drug conjugates, and ligand-targeted drugs. In this study, CAIX-targeted fluorescent reporter molecules were initially exploited to investigate CAIX-specific binding to multiple cancer cell lines, where they were shown to display potent and selective binding to CAIX positive cells. A small molecule CAIX-targeted tubulysin B conjugate was then synthesized and examined for its ability to kill CAIX-expressing tumor cells *in vitro*. Potent therapeutic conjugates were subsequently tested *in vivo* and demonstrated to eliminate solid human tumor xenografts in murine tumor models without exhibiting overt signs of toxicity. Because most solid tumors contain hypoxic regions where CAIX is overexpressed, development of a method to selectively deliver drugs to these hypoxic regions could aid in the therapy of otherwise difficult to treat tumors.

1.2 Introduction

Rapidly growing tumors can outgrow their nascent vasculature, resulting in the formation of hypoxic regions that rely on anaerobic metabolism to survive.¹ While such hypoxic niches may comprise only a small portion of the total tumor volume,^{2,3} their importance in cancer survival and progression cannot be overstated. Thus, as a result of the induction of hypoxia-inducible factor 1a (HIF-1a), genes that control the epithelial to mesenchymal transition (EMT) are stimulated, leading to the transformation of cancer cells into migratory stem cell-like mesenchymal cells that have been repeatedly implicated in disease progression, metastasis, and overall poor prognosis.⁴

In addition to their propensity to metastasize, cells that have undergone EMT can become mitotically quiescent and thereby insensitive to antimetabolic drugs. EMT cells may also upregulate other drug resistance mechanisms, including expression of multidrug resistance pumps,⁵ enhanced DNA repair,⁶ and dysregulated apoptotic pathways.⁷ As a consequence, tumors that initially shrink in response to chemotherapy may rebound when their drug-resistant hypoxic cells revert to a highly proliferative state after termination of treatment.⁸

One of the hallmarks of tumor hypoxia is the production of acidic metabolites such as lactic and carbonic acids that induce a decrease in pH that in turn activates adaptive mechanisms to mitigate these harsh conditions.⁹ One such mechanism involves the expression of a membrane-spanning carbonic anhydrase (carbonic anhydrase IX) that catalyzes the reversible consumption of CO₂ and water to form H⁺ + HCO₃⁻. In this reaction, the resulting bicarbonate can be transported across the membrane, thereby preventing the drop in intracellular pH that would have otherwise inhibited many metabolic pathways.¹⁰

Based upon these considerations, we hypothesize that delivery of appropriate drugs selectively to hypoxic carbonic anhydrase IX (CAIX)-expressing cancer cells can contribute to the treatment of many solid tumors. Immunohistochemistry and gene expression studies demonstrate that CAIX is upregulated in most cancers of the lung,^{11,12} colon,^{13,14} pancreas,^{15,16} breast,^{17,18} cervix,^{19,20} bladder^{21,22} ovaries,^{23,24} brain,^{25,26} head and neck,²⁷ and kidneys.^{28,29} Moreover, CAIX expression in healthy tissues is limited to low levels in the gastric mucosa of the stomach, duodenum, and gall bladder.^{30,31} Because of this upregulation in malignant tissues, strategies have been explored to develop cancer cell-specific therapies for such diseases. The most common therapeutic approaches have included use of anti-CAIX antibodies,³² anti-CAIX antibody–drug conjugates (ADCs),³³ pan-carbonic anhydrase-targeted small-molecule drug conjugates,^{34–36} and CAIX inhibitors.^{37–40} Herein, we describe the design, synthesis, and biological evaluation of a highly specific low molecular weight CAIX-targeted microtubule inhibitor. We demonstrate that selective delivery of tubulysin B hydrazide to multiple CAIX-expressing solid tumors leads to rapid cancer cell death and tumor shrinkage.

1.3 Materials and Methods

1.3.1 Materials

H-Cys(Trt)-2-chlorotrityl resin and l-aspartic acid β -tert-butyl 2-chlorotrityl resins were obtained from Novabiochem (San Diego, CA). Amino acids were purchased from Chem-Impex International (Chicago, IL). Tubulysin B hydrazide (TubBH) was provided by Endocyte Inc. (West Lafayette, IN). HATU was obtained from Genscript Inc. (Piscataway, NJ). Sulfuric acid, MeOH, DMSO, DMF, TFA, IPA, DIPEA, piperidine, DCM, K₂CO₃, and all other chemical reagents were purchased from Sigma-Aldrich (St. Louis, MO). Amine-coated 24-well microtiter plates were purchased from BD Biosciences (San Jose, CA). [3H]-Thymidine was obtained from Moravsek Biochemicals (Brea, CA). All other cell culture reagents, syringes, and disposable items were purchased from VWR (Chicago, IL). NMR spectra were recorded on a 500 MHz Bruker AV500HD Spectrometer. All preparative HPLC was performed with an Agilent 1200 Instrument with a reverse-phase XBridge OBD preparative column (19 × 150 mm, 5 μ m) manufactured by Waters (Milford, MA) with UV detection at 254 nm. LRMS–LC/MS was performed on an Agilent 1220 Infinity LC with a reverse-phase XBridge Shield RP18 column (3.0 × 50 mm, 3.5 μ m).

1.3.2 Synthesis CAIX Conjugates

Synthesis of CAL-PEG2-Cys (Compound 2)

The fluoro-benzosulfonamide (CAL) CAIX targeting ligand was synthesized as previously described⁴¹ with the exception that 3-mercaptopropanoic acid was employed in place of 3-mercaptopropanol for subsequent attachment to amine-terminated drugs (Scheme S1). H-Cys(Trt)-2-chlorotrityl resin 1 (100 mg, 0.64 mmol/g) was swollen with DCM (3 mL) for 20 min followed by DMF (3 mL) for 20 min. After swelling, a solution of 3-[2-[2-(9H-fluoren-9-ylmethoxycarbonylamino)ethoxy]ethoxy]propanoic acid (51.1 mg, 0.128 mmol), HATU (60.8 mg, 0.16 mmol), and DIPEA (0.056 mL, 0.32 mmol) in DMF (3 mL) was added. Argon was bubbled for 2 h, and the resin was subsequently washed with DMF (3 × 3 mL) and i-PrOH (3 × 3 mL). The Fmoc was deprotected with piperidine (20% piperidine in DMF, 3 × 5 mL), and the resin was washed with DMF (3 × 3 mL) and i-PrOH (3 × 3 mL).

A solution of 3-((2-(cyclooctylamino)-3,5,6-trifluoro-4-sulfamoylphenyl)sulfonyl)propanoic acid (9) (33.3 mg, 0.074 mmol), HATU (24.3 mg, 0.064 mmol), and DIPEA (0.034 mL, 0.192 mmol)

in DMF was added. Argon was bubbled for 2 h, and resin was washed DMF (3 × 3 mL) and i-PrOH (3 × 3 mL). Compound 2 was cleaved from the resin using a TFA/TIPS/H₂O/EDT cocktail (95:2.5:2.5:2.5) and concentrated under vacuum. The concentrated product was precipitated in Et₂O and dried under vacuum. Crude conjugate was purified by RP-HPLC [A = 2 mM ammonium acetate buffer (pH 5.0), B = CH₃CN, solvent gradient 0% B to 100% B in 30 min, retention time = 18.8 min] to yield the product as a clear oil (18.5 mg, 34%). LRMS–LC/MS (m/z): [M + H]⁺ calcd for C₂₇H₄₁F₃N₄O₁₀S₃, 735.2; found, 735.2.

Synthesis of CAL-PEG2-FITC (Compound 3)

To a solution of 2 (5 mg, 0.0068 mmol) in DMF (1 mL) was added fluorescein-5-maleimide (3.2 mg, 0.0075 mmol) and DIPEA (0.006 mL, 0.034 mmol) and stirred for 1 h at room temperature. The crude reaction mixture was purified RP-HPLC [A = 2 mM ammonium acetate buffer (pH 7.0), B = CH₃CN, solvent gradient 0% B to 100% B in 30 min, retention time = 22.1 min] to yield the product 3 as a yellow powder (4.8 mg, 61%). LRMS–LC/MS (m/z): [M + H]⁺ calcd for C₅₁H₅₄F₃N₅O₁₇S₃, 1162.3; found, 1162.2.

Synthesis of CAL-PEG2-D-R-D-Dap-D-C (Compound 4)

H-Cys(Trt)-2-chlorotrityl resin 1 (100 mg, 0.64 mmol/g) was swollen with DCM (3 mL) for 20 min followed by DMF (3 mL) for 20 min. After swelling, a solution of Fmoc-Asp(tBu)-OH (52.7 mg, 0.128 mmol), HATU (60.8 mg, 0.16 mmol), and DIPEA (0.056 mL, 0.32 mmol) in DMF (3 mL) was added. Argon was bubbled for 2 h, and resin was washed with DMF (3 × 3 mL) and i-PrOH (3 × 3 mL). The Fmoc was removed with a piperidine solution (20% in DMF, 3 × 5 mL), and the resin was washed with DMF (3 × 3 mL) and i-PrOH (3 × 3 mL). The same protocol was followed for the remaining steps. Compound 4 was cleaved from the resin using a TFA/TIPS/H₂O/EDT cocktail (95:2.5:2.5:2.5) and concentrated under vacuum. The concentrated product was precipitated in diethyl ether and dried under vacuum. Crude conjugate was purified by RP-HPLC [A = 2 mM ammonium acetate buffer (pH 5.0), B = CH₃CN, solvent gradient 0% B to 100% B in 30 min, retention time = 19.7 min] to yield the product as a clear oil (36 mg, 43%). LRMS–LC/MS (m/z): [M + H]⁺ calcd for C₄₈H₇₄F₃N₁₃O₂₁S₃, 1322.43; found, 1322.38.

Synthesis of CAL-PEG2-D-R-D-Dap-D-C-tubulysin B (Compound 6)

A solution of saturated sodium bicarbonate (10 mL) in distilled water was bubbled with argon continuously for 30 min. Compound 4 (1.2 mg, 0.0009 mmol) was dissolved in argon-purged HPLC grade water (2.0 mL), and the pH of the reaction mixture was increased to 7 using the argon-

purged sodium bicarbonate solution. A solution of disulfide activated-tubulysin B (5), supplied by Endocyte, 1.27 mg, 0.0012 mmol) in THF (0.5 mL) was then added to the reaction mixture. The progress of the reaction was monitored using LCMS, and after stirring for 30 min, the reaction was found to reach completion. Compound 6 was purified by RP-HPLC [A = 2 mM ammonium acetate buffer (pH 7.0), B = CH₃CN, solvent gradient 0% B to 100% B in 30 min, retention time = 23.4 min] to yield the requisite product. LRMS–LC/MS (m/z): [M + H]⁺ calcd for C₉₃H₁₄₁F₃N₂₀O₃S₅, 2267.86; found, 1134.57 (half mass).

1.3.3 Cell Culture and Animal Husbandry

Cell lines were purchased from American Type Culture Collection (ATCC) and cultured as monolayers in 1640 rpmI supplemented with 10% heat-inactivated fetal bovine serum, and 1% of penicillin–streptomycin at 37 °C in a 5% CO₂/95% humidified-air atmosphere. Female athymic nu/nu mice were purchased from Harlan Laboratories, housed in a sterile environment on a standard 12 h light–dark cycle, and maintained on normal rodent chow. All animal procedures were approved by the Purdue Animal Care and Use Committee in accordance with National Institutes of Health guidelines.

1.3.4 Fluorescent microscopy of CAL-PEG2-FITC Conjugate (Compound 3)

SKRC52 cells (10⁵) were seeded into chambered cover glass plates and allowed to grow to confluence over 24 h. Spent medium was replaced with 0.5 mL of fresh medium containing 10% fetal bovine serum containing 25 nM conjugate 3, alone or in combination with 100-fold excess CAIX inhibitor (9). After incubation for 1 h at 37 °C, cells were rinsed twice with 1 mL of media to remove unbound fluorescence, and 0.5 mL of fresh incubation medium was added to the wells. Images were acquired using confocal microscopy (FV 1000, Olympus; 60× objective, NA: 1.42) and analyzed with Olympus Fluoview software (Ver. 4.2).

1.3.5 General Procedure for Determination of Binding Affinity of CAIX-FITC Conjugates

Untransfected cells (SKRC52, HT29, A549) or HEK293 cells transfected with CAIX (0.25 × 10⁶) were placed into 1.5 mL centrifuge tubes with 0.3 mL of fresh DMEM or RPMI medium containing increasing concentrations of CAL-FITC conjugates in the presence or absence of 100-

fold excess CAL inhibitor (Scheme S1, compound 9). All concentrations were examined in duplicate or triplicate. After incubating for 1 h at 25 °C, cells were rinsed twice with 1 mL of medium. The cells were transferred into a 96-well plate, and the mean fluorescence intensity (MFI) was read by flow cytometry (BD Accuri C6, BD Biosciences). Apparent KD was calculated by plotting mean fluorescence intensity versus concentration of FITC conjugates using GraphPad Prism 4. For hypoxia experiments, cells were incubated under an atmosphere containing 1% oxygen, 5% carbon dioxide, and 94% nitrogen for 24–48 h in a sealed chamber.

1.3.6 In Vitro Cytotoxicity Determination by 3H-Thymidine Uptake Assay

Cells were seeded on amine-coated, 24-well plates (BD Purecoat Amine, BD Biosciences) and allowed to form monolayers. The spent medium in each well was replaced with fresh medium (0.5 mL) containing various concentrations of compound 6. After incubating for 2 h at 37 °C, cells were rinsed 3× with fresh medium and then incubated an additional 66 h at 37 °C in fresh medium. Spent medium in each well was again replaced with fresh medium (0.5 mL) containing 3H-thymidine (1 µCi/mL), and the cells were incubated for an additional 4 h to allow for [3H]-thymidine incorporation. The cells were then washed with media (3 × 0.5 mL), treated with 5% trichloroacetic acid (0.5 mL) for 10 min at room temperature, and dissolved in 0.25 N NaOH (0.5 mL), and 0.45 mL was transferred to individual scintillation vials containing Ecolume scintillation cocktail (3.0 mL). After thoroughly mixing to form a homogeneous liquid, the vials were counted in a liquid scintillation analyzer. The IC₅₀ values were derived from a plot of the percent 3H-thymidine incorporation versus log concentration using Graph Pad Prism 4.

1.3.7 Evaluation of in Vivo Efficacy of Tubulysin Conjugates in Tumor Xenografts

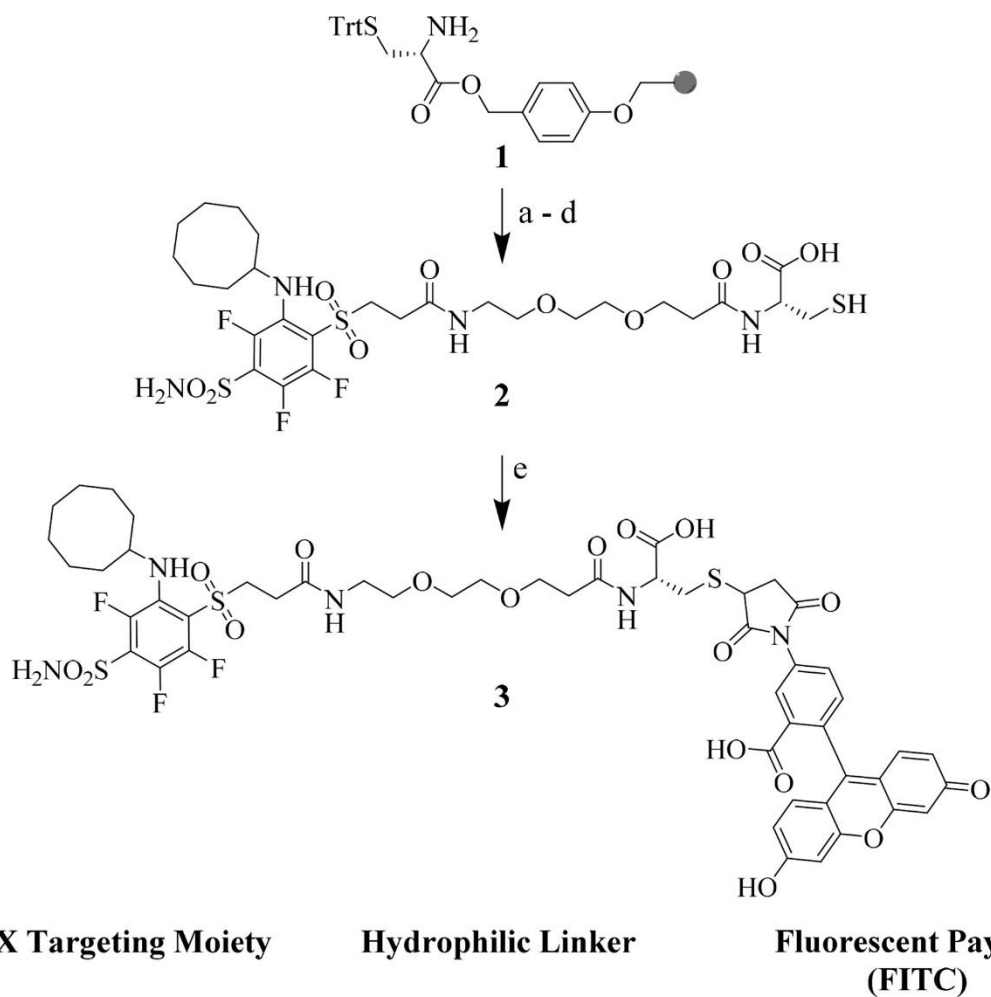
HT29 or A540 cells (2×10^6) were injected subcutaneously into 5–6 week old female nu/nu mice. Tumors were measured in two perpendicular directions 3× weekly with vernier calipers, and tumor volume was calculated as $0.5 \times L \times W^2$, where L is the longest axis (in millimeters) and W is the axis perpendicular to L (in millimeters). Dosing of CAL-TubB compounds was initiated when the subcutaneous tumors reached 100–275 mm³ in volume. Dosing solutions were prepared in saline, adjusted to 100 µL total injection volume per mouse, and filtered through a 0.22 µm filter. Solutions were administered via tail vein injection.

1.4 Results

1.4.1 Design and Synthesis of a CAIX-Targeted Drug Conjugate

After reviewing the properties of multiple carbonic anhydrase inhibitors described in the literature, the inhibitor shown in Scheme 1 was selected for further analysis based on its affinity and selectivity for CAIX. This inhibitor, developed by Dudutiene and co-workers,(41) exhibited the highest affinity (50 pM) and specificity (66-fold over the closely related CAXII) of all carbonic anhydrase inhibitors we examined. As shown in Scheme S1, a modified version of this inhibitor, containing a carboxylic acid instead of a hydroxyl on the sulfone, was synthesized to facilitate attachment of the ligand to a flexible linker.

To determine the length of the flexible linker that might best enable the CAIX ligand to reach the bottom of its binding pocket, the depth of the binding pocket in CAIX was estimated using its crystal structure CAIX (PDB code: 4Q07). Analysis showed that a linker of about 20 Å would be required for optimal docking. To confirm this assessment, several CAL-FITC conjugates with spacers of different lengths were synthesized and tested for their binding affinities. As shown in Figure S1, a minimal linker length of 20 Å was required to achieve maximal binding affinity; i.e., in good agreement with the crystal structure analysis.



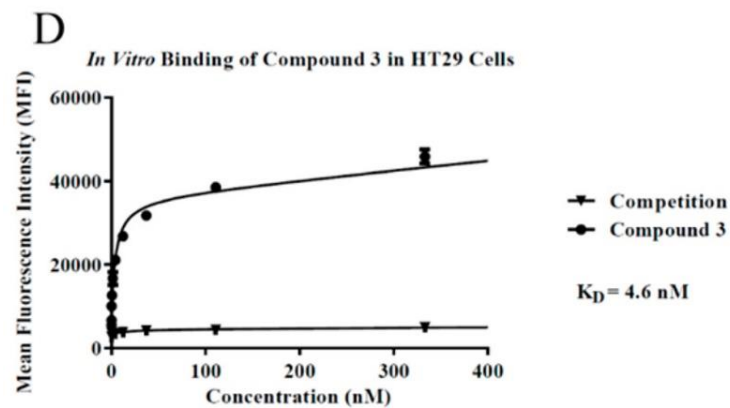
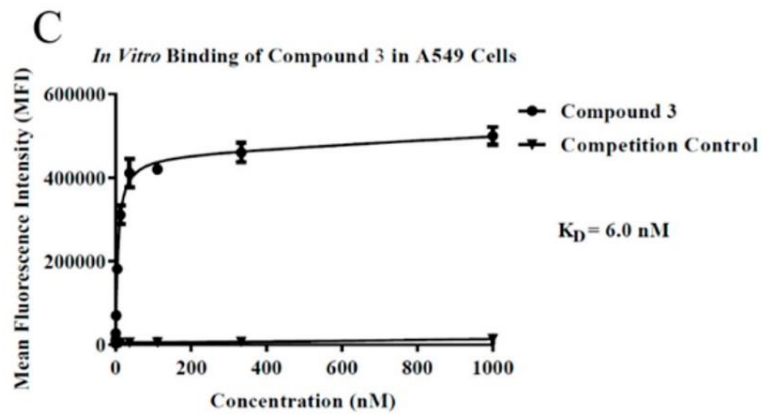
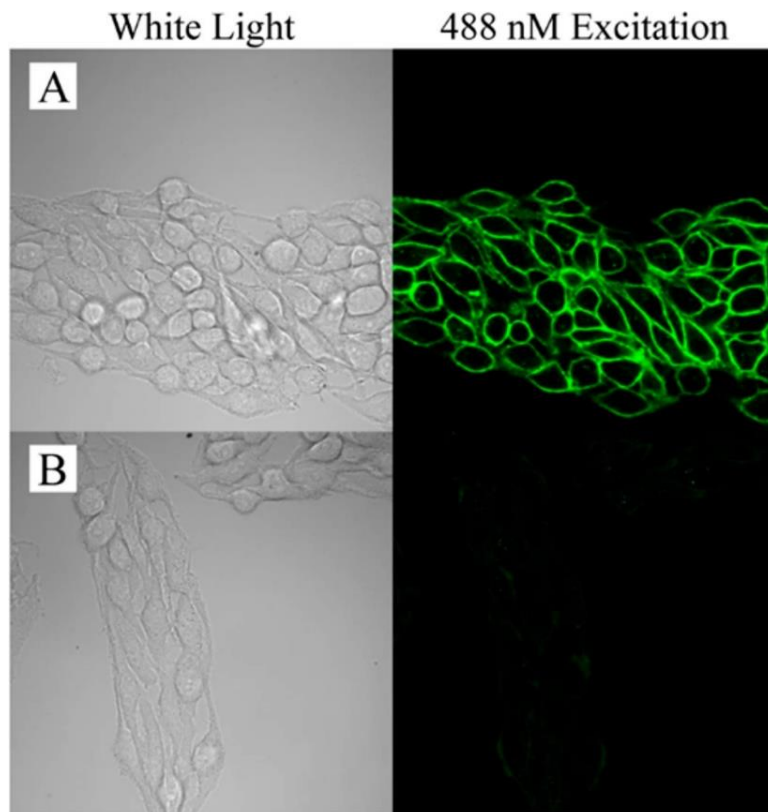
Scheme 1. Synthesis of CAL-PEG2-FITC (Compound 3). Reagents and conditions: (a) Fmoc-N-amido-PEG2-acid, HATU, DIPEA, DMF, 2 h; (b) 20% piperidine/DMF, rt, 3 × 10 min; (c) CAL-COOH, HATU, DIPEA, DMF, 2 h; (d) TFA/TIPS/H₂O/EDT (95:2.5:2.5:2.5), 3 × 10 min; (e) fluorescein-5-maleimide, DIPEA, DMF, rt, 2 h.

1.4.2 In Vitro Binding to CAIX-Expressing Cells

To obtain an initial indication of which human cancer cell lines might upregulate CAIX, we incubated SKRC-52 (human renal cell carcinoma), HT29 (human colon adenocarcinoma), and A549 (human lung carcinoma) cells, as well as HEK293 (human embryonic kidney) cells that were transfected with CAIX (positive control), with 25 nM of the FITC-labeled compound 3, and then examined the cells by confocal microscopy. As shown in the representative data of Figure 1, compound 3 labeled the plasma membranes of SKRC-52 cells brightly (panel A) in a manner that was readily competed by the addition of 100-fold excess of unlabeled CAIX targeting ligand (panel B). Importantly, similar data were also found for HT-29, A549, and transfected HEK293 cells. These results demonstrate that all four of the examined cell lines express CAIX receptors that can bind compound 3. Expression of CAIX on each of the above cell lines was further confirmed by staining with an anti-CAIX specific antibody (data not shown).

To obtain a more accurate assessment of the binding affinity of compound 3 for the aforementioned cell lines, cells were incubated with increasing concentrations of compound 3 and analyzed for mean fluorescence intensity (MFI) by flow cytometry. As shown in Figure 1, analysis of MFI yields a binding affinity of ~5 nM for both HT-29 and A549 cells (which was similar to the KD for SKRC-52 and HEK293 cells that have stability with CAIX shown in Figures S2–S4), suggesting that attachment of fluorescein to CAL has only a minor effect on its affinity for CAIX. The fact that MFI was reduced to near background levels upon the addition of excess unlabeled CAL further establishes that virtually all of compound 3's binding is CAIX specific. These data therefore argue that a CAL-linked drug can be targeted to CAIX-expressing cancer cells with high affinity and specificity.

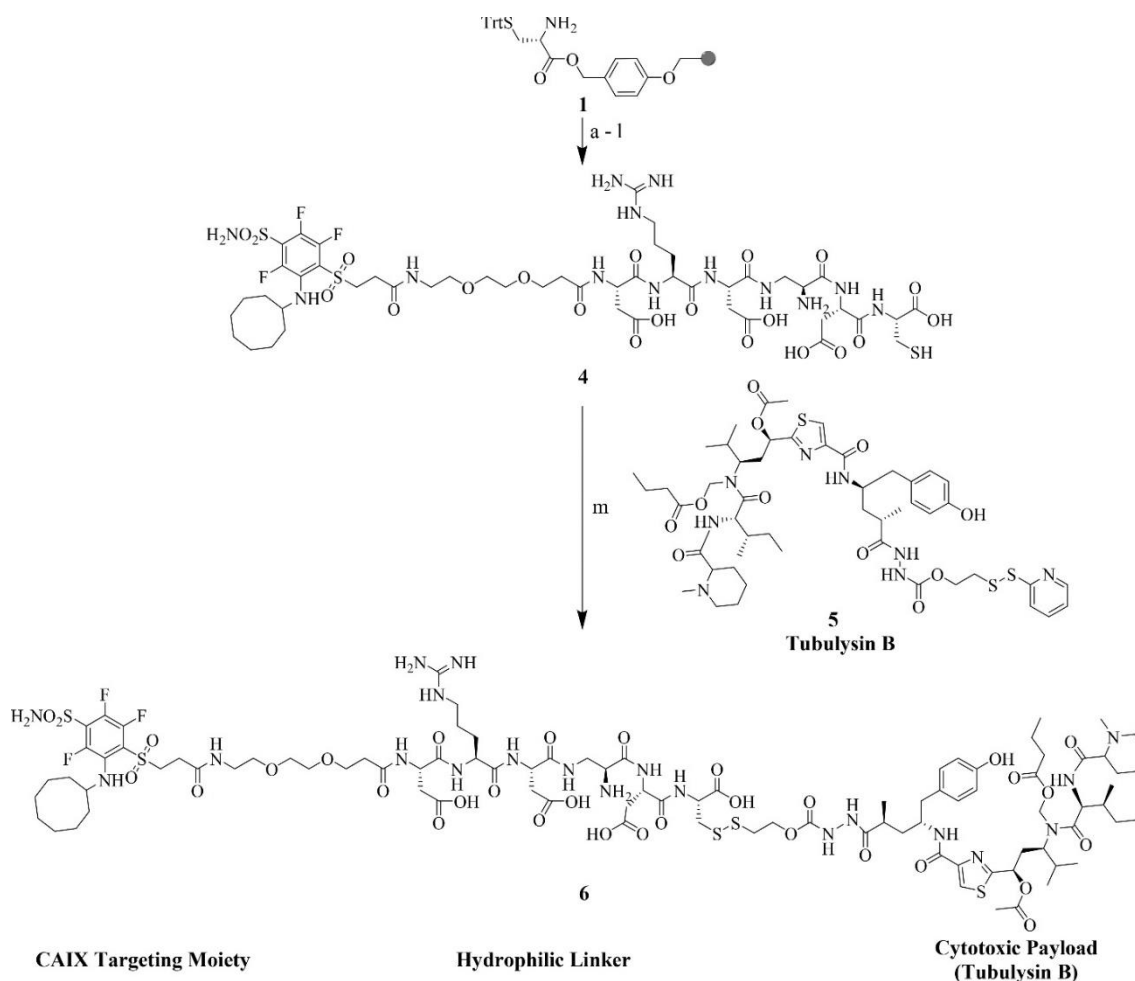
Figure 1.1 Binding of CAL-FITC (3) to SKRC-52 renal cell carcinoma cells. Twenty-five nanomolar CAL-PEG2-FITC was incubated with SKRC-52 cells for 1 h at 37 °C under normoxic conditions in the absence (A) or presence (B) of excess CAL to block available ligand binding sites. After washing, cells were analyzed for fluorescein fluorescence by confocal microscopy. (C,D) Analysis of the binding affinity of CAIX-FITC (conjugate 3) for A549 (lung carcinoma) (C) and HT29 (colorectal adenocarcinoma) (D) cells in the absence (triangles) and presence (circles) of 100-fold excess unconjugated inhibitor. Please note that data from different cell lines were shown in different panels to demonstrate the ability of CAL to target attached molecules to a diversity of cell lines.



1.4.3 Evaluation of the in Vivo Efficacy of Compound 6 in CAIX-Positive Cells

Motivated by a need for a chemotherapeutic agent that could target hypoxic regions in solid tumors, we next used CAL to construct a therapeutic drug conjugate comprising CAL linked to the highly potent chemotherapeutic agent, tubulysin B, via a flexible, self-immolative linker (Scheme 2). However, because the initial conjugate constructed with the PEG-based linker employed in compound 3 was found to be too insoluble for in vivo applications (Scheme S4), the linker was redesigned to render the final tubulysin conjugate more water-soluble by adding several hydrophilic amino acids. A self-immolative linker was also inserted (Scheme 2) between the linker and the therapeutic payload to facilitate release of unmodified tubulysin B hydrazide upon internalization of the conjugate into the strongly reducing environment of intracellular endosomes.⁴² The in vitro potency and specificity of the final product (compound 6) was then evaluated in the stably transfected HEK293 cells using a ³H-thymidine incorporation assay. As shown in Figure 2A, compound 6 successfully killed these CAIX-transfected cells with an IC₅₀ of 1.05 ± 0.01 nM.

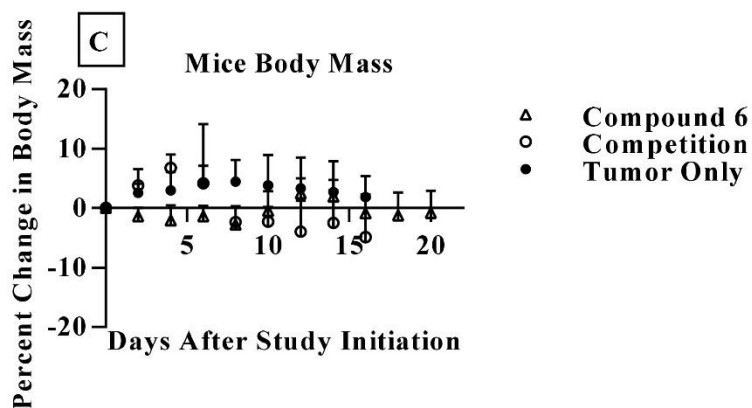
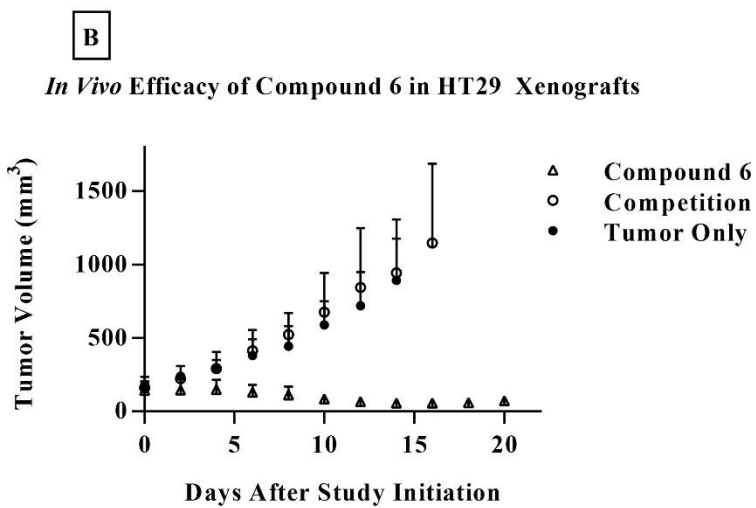
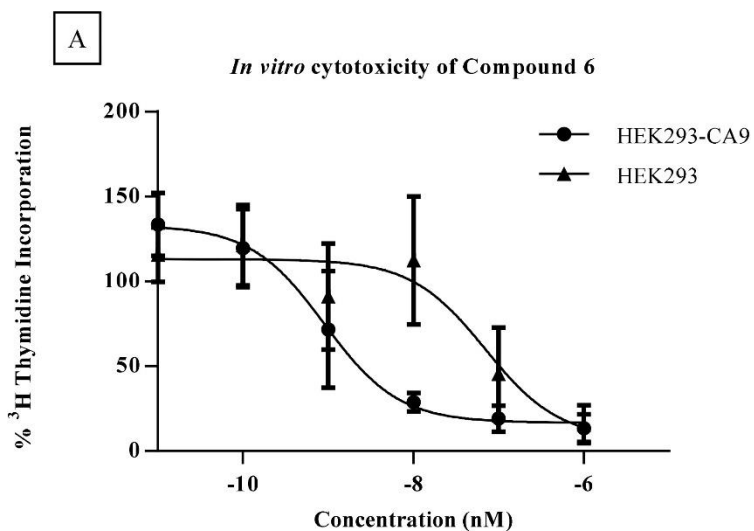
In vivo efficacy of compound 6 was then evaluated in athymic nude mice bearing 200 mm³ HT29 tumor xenografts after determining its maximum tolerated dose (MTD) by treating mice TIW with increasing concentrations of conjugate (Figures S5–S6). Based on an estimated MTD of 2.0 μmol/kg, all subsequent live mouse studies were performed by intravenous injection of 1.25 μmol/kg TIW. As shown in Figure 2B, the aforementioned treatment regimen caused dramatic tumor shrinkage when no competing ligand was added. However, upon coinjection of 100-fold excess CAL containing no TubB (compound 16, Scheme S5; competing ligand), tumor growth increased to the rate seen in untreated controls. These data demonstrate that treatment of HT29 tumors was CAIX-specific and that little or no cancer cell death derived from nonspecific extracellular release of nontargeted drug. This lack of significant premature drug release was further confirmed by demonstrating that conjugate-treated animals show no weight loss; i.e., an outcome that would not have been expected if the highly toxic free tubulysin were released systemically during transit to the tumor. Importantly, an analogous but smaller study was conducted using A549 mouse xenografts to ensure that the targeted efficacy was not cell-type-specific and that similar efficacy was observed (Figures S7–S8).



Scheme 2. Solid Phase Peptide Synthesis of CAL-PEG22-D-R-D-Dap-D-C-Tubulysin B

Reagents and conditions: (a) Fmoc-Asp(OtBu)-OH, HATU, DIPEA, DMF, 2 h; (b) 20% piperidine/DMF, rt, 3 × 10 min; (c) Fmoc-Dap(Boc)-OH, HATU, DIPEA, DMF, 2 h; (d) 20% piperidine/DMF, rt, 3 × 10 min; (e) Fmoc-Asp(OtBu)-OH, HATU, DIPEA, DMF, 2 h; (f) 20% piperidine/DMF, rt, 3 × 10 min; (g) Fmoc-Arg(Pbf)-OH, HATU, DIPEA, DMF, 2 h; (h) 20% piperidine/DMF, rt, 3 × 10 min; (i) N-amido-PEG2-acid, HATU, DIPEA, DMF, 2 h; (j) 20% piperidine/DMF, rt, 3 × 10 min; (k) CAL-COOH, HATU, DIPEA, DMF, 2 h; (l) TFA/TIPS/H₂O/EDT (95:2.5:2.5:2.5), 3 × 15 min; (m) 5, NaHCO₃, THF/H₂O (1:1), rt, 30 min.

Figure 1.2 (A) In vitro cytotoxicity of compound 6 in unmodified (triangles) and CAIX-transfected (circles) HEK293 cells. Incorporation of ³H-thymidine was assayed in triplicate in cells treated for 2 h with different concentrations of compound 6. Error bars represent the standard deviation. (B) In vivo efficacy of compound 6 in nu/nu mice bearing HT29 xenografts (n = 5 in each group). Compound 6 was administered TIW at 1.25 μmol/kg in the presence (open circles) or absence (triangles) of 100-fold excess CAL containing no TubB (16). The competition and untreated groups were sacrificed when tumors exceeded 1500 mm³ as per the study's humane guidelines (day 16). (C) Whole body masses of mice treated in panel B.



1.5 Discussion.

Because of its upregulation in many cancers, carbonic anhydrase IX has attracted increasing interest as a possible target for ligand-targeted therapeutic interventions in solid tumors. For example, Cazzamalli et al.⁴³ and Krall et al.⁴⁴ have used the FDA-approved small molecule CAIX inhibitor, acetazolamide (KI \approx 25 nM), as a targeting ligand to deliver cytotoxic compounds including monomethyl auristatin E (MMAE), PNU-159682, maytansine, and duocarmycin. Similarly, Lv et al., exploiting a tubulysin conjugate of a different small molecule inhibitor (KI \approx 7.8 nM), reported only stable disease when dosed TIW at 2 μ mol/kg for 3 weeks.⁴⁵ Because off-tumor toxicity commonly limits the amount of drug that can be administered, we reasoned that use of a much higher affinity targeting ligand for delivery of our cytotoxic payload might allow a more complete response since saturation of tumor receptors at much lower conjugate concentrations should reduce off-target toxicities associated with unwanted drug release in healthy tissues. For this purpose, we scrutinized the literature for high affinity inhibitors of CAIX and found the fluoro-benzosulfonamide developed by Dudutiene and co-workers⁴¹ to bind CAIX with much higher affinity and specificity. Not surprisingly, conjugation of this inhibitor to tubulysin B yielded better responses in tumor-bearing mice implanted with multiple tumor types at a dose lower than was achieved with earlier tubulysin B conjugates. While Janoniene and co-workers previously modified a porous silicon nanosystem to display CAL on the surface to achieve CAIX targeting, the work described in this report is the first use of CAL as the targeting moiety in a small molecule drug conjugate for CAIX positive tumors.⁴⁶

While most previous ligand–drug conjugates developed in our lab have been targeted to tumor-specific receptors that readily internalize (i.e., and thereby delivering their cargoes into intracellular compartments), the CAL ligand used in this study was not found to internalize. The question therefore arises whether this inability to rapidly deliver an attached drug into the target cell’s interior might compromise the ligand–drug conjugate’s potency. While delivery of a ligand-targeted drug to an endocytosing receptor is always preferred,⁴⁷ we have also previously observed that even a noninternalizing receptor can be exploited for potent tumor-specific cytotoxicity⁴⁸ Virtually all cell surface receptors naturally internalize during the normal process of membrane recycling (which occurs within hours in many cells),^{48,49} and even payloads that are not internalized can be engineered for facile cell surface release if they are conjugated to their tumor targeting ligands via a disulfide bond.^{50,51} Thus, because many cancer cells upregulate a

transplasma membrane redox pathway that continuously generates extracellular reducing power,⁵² disulfide bonds are much more rapidly reduced in a tumor microenvironment than in the extracellular milieu of healthy tissues.^{53,54} Because the targeted drugs employed in our studies are all naturally membrane permeable, their probabilities of entering a cancer cell over a normal cell must be very high. Thus, assuming the average diameter of a tumor nodule to be ~1 cm and the average diameter of a cancer cell to be ~20 μm , a drug released near the middle of the nodule would have to pass by ~250 cancer cells before it could leave the tumor mass. This must increase the probability that the cytotoxic warhead will preferentially kill a cancer cell over a normal cell.

CAL targeting of CAIX can also be used for applications other than the targeted delivery of tubulysin B to CAIX positive cells. Because some of the cells that are present in hypoxic regions of solid tumors may slowly divide, there are cytotoxic cargos other than tubulysin B that merit further exploration, including spliceostatins and pyrolobenzodiazepines. Additionally, CAL could be used to target therapeutic radionuclides to CAIX positive cancers. Beyond the therapeutic applications, there are also targeted imaging applications, including CAL-targeted fluorescent dyes for the fluorescence-guided surgical resection of CAIX positive tumors and CAL-targeted PET and SPECT/CT radioimaging agents for whole body diagnosis and monitoring of cancer.

1.6 References

1. Eales, K. L.; Hollinshead, K. E.; Tennant, D. A. Hypoxia and metabolic adaptation of cancer cells. *Oncogenesis* 2016, 5, e190.
2. Raleigh, J. A.; Calkins-Adams, D. P.; Rinker, L. H.; et al. Hypoxia and vascular endothelial growth factor expression in human squamous cell carcinomas using Pimonidazole as a hypoxia marker. *Cancer Res.* 1998, 58(17), 3765–3768.
3. Verstraete, M.; Debucquoy, A.; Devos, E.; et al. Investigation of possible endogenous hypoxia markers in colorectal cancer. *Int. J. Radiat. Biol.* 2013, 89(1), 9–15.
4. Das, B.; Tsuchida, R.; Malkin, D.; et al. Hypoxia enhances tumor stemness by increasing the invasive and tumorigenic side population fraction. *Stem Cells* 2008, 26(7), 1818–30.

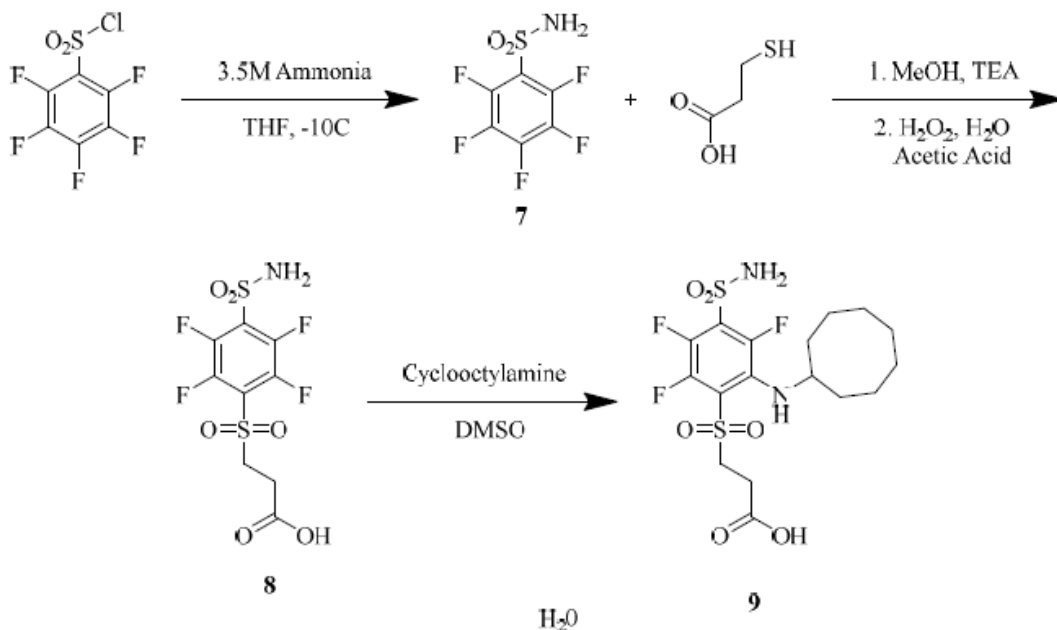
5. Dean, M. ABC transporters, drug resistance, and cancer stem cells. *J. Mammary Gland Biol. Neoplasia*.2009,14(1), 3–9.
6. Wang, Q. E. DNA damage responses in cancer stem cells: Implications for cancer therapeutic strategies. *World J. Biol. Chem.*2015,6(3), 57–64.
7. Eyler, C. E.; Rich, J. N. Survival of the fittest: cancer stem cells in therapeutic resistance and angiogenesis. *J. Clin. Oncol.*2008,26(17),2839–45.
8. Yu, Y.; Ramena, G.; Elble, R. C. The role of cancer stem cells in relapse of solid tumors. *Front. Biosci., Elite Ed.*2012,4, 1528–41.
9. Warburg, O. On the Origin of Cancer Cells.*Science*1956,123(3191), 309–314.
10. Chiche, J.; Ilc, K.; Laferriere, J.; et al. Hypoxia-inducible carbonic anhydrase IX and XII promote tumor cell growth by counteracting acidosis through the regulation of the intracellular pH. *Cancer Res.*2009,69(1), 358–68.
11. Ilie, M.; Mazure, N. M.; Hofman, V.; et al. High levels of carbonic anhydrase IX in tumour tissue and plasma are biomarkers of poor prognostic in patients with non-small cell lung cancer.*Br. J. Cancer*2010,102(11), 1627–35.
12. Stewart, D. J.; Nunez, M. I.; Behrens, C.; et al. Membrane carbonic anhydrase IX expression and relapse risk in resected stage I-II non-small-cell lung cancer. *J. Thorac. Oncol.*2014,9(5), 675–84.
13. Niemela, A. M.; Hynninen, P.; Mecklin, J. P.; et al. Carbonic anhydrase IX is highly expressed in hereditary nonpolyposis colorectal cancer. *Cancer Epidemiol., Biomarkers Prev.*2007,16(9), 1760–6.
14. Korkeila, E.; Talvinen, K.; Jaakkola, P. M.; et al. Expression of carbonic anhydrase IX suggests poor outcome in rectal cancer.*Br. J. Cancer*2009,100(6), 874–80.
15. Juhasz, M.; Chen, J.; Lendeckel, U.; et al. Expression of carbonic anhydrase IX in human pancreatic cancer. *Aliment. Pharmacol. Ther.*2003,18(8), 837–46.
16. Li, Y.; Dong, M.; Sheng, W.; Huang, L. Roles of Carbonic Anhydrase IX in Development of Pancreatic Cancer. *Pathol. Oncol. Res.*2016,22(2), 277–86.
17. Chia, S. K.; Wykoff, C. C.; Watson, P. H.; et al. Prognostic significance of a novel hypoxia-regulated marker, carbonic anhydrase IX, in invasive breast carcinoma. *J. Clin. Oncol.*2001,19(16), 3660–8.
18. Hussain, S. A.; Ganesan, R.; Reynolds, G.; et al. Hypoxia-regulated carbonic anhydrase IX expression is associated with poor survival in patients with invasive breast cancer.*Br. J. Cancer*2007,96(1), 104–9.

19. Loncaster, J. A.; Harris, A. L.; Davidson, S. E.; et al. Carbonic anhydrase (CA IX) expression, a potential new intrinsic marker of hypoxia: correlations with tumor oxygen measurements and prognosis in locally advanced carcinoma of the cervix. *Cancer Res.*2001,61(17),6394–9.
20. Hedley, D.; Pintilie, M.; Woo, J.; et al. Carbonic anhydrase IX expression, hypoxia, and prognosis in patients with uterine cervical carcinomas. *Clin. Cancer Res.*2003,9(15), 5666–74.
21. Klatte, T.; Seligson, D. B.; Rao, J. Y.; et al. Carbonic anhydrase IX in bladder cancer: a diagnostic, prognostic, and therapeutic molecular marker. *Cancer*2009,115(7), 1448–58.
22. Hussain, S.; Palmer, D.; Ganesan, R.; et al. Carbonic anhydrase IX, a marker of hypoxia: Correlation with clinical outcome in transitional cell carcinoma of the bladder. *Oncol. Rep.*2004,11(5), 1005–10.
23. Hynninen, P.; Vaskivuo, L.; Saarnio, J.; et al. Expression of transmembrane carbonic anhydrases IX and XII in ovarian tumours. *Histopathology*2006,49(6), 594–602.
24. Choschzick, M.; Oosterwijk, E.; Muller, V.; et al. Over expression of carbonic anhydrase IX (CAIX) is an independent unfavorable prognostic marker in endometrioid ovarian cancer. *Virchows Arch.*2011,459(2), 193–200.
25. Jarvela, S.; Parkkila, S.; Bragge, H.; et al. Carbonic anhydrase IX in oligodendroglial brain tumors. *BMC Cancer*2008,8,1.
26. Haapasalo, J. A.; Nordfors, K. M.; Hilvo, M.; et al. Expression of carbonic anhydrase IX in astrocytic tumors predicts poor prognosis. *Clin. Cancer Res.*2006,12(2), 473–7.
27. Beasley, N. J.; Wykoff, C. C.; Watson, P. H.; et al. Carbonic anhydrase IX, an endogenous hypoxia marker, expression in head and neck squamous cell carcinoma and its relationship to hypoxia, necrosis, and microvessel density. *Cancer Res.*2001,61(13), 5262–7.
28. Stillebroer, A. B.; Mulders, P. F.; Boerman, O. C.; Oyen, W. J.; Oosterwijk, E. Carbonic anhydrase IX in renal cell carcinoma: implications for prognosis, diagnosis, and therapy. *Eur. Urol.*2010,58(1), 75–83.
29. Genega, E. M.; Ghebremichael, M.; Najarian, R.; et al. Carbonic anhydrase IX expression in renal neoplasms: correlation with tumor type and grade. *Am. J. Clin. Pathol.*2010,134(6), 873–9.
30. Karhumaa, P.; Kaunisto, K.; Parkkila, S.; et al. Expression of the transmembrane carbonic anhydrases, CA IX and CA XII, in the human male excurrent ducts. *Mol. Hum. Reprod.*2001,7(7), 611–6.
31. Saarnio, J.; Parkkila, S.; Parkkila, A. K.; et al. Immunohistochemistry of carbonic anhydrase isozyme IX (MN/CA IX) in human gut reveals polarized expression in the epithelial cells with the highest proliferative capacity. *J. Histochem. Cytochem.*1998,46(4), 497–504.

32. Ahlskog, J. K.; Schliemann, C.; Marlind, J.; et al. Human monoclonal antibodies targeting carbonic anhydrase IX for the molecular imaging of hypoxic regions in solid tumours. *Br. J. Cancer* 2009, 101(4), 645–57.
33. Petrul, H. M.; Schatz, C. A.; Kopitz, C. C.; et al. Therapeutic mechanism and efficacy of the antibody-drug conjugate BAY 79–4620 targeting human carbonic anhydrase 9. *Mol. Cancer Ther.* 2012, 11(2), 340–9.
34. Krall, N.; Pretto, F.; Neri, D. A bivalent small molecule-drug conjugate directed against carbonic anhydrase IX can elicit complete tumour regression in mice. *Chemical Science* 2014, 5(9), 3640–3644.
35. Krall, N.; Pretto, F.; Decurtins, W.; Bernardes, G. J. L.; Supuran, C. T.; Neri, D. A Small-Molecule Drug Conjugate for the Treatment of Carbonic Anhydrase IX Expressing Tumors. *Angew. Chem., Int. Ed.* 2014, 53(16), 4231–4235.
36. Wichert, M.; Krall, N. Targeting carbonic anhydrase IX with small organic ligands. *Curr. Opin. Chem. Biol.* 2015, 26, 48–54.
37. Alafeefy, A. M.; Carta, F.; Ceruso, M.; Al-Tamimi, A. M.; Al-Kahtani, A. A.; Supuran, C. T. Development of 3-(4-aminosulphonyl)-phenyl-2-mercapto-3H-quinazolin-4-ones as inhibitors of carbonic anhydrase isoforms involved in tumorigenesis and glaucoma. *Bioorg. Med. Chem.* 2016, 24(6), 1402–7.
38. Durgun, M.; Turkmen, H.; Ceruso, M.; Supuran, C. T. Synthesis of 4-sulfamoylphenyl-benzylamine derivatives with inhibitory activity against human carbonic anhydrase isoforms I, II, IX and XII. *Bioorg. Med. Chem.* 2016, 24(5), 982–988.
39. Eldehna, W. M.; Fares, M.; Ceruso, M.; Ghabbour, H. A.; et al. Amido/ureido substituted benzenesulfonamides-isatin conjugates as low nanomolar/subnanomolar inhibitors of the tumor-associated carbonic anhydrase isoform XII. *Eur. J. Med. Chem.* 2016, 110, 259–66.
40. Goksu, H.; Topal, M.; Keskin, A.; et al. 9,10-Dibromo-N-aryl-9,10-dihydro-9,10-[3,4]epipyrroloanthracene-12,14-diones: Synthesis and Investigation of Their Effects on Carbonic Anhydrase Isozymes I, II, IX, and XII. *Arch. Pharm.* 2016, 349(6), 466–74.
41. Dudutiene, V.; Matuliene, J.; Smirnov, A.; et al. Discovery and characterization of novel selective inhibitors of carbonic anhydrase IX. *J. Med. Chem.* 2014, 57(22), 9435–46.
42. Vlahov, I. R.; Santhapuram, H. K.; You, F.; et al. Carbohydrate-based synthetic approach to control toxicity profiles of folate-drug conjugates. *J. Org. Chem.* 2010, 75(11), 3685–91.
43. Cazzamalli, S.; Dal Corso, A.; Neri, D. Acetazolamide Serves as Selective Delivery Vehicle for Dipeptide-Linked Drugs to Renal Cell Carcinoma. *Mol. Cancer Ther.* 2016, 15(12), 2926–2935.

44. Krall, N.; Pretto, F.; Decurtins, W.; Bernardes, G. J.; Supuran, C.T.; Neri, D. A small-molecule drug conjugate for the treatment of carbonic anhydrase IX expressing tumors. *Angew. Chem., Int. Ed.*2014,53(16), 4231–5.
45. Lv, P. C.; Roy, J.; Putt, K. S.; Low, P. S. Evaluation of Nonpeptidic Ligand Conjugates for the Treatment of Hypoxic and Carbonic Anhydrase IX-Expressing Cancers. *Mol. Cancer Ther.*2017,16(3),453–460.
46. Janoniene, A.; Liu, Z.; Baranauskiene, L.; et al. A Versatile Carbonic Anhydrase IX Targeting Ligand-Functionalized Porous Silicon Nanoplatfrom for Dual Hypoxia Cancer Therapy and Imaging. *ACS Appl. Mater. Interfaces*2017,9(16), 13976–13987.
47. Srinivasarao, M.; Galliford, G.; Low, P. Principles in the Design of Ligand-Targeted Cancer Therapeutics and Imaging Agents. *Nat. Rev. Drug Discovery*2015,14, 203–219.
48. Steinman, R.; Brodie, S.; Cohn, Z. Membrane flow during pinocytosis. A stereologic analysis. *J. Cell Biol.*1976,68(3), 665–687.
49. Steinman, R.; Mellman, I.; Muller, W.; Cohn, Z. Endocytosis and the Recycling of Plasma Membrane. *J. Cell Biol.*1983,96(1), 1–27.
50. Kanduluru, A. K.; Low, P. S. Development of a Ligand-Targeted Therapeutic Agent for Neurokinin-1 Receptor Expressing Cancers.*Mol. Pharmaceutics*2017,14(11), 3859–3865.
51. Cazzamalli, S.; Dal Corso, A.; Neri, D. Acetazolamide Serves as Selective Delivery Vehicle for Dipeptide-Linked Drugs to Renal Cell Carcinoma. *Mol. Cancer Ther.*2016,15(12), 2926–2935.
52. Crane, F.; Sun, I.; Sun, E.; Crowe, R. Plasma membrane redox and regulation of cell growth.*Protoplasma*1995,184(1), 3–7.
53. Gébleux, R.; Wulhfard, S.; Casi, G.; Neri, D. Antibody Format and Drug Release Rate Determine the Therapeutic Activity of Non-internalizing Antibody–Drug Conjugates. *Mol. Cancer Ther.*2015,14(11), 2606–2612.
54. Perrino, E.; Steiner, M.; Krall, N.; Bernardes, G.; Pretto, F.; Casi,G.; et al. Curative properties of noninternalizing antibody-drugconjugates based on maytansinoids. *Cancer Res.*2014,74, 2569–2578.

1.7 Appendix A Supplemental Information



Scheme S1. Synthesis of CAL-COOH, a CAIX inhibitor with carboxylic acid functionality

Synthesis of pentafluorobenzenesulfonamide, Compound 7.

A stirring mixture of pentafluorobenzene sulfonyl chloride (2.60 mL) in tetrahydrofuran was chilled to -10 °C using an ice/NaCl cooling bath. Then 3.5M ammonia in methanol/ethanol (6.00 mL) was added dropwise, the reaction warmed to room temperature, and stirred for 3.5 hours. The solvent was then removed under vacuum and recrystallized in water. Yield: 2.7404 g, MP: 153.2-154.8 °C (Lit: 156°C¹), IR(cm⁻¹): 3343.00 (-NH₂, Asym), 3264 (-NH₂, Sym).

Synthesis of 3-((2,3,5,6-tetrafluoro-4-sulfamoylphenyl)sulfonyl)propanoic acid, Compound 8
Pentafluorobenzenesulfonamide (950.4 mg), triethylamine (1.400 mL) and 3-mercaptopropanoic acid (368 µL) were added to methanol (40 mL). The reaction was then refluxed for 24 hours, then dried under vacuum. The resulting residue was then dissolved in a 2:1 mixture of acetic acid to water, respectively. This mixture was then heated to 70°C and 2mL portions of 30% hydrogen peroxide were added every 2 hours until the total volume of peroxide added reached 10 mL. The reaction was then allowed to stir at 70 °C for a total of 24 hours. Acetic acid was removed under vacuum and the resulting precipitate was filtered, washed with water and carried forward with no further purification. Yield: 0.5679 g, LRMS-LC/MS (m/z): [M + H₂O]⁺ calcd for C₉H₈F₄NO₆S₂,

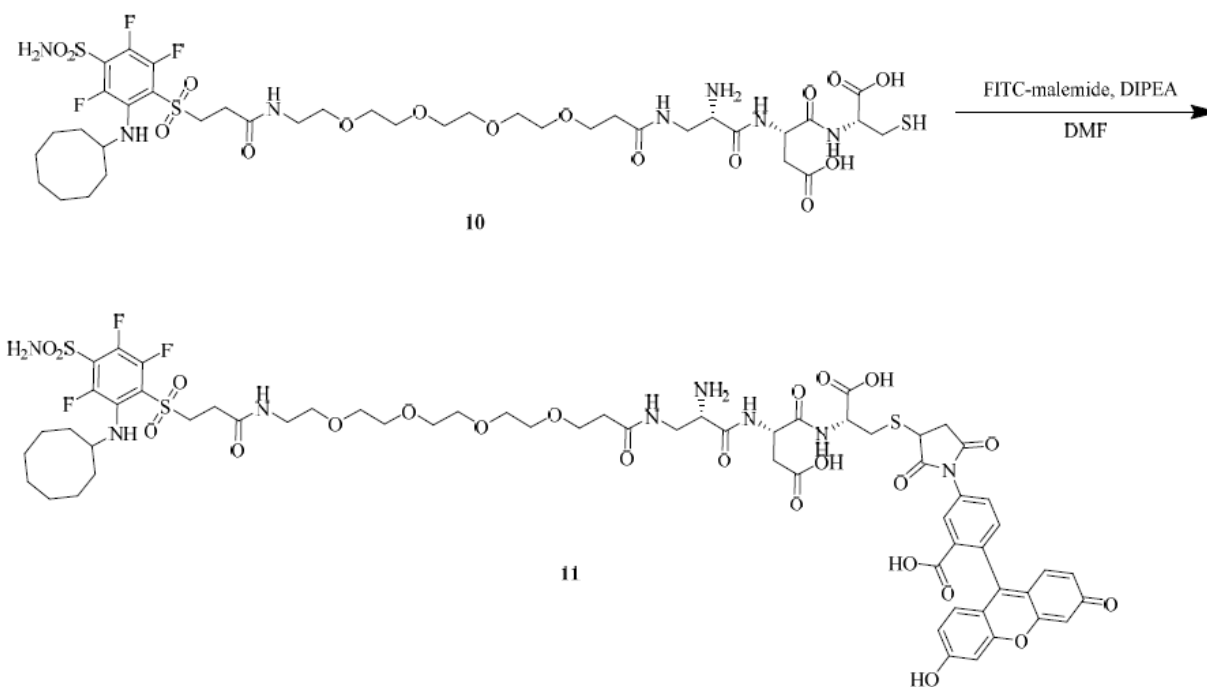
366.0; found, 383.0.

Synthesis of 3-((2-(cyclooctylamino)-3,5,6-trifluoro-4-sulfamoylphenyl)sulfonyl)propanoic acid (CAL-COOH, Compound 9)

Compound 8 (400 mg) was dissolved in DMSO (2 mL) and cyclooctylamine (2 equivalents) was added and the reaction mixture was stirred at room temperature for 24 hours. The reaction was quenched with water and concentrated ammonium chloride. The resulting precipitate was extracted with ethyl acetate and dried over sodium sulfate. The extract was then dried on silica and purified by flash chromatography. (Yield: 0.1662 g) The resulting oil was then purified using RP-HPLC [A = 20 mM ammonium acetate buffer (pH 7.0), B = CH₃CN, solvent gradient: 0% B to 100% B in 30 min, retention time: 17.5 min]. ¹H NMR (500 MHz, DMSO-d₆) δ 7.28 (bs, 6H*), 6.65 (q, J = 9.0 Hz, 1H), 3.83 – 3.66 (m, 1H), 3.60 (dt, J = 22.1, 7.9 Hz, 2H), 2.49 (t, J = 20.5 Hz, 1H), 2.31 (dt, J = 14.4, 7.6 Hz, 2H), 1.89 – 1.70 (m, 3H), 1.70 – 1.11 (m, 10H). ¹⁹F NMR (471 MHz, DMSO-d₆) δ -126.01 (t, J = 8.3 Hz), -135.46 (dd, J = 27.0, 12.5 Hz), -151.62 (dd, J = 27.1, 6.7 Hz).

*Integration sulfonamide protons may be affected by carboxylic acid

LRMS-LC/MS (m/z): [M + H]⁺ calcd for C₁₇H₂₄F₃N₂O₆S₂, 473.1; found, 473.2.



Scheme S2. Synthesis of CAL-PEG4-FITC, compound 11.

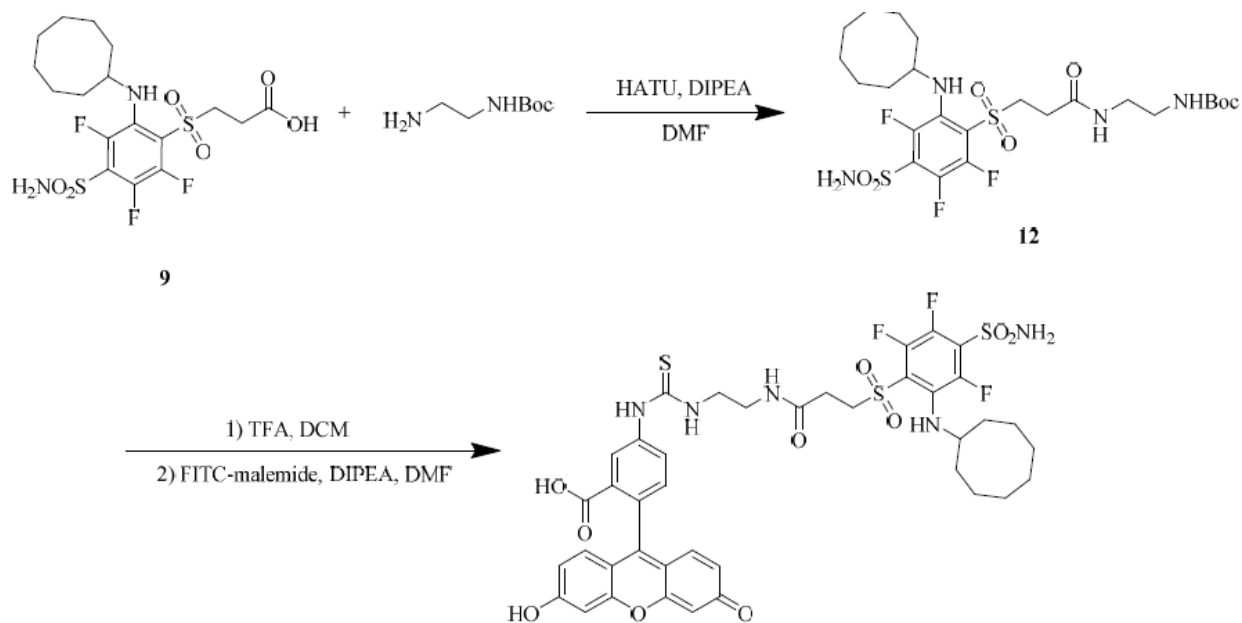
Synthesis of (2R,5S,8S)-8-amino-5-(carboxymethyl)-29-((2-(cyclooctylamino)-3,5,6-trifluoro-4-sulfamoylphenyl)sulfonyl)-2-(mercaptomethyl)-4,7,11,27-tetraoxo-14,17,20,23-tetraoxa-3,6,10,26-tetraazanonacosanoic acid, Compound 10.

Compound 10 was synthesized by the following solid phase methodology: H-Cys(Trt)-2-chlorotrityl resin (100 mg, 0.64 mmole/g) was swollen with 3 mL of DCM followed by 3 mL of DMF. After swelling the resin in DMF, a solution of Fmoc-Asp(tBu)-OH (52.7 mg, 0.128 mmoles), HATU (60.8 mg, 0.16 mmoles) and DIPEA (0.056 ml, 0.32 mmoles) in DMF (3 mL) was added. Argon was bubbled for 2 h, and resin was washed with DMF (3 x 3 mL) and i-PrOH (3 x 3 mL). The Fmoc was removed with a piperidine solution (20% in DMF, 3x5 ml) and the resin was washed with DMF (3 x 3 mL) and i-PrOH (3 x 3 mL). A solution of Boc-DAP(Fmoc)-OH (54.6 mg, 0.128 mmoles), HATU (60.8 mg, 0.16 mmoles) and DIPEA (0.056 ml, 0.32 mmoles) in DMF (3 mL) was added. Argon was bubbled for 2 h, and resin was washed with DMF (3 x 3 mL) and i-PrOH (3 x 3 mL). The Fmoc was removed with a piperidine solution (20% in DMF, 3X 5 ml) and the resin was washed with DMF (3 x 3 mL) and i-PrOH (3 x 3 mL). A solution of Fmoc-15-amino-4,7,10,13-tetraoxapentadecanoic acid (62.4 mg, 0.128 mmoles), HATU (60.8 mg, 0.16 mmoles) and DIPEA (0.056 ml, 0.32 mmoles) in DMF was added. Argon was bubbled for 2 h, and resin was washed with DMF (3 x 3 mL) and i-PrOH (3 x 3 mL). The Fmoc was removed with a piperidine solution (20% in DMF, 3X 5 ml) and the resin was washed with DMF (3 x 3 mL) and i-PrOH (3 x 3 mL). A solution of CAL-COOH (9, 33.3mg, 0.074 mmoles), HATU (24.3 mg, 0.064 mmoles) and DIPEA (0.034 ml, 0.192 mmoles) in DMF was added. Argon was bubbled for 2 h, and resin was washed with DMF (3 x 3 mL) and i-PrOH (3 x 3 mL). Compound 10 was cleaved from the resin using a TFA:TIPS:H₂O:EDT cocktail (95:2.5:2.5:2.5) and concentrated under vacuum. The concentrated product was precipitated in diethyl ether and dried under vacuum. Crude conjugate was purified by RP-HPLC [A = 20 mM ammonium acetate buffer (pH 5.0), B = CH₃CN, solvent gradient: 0% B to 100% B in 30 min, retention time: 9.8 min] to yield the product as a clear oil (62%). LRMS-LC/MS (m/z): [M + H]⁺ calcd for C₃₈H₆₀F₃N₇O₁₆S₃, 1024.33; found, 1024.3.

Synthesis of 5-(3-(((2R,5S,8S)-8-amino-2-carboxy-5-(carboxymethyl)-29-((2-(cyclooctylamino)-3,5,6-trifluoro-4-sulfamoylphenyl)sulfonyl)-4,7,11,27-tetraoxo-14,17,20,23-tetraoxa-3,6,10,26-

tetraazanonacosyl)thio)-2,5-dioxopyrrolidin-1-yl)-2-(6-hydroxy-3-oxo-3H-xanthen-9-yl)benzoic acid, Compound 11.

To a solution of 10 (2 mg, 0.002 mmoles) in DMF (1 mL) was added fluorescein-5-maleimide (0.85 mg, 0.002 mmoles) and DIPEA (0.002 ml, 0.01 mmoles) and stirred for 1 hour at room temperature. The crude reaction mixture was purified using RP-HPLC [A = 2 mM ammonium acetate buffer (pH 7.0), B = CH₃CN, solvent gradient: 0% B to 80% B in 30 min, retention time: 21.9 min] to yield the product as a yellow powder (76%). LRMS-LC/MS (m/z): [M + H]⁺ calcd for C₆₂H₇₃F₃N₈O₂₃S₃, 1451.40; found, 1451.3.



Scheme S3. Synthesis of CAL-EDA-FITC, compound 13.

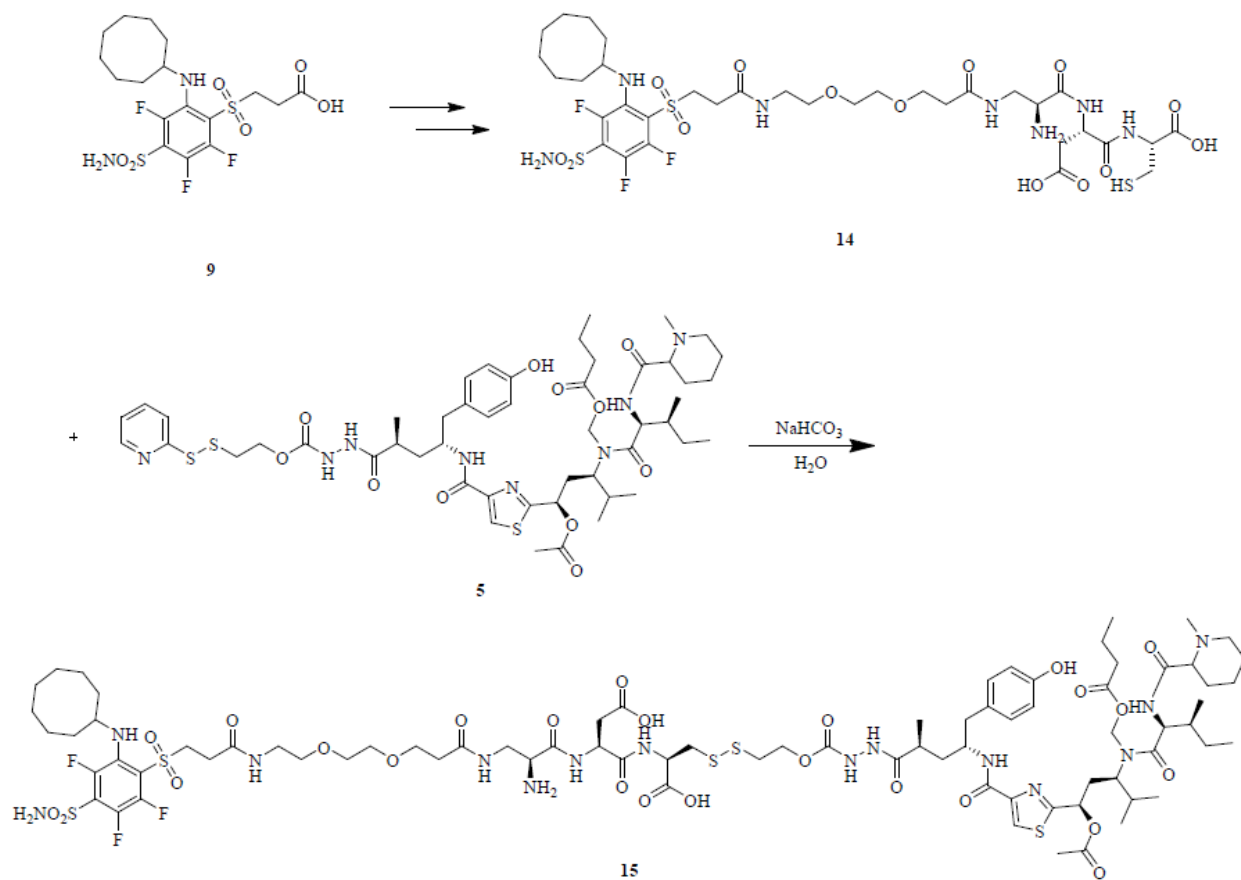
Synthesis of tert-butyl (2-(3-((2-(cyclooctylamino)-3,5,6-trifluoro-4-sulfamoylphenyl)sulfonyl)propanamido)ethyl)carbamate, Compound 12.

To a solution of 3-((2-(cyclooctylamino)-3,5,6-trifluoro-4-sulfamoylphenyl)sulfonyl)propanoic acid (20 mg, 0.042 mmoles) in DMF (2 ml) was added tert-butyl (2-aminoethyl)carbamate (7.40 mg, 0.0462 mmoles) and allowed to stir under argon for 10 minutes at room temperature. HATU

(16 mg, 0.042 mmoles) and DIPEA (0.022 ml, 0.126 mmoles) were then added. The reaction was stirred for 1 hour before quenching with water (10 ml) and extracted with ethyl acetate (3 x 25 ml). The organic layers were combined, washed with brine, and dried over anhydrous sodium sulfate. The solvent was concentrated under vacuum, and the crude mixture was purified on silica gel using 10% methanol/dichloromethane to obtain 12 as a colorless oil (21.4 mg, 83%). LRMS-LC/MS (m/z): [M + H]⁺ calcd for C₂₄H₃₇F₃N₄O₇S₂, 615.21; found, 615.2. ¹H NMR (500 MHz, DMSO-d₆) δ 8.29 (bs, 2H), 8.12 (t, J = 5.7 Hz, 1H), 6.79 (t, J = 5.7 Hz, 1H), 6.62 (d, J = 8.4 Hz, 1H), 3.81 (d, J = 9.1 Hz, 1H), 3.76 (t, J = 7.4 Hz, 2H), 3.07 – 2.93 (m, 4H), 2.62 – 2.57 (m, 2H), 1.91 – 1.84 (m, 2H), 1.73 – 1.63 (m, 2H), 1.62 – 1.48 (m, 10H), 1.40 (d, J = 1.4 Hz, 9H). ¹⁹F NMR (471 MHz, DMSO-d₆) δ -126.12 (d, J = 11.7 Hz), -135.38 (dd, J = 27.3, 12.2 Hz), -151.64 (d, J = 26.9 Hz).

Synthesis of 5-(3-(2-(3-((2-(cyclooctylamino)-3,5,6-trifluoro-4-sulfamoylphenyl)sulfonyl)propanamido)ethyl)thioureido)-2-(6-hydroxy-3-oxo-3H-xanthen-9-yl)benzoic acid, Compound 13.

The tert-butyloxycarbonyl protecting group of compound 13 (10 mg, 0.008 mmoles) was removed with a mixture of TFA/DCM (20%, 2 ml) for 30 minutes. The TFA/DCM mixture was removed under vacuum and the product brought forward without purification. To the vial containing the deprotected 13, was added DMF (1 ml) and DIPEA (0.007 ml, 0.04 mmoles) and allowed to stir for 5 minutes before fluorescein-5-maleimide (3.8 mg, 0.0088 mmoles) was added and allowed to stir for an additional hour. The crude mixture was purified without workup by purified RP-HPLC [A = 2 mM ammonium acetate buffer (pH 7.0), B = CH₃CN, solvent gradient: 0% B to 100% B in 30 min, retention time: 26.1 min] to yield the product as a yellow powder (76%). LRMS-LC/MS (m/z): [M + H]⁺ calcd for C₄₀H₄₀F₃N₅O₁₀S₃, 904.19; found, 904.2



Scheme S4. Synthesis of CAL-PEG2-TubB, compound 15

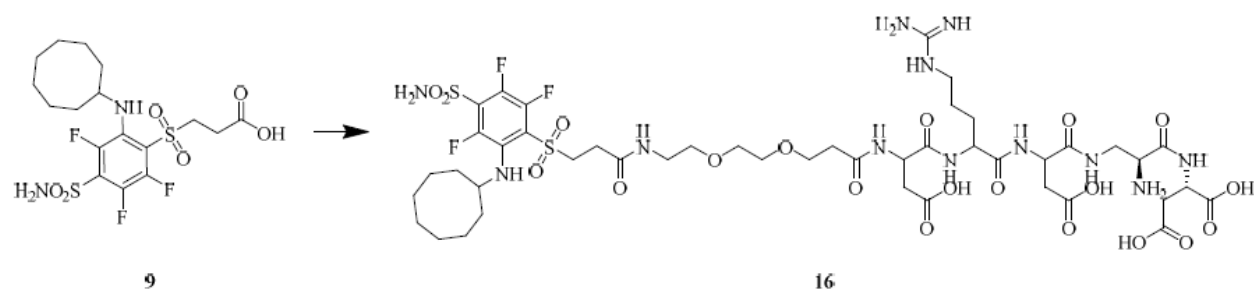
Synthesis of (2R,5S,8S)-8-amino-5-(carboxymethyl)-23-((2-(cyclooctylamino)-3,5,6-trifluoro-4-sulfamoylphenyl)sulfonyl)-2-(mercaptomethyl)-4,7,11,21-tetraoxo-14,17-dioxo-3,6,10,20-tetraazatricosanoic acid, Compound 14.

Compound 14 was synthesized by the following solid phase methodology. H-Cys(Trt)-2-chlorotrityl resin (100 mg, 0.64 mmole/g) was swollen with 3 mL of DCM followed by 3 mL of DMF. After swelling the resin in DMF, a solution of Fmoc-Asp(tBu)-OH (52.7 mg, 0.128 mmoles), HATU (60.8 mg, 0.16 mmoles) and DIPEA (0.056 ml, 0.32 mmoles) in DMF (3 mL) was added. Argon was bubbled for 2 h, and resin was washed (3x3 mL) with DMF and i-PrOH (3x3 mL). The Fmoc was removed with a piperidine solution (20% in DMF, 3x5 ml) and the resin was washed with DMF (3 x 3 mL) and i-PrOH (3 x 3 mL). A solution of Boc-DAP(Fmoc)-OH (54.6 mg, 0.128 mmoles), HATU (60.8 mg, 0.16 mmoles) and DIPEA (0.056 ml, 0.32 mmoles) in DMF (3 mL) was added. Argon was bubbled for 2 h, and resin was washed with DMF (3 x 3 mL) and i-PrOH (3 x 3 mL). The Fmoc was removed with a piperidine solution

(20% in DMF, 3X 5 ml) and the resin was washed with DMF (3 x 3 mL) and i-PrOH (3 x 3 mL). A solution of Fmoc-9-amino-4,7-dioxanonanoic acid (51.12 mg, 0.128 mmoles), HATU (60.8 mg, 0.16 mmoles) and DIPEA (0.056 ml, 0.32 mmoles) in DMF was added. Argon was bubbled for 2 h, and resin was washed with DMF (3 x 3 mL) and i-PrOH (3 x 3 mL). The Fmoc was removed with a piperidine solution (20% in DMF, 3X 5 ml) and the resin was washed with DMF (3 x 3 mL) and i-PrOH (3 x 3 mL). A solution of 3-((2-(cyclooctylamino)-3,5,6-trifluoro-4-sulfamoylphenyl)sulfonyl)propanoic acid (compound 9, 33.3mg, 0.074 mmoles), HATU (24.3 mg, 0.064 mmoles) and DIPEA (0.034 ml, 0.192 mmoles) in DMF was added. Argon was bubbled for 2 h, and resin was washed with DMF (3 x 3 mL) and i-PrOH (3 x 3 mL). Compound 14 was cleaved from the resin using a TFA:TIPS:H₂O:EDT cocktail (95:2.5:2.5:2.5) and concentrated under vacuum. The concentrated product was precipitated in diethyl ether and dried under vacuum. Crude conjugate was purified by RP-HPLC [A = 20 mM ammonium acetate buffer (pH 5.0), B = CH₃CN, solvent gradient: 0% B to 100% B in 30 min, retention time: 15.6 min] to yield the product as a clear oil (62%). LRMS-LC/MS (m/z): [M + H]⁺ calcd for C₃₄H₅₂F₃N₇O₁₄S₃, 935.27; found, 935.2.

Synthesis of (3R,5S,16R,19S)-1-(2-((1R,3R)-1-acetoxy-3-((2S,3S)-N-((butyryloxy)methyl)-3-methyl-2-(1-methylpiperidine-2-carboxamido)pentanamido)-4-methylpentyl)thiazol-4-yl)-19-((S)-16-amino-1-((2-(cyclooctylamino)-3,5,6-trifluoro-4-sulfamoylphenyl)sulfonyl)-3,13-dioxo-7,10-dioxo-4,14-diazaheptadecan-17-amido)-16-carboxy-3-(4-hydroxybenzyl)-5-methyl-1,6,9,18-tetraoxo-10-oxa-13,14-dithia-2,7,8,17-tetraazahenicosan-21-oic acid, Compound 15.

A solution of saturated sodium bicarbonate (10 mL) in distilled water was bubbled with argon continuously for 30 min. Compound 14 (1.5 mg, 0.0016 mmol) was dissolved in argon-purged HPLC grade water (2.0 mL) and the pH of the reaction mixture was increased to 7 using argon purged sodium bicarbonate. A solution of activated-Tubulysin B, supplied by Endocyte, (compound 5, 1.86 mg, 0.018 mmol) in THF (0.5 mL) was then added to the reaction mixture. The progress of the reaction was monitored using analytical LCMS, and after stirring for 30 min, the reaction was found to reach completion. Compound 15 was purified by RP-HPLC [A = 20 mM ammonium acetate buffer (pH 7.0), B = CH₃CN, solvent gradient: 0% B to 100% B in 30 min, retention time: 22.2 min] to yield the requisite product. LRMS-LC/MS (m/z): [M + H]⁺ calcd for C₇₉H₁₁₉F₃N₁₄O₂₅S₅, 1881.70; found, 1881.5.



Scheme S5. Synthesis of CAL-PEG2-D-R-D-Dap-D, compound 16.

Synthesis of ((2S)-2-amino-3-(3-carboxy-2-(2-(3-carboxy-2-(3-(2-(2-(3-((2-(cyclooctylamino)-3,5,6-trifluoro-4-sulfamoylphenyl)sulfonyl)propanamido)ethoxy)ethoxy)propanamido)propanamido)-5-guanidinopentanamido)propanamido)propanoyl)-L-aspartic acid, Compound 16.

Compound 16 was synthesized by the following solid phase methodology: H-Cys(Trt)-2-chlorotrityl resin (100 mg, 0.64 mmole/g) was swollen with 3 mL of dichloromethane (DCM) followed by 3 mL of dimethylformamide (DMF). After swelling the resin in DMF, a solution of Boc-DAP(Fmoc)-OH (54.6 mg, 0.128 mmoles), HATU (60.8 mg, 0.16 mmoles) and DIPEA (0.056 ml, 0.32 mmoles) in DMF (3 mL) was added. Argon was bubbled for 2 h, and resin was washed with DMF (3 x 3 mL) and i-PrOH (3 x 3 mL). The Fmoc was removed with a piperidine solution (20% in DMF, 3X 5 ml) and the resin was washed with DMF (3 x 3 mL) and i-PrOH (3 x 3 mL). The other residues were added in using the same stoichiometry. Compound 16 was cleaved from the resin using a TFA:TIPS:H₂O:EDT (95:2.5:2.5:2.5) and concentrated under vacuum. The concentrated product was precipitated in diethyl ether and dried under vacuum. Crude conjugate was purified by RP-HPLC [A = 20 mM ammonium acetate buffer (pH 7.0), B = CH₃CN, solvent gradient: 0% B to 60% B in 30 min, retention time: 18.0 min] to yield the product as a clear oil (62%). LRMS-LC/MS (m/z): [M + H]⁺ calcd for C₄₅H₆₉F₃N₁₂O₂₀S₂, 1219.41; found, 1219.09.

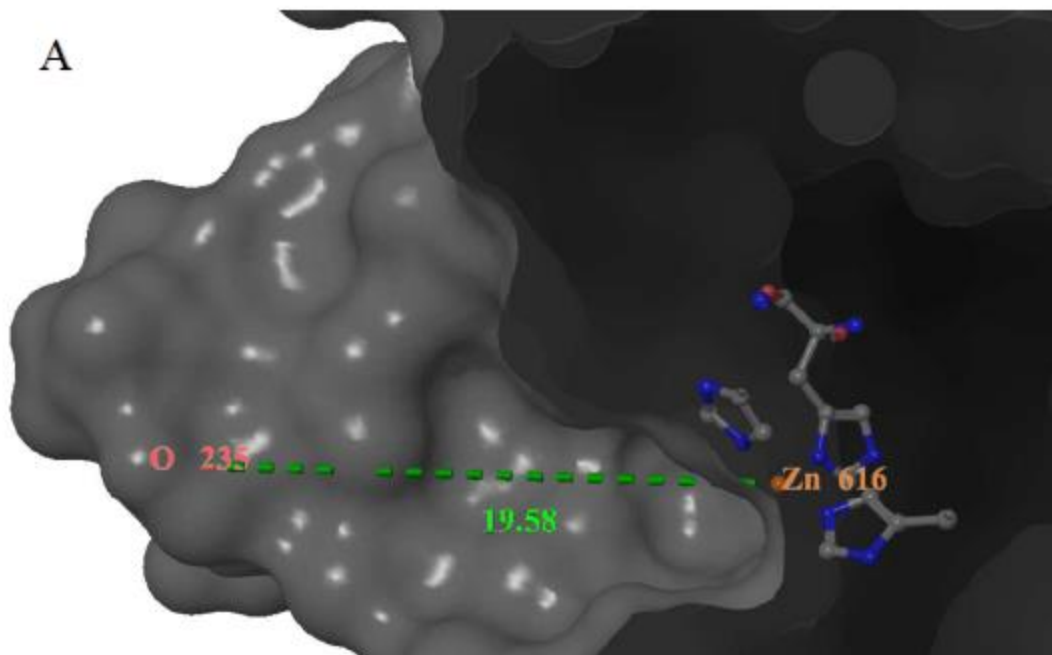


Figure S1. (A) Measurement of the depth of the binding pocket of CAIX active site (PDB: 4Q07) shows that a SMDC must have a linker length of about 20 Å to avoid steric interference with the protein surface

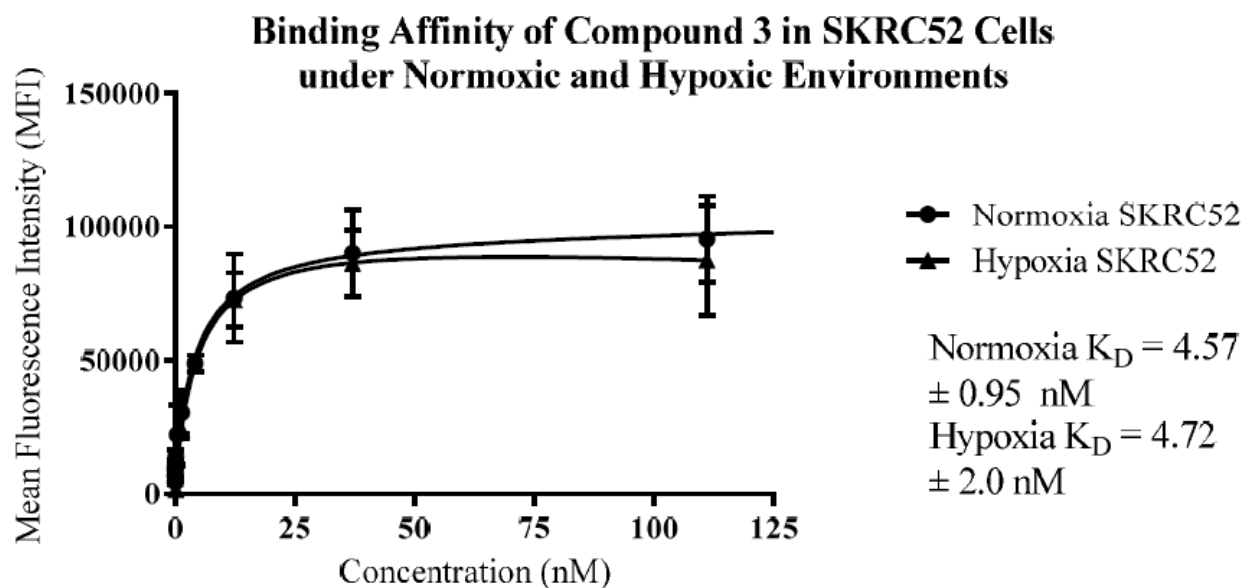


Figure S2. Binding affinity of CAL-FITC conjugate 3 in SKRC52 cells with or without hypoxia showing that conjugate 3 binds to CAIX irrespective of whether or not hypoxia is present.

Binding Affinity of CAIX FITC Conjugates 3, 11, and 13 in SKRC52 Cells

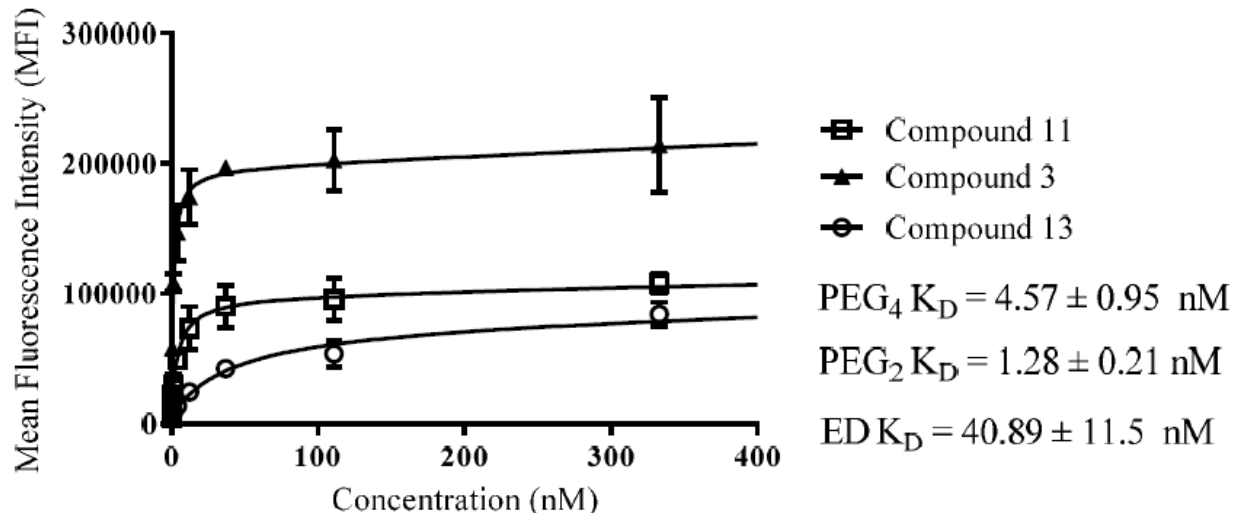


Figure S3. Binding Affinity of CAIX FITC conjugates 3, 11, and 13 in SKRC52 cells shows that the compound with PEG2 linker (compound 3) has the highest binding affinity at 1.28 nM.

Binding Affinity of CAIX FITC conjugates 3, 11, and 13 in HEK293-CA9 Cells

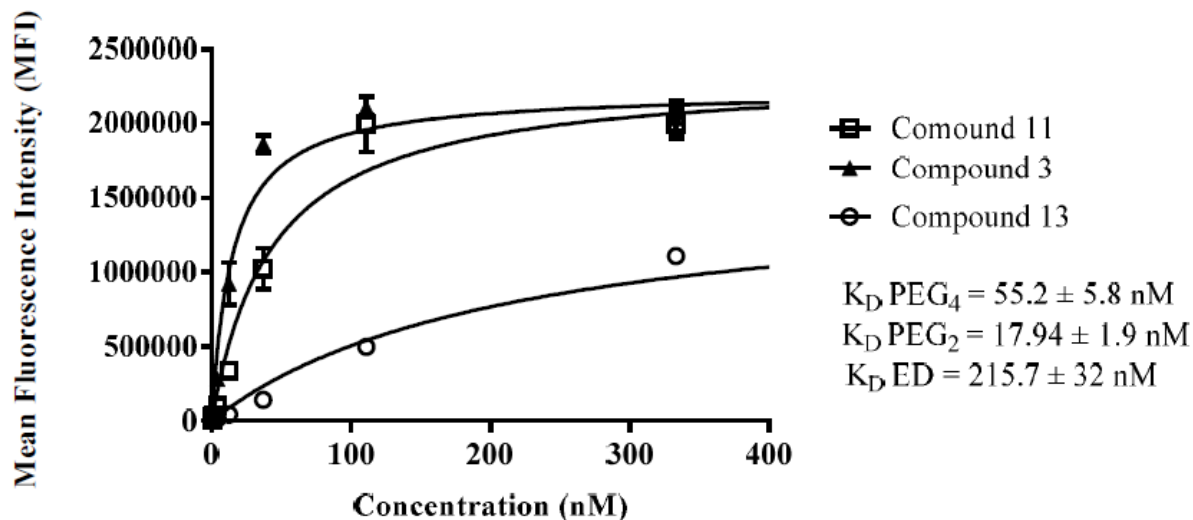
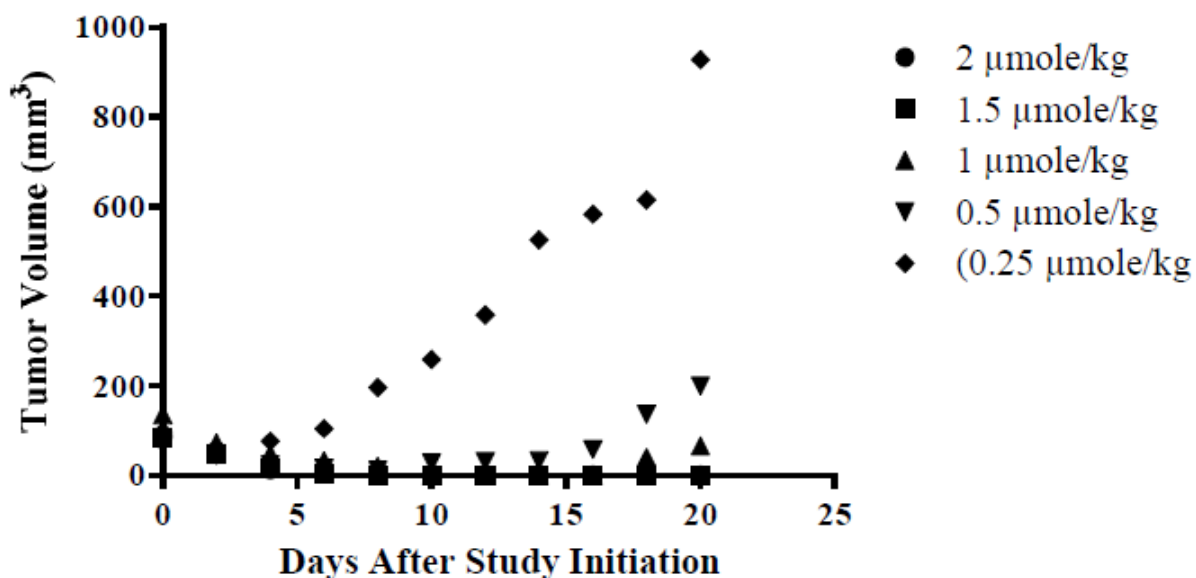


Figure S4. Binding affinity of CAL-FITC conjugates 3, 11, and 13 in HEK293-CA9 cells

Dose Escalation of Compound 6 in HT29 Xenograph Model



showing that the PEG2 linker (compound 3) has the highest binding affinity at 17.94 nM. Figure S5. Dose escalation in vivo efficacy of compound 6 in HT29 xenografts (n=1 in for each dose). After tumor disappeared, the mice were treated with one additional dose. The last treatment was Day 6, 8, 12 and 14 for Mouse 1, 2, 3, and 4/5, respectively. Doses 2, 1.5, and 1 $\mu\text{mole/kg}$ all shrink tumors equally fast, but 1 $\mu\text{mole/kg}$ shows tumor reemergence starting on day 16.

Dose Escalation of Compound 6 in HT29 Xenografts: Mice Body Mass

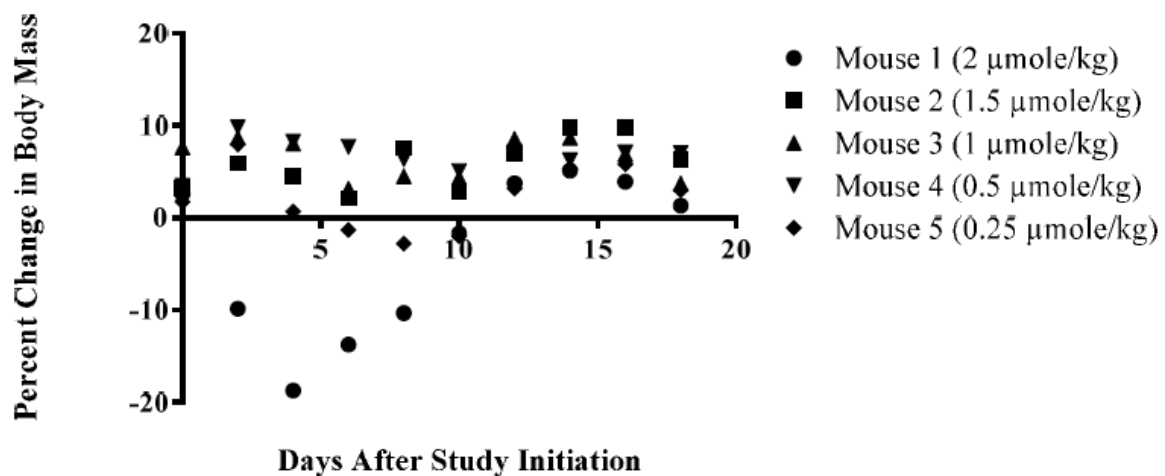


Figure S6. Whole body masses of HT29 xenograft mice treated with various doses of compound 6 (n=1 in for each dose). The highest dose of compound 6 still shows loss of body mass when compared to compound 15 (data not shown) but the other (lower) doses show acceptable body mass profiles.

***In Vivo* Efficacy of Compound 6 in A549 Xenografts**

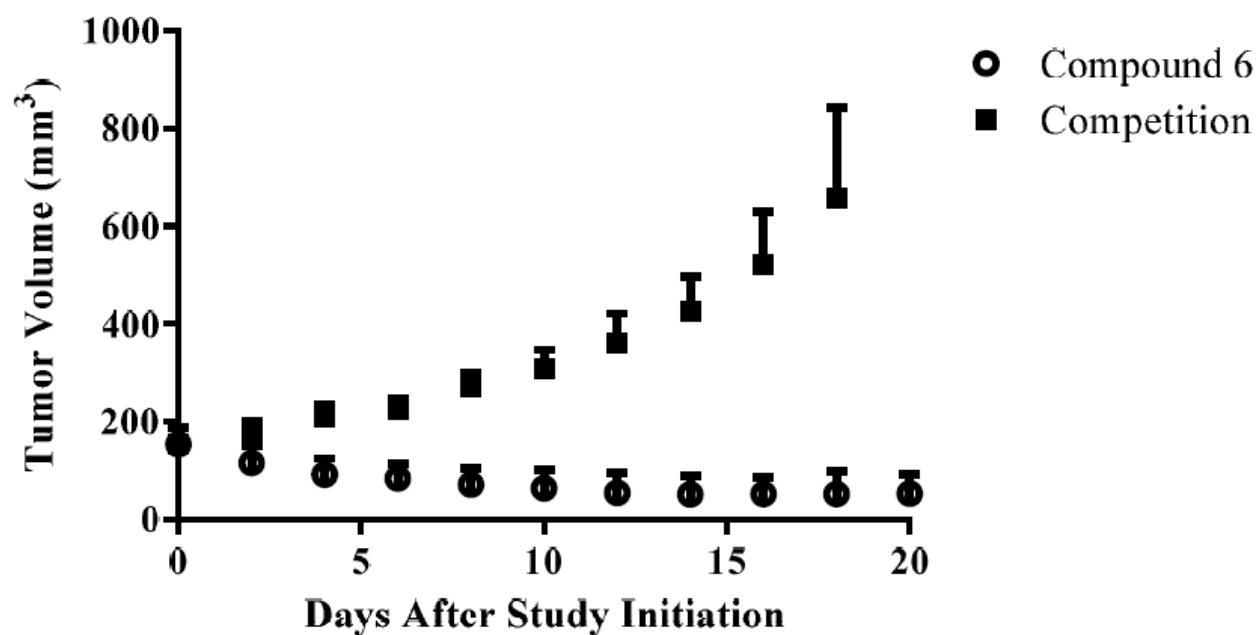


Figure S7. *In vivo* efficacy of compound 6 in A549 xenografts. Treatment was administered TIW for three weeks at 1.25 $\mu\text{mole/kg}$ of compound 6 and the competition was treated with 1.25 $\mu\text{mole/kg}$ of compound 6 with 100-fold excess of compound 16. The competition group was sacrificed as per the study's humane guidelines on Day 18. The treatment group shows displays stable tumor regression and stable disease until treatment cessation.

In Vivo Efficacy of Compound 6 in A549 Xenografts: Mice Body Mass

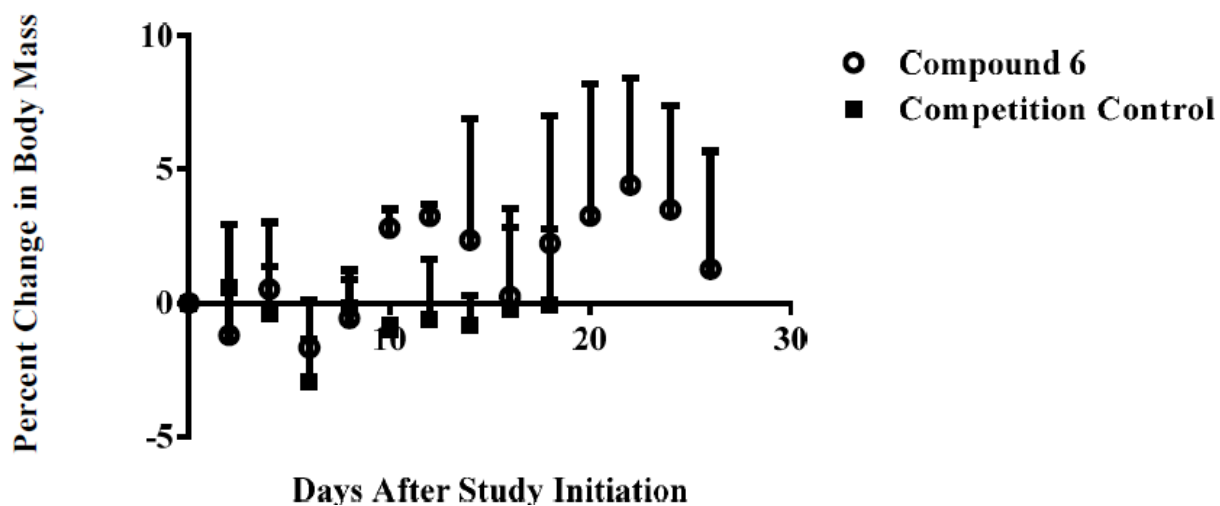


Figure S8. Whole body masses of A549 xenograft mice treated with 1.25 $\mu\text{mole/kg}$ of compound 6 and the competition group 1.25 $\mu\text{mole/kg}$ of compound 6 with 100-fold excess of compound 16.

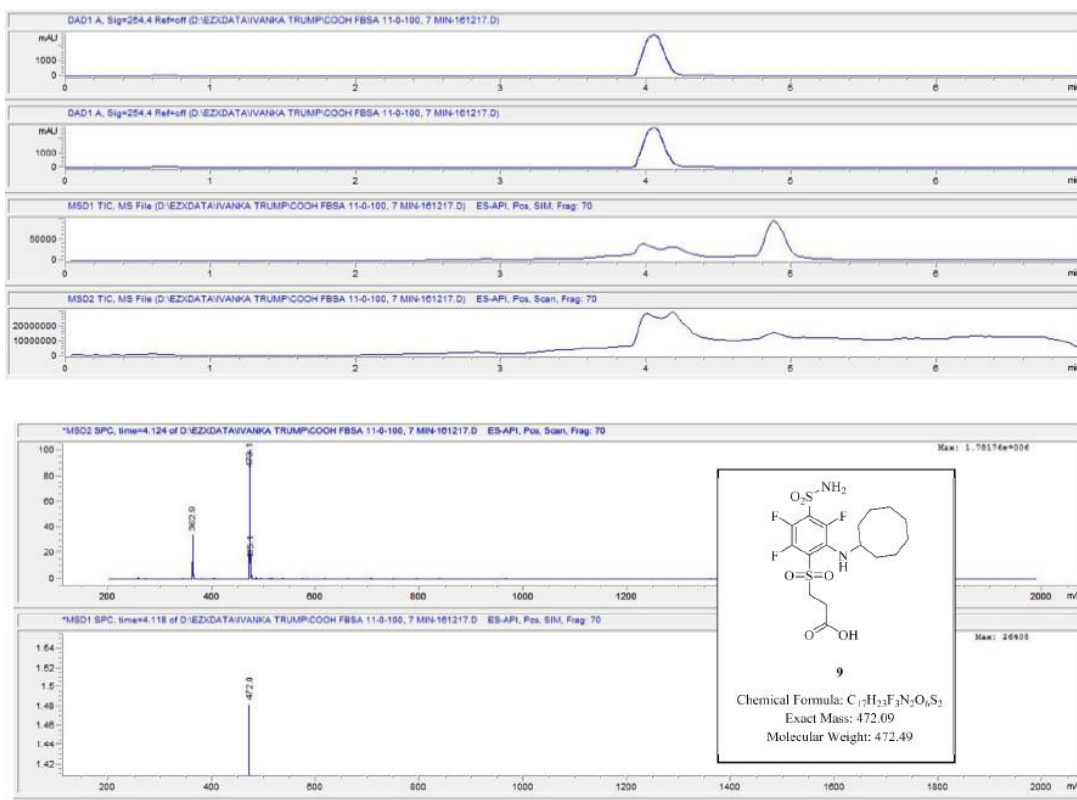


Figure S9. LC-MS characterization of compound 9.

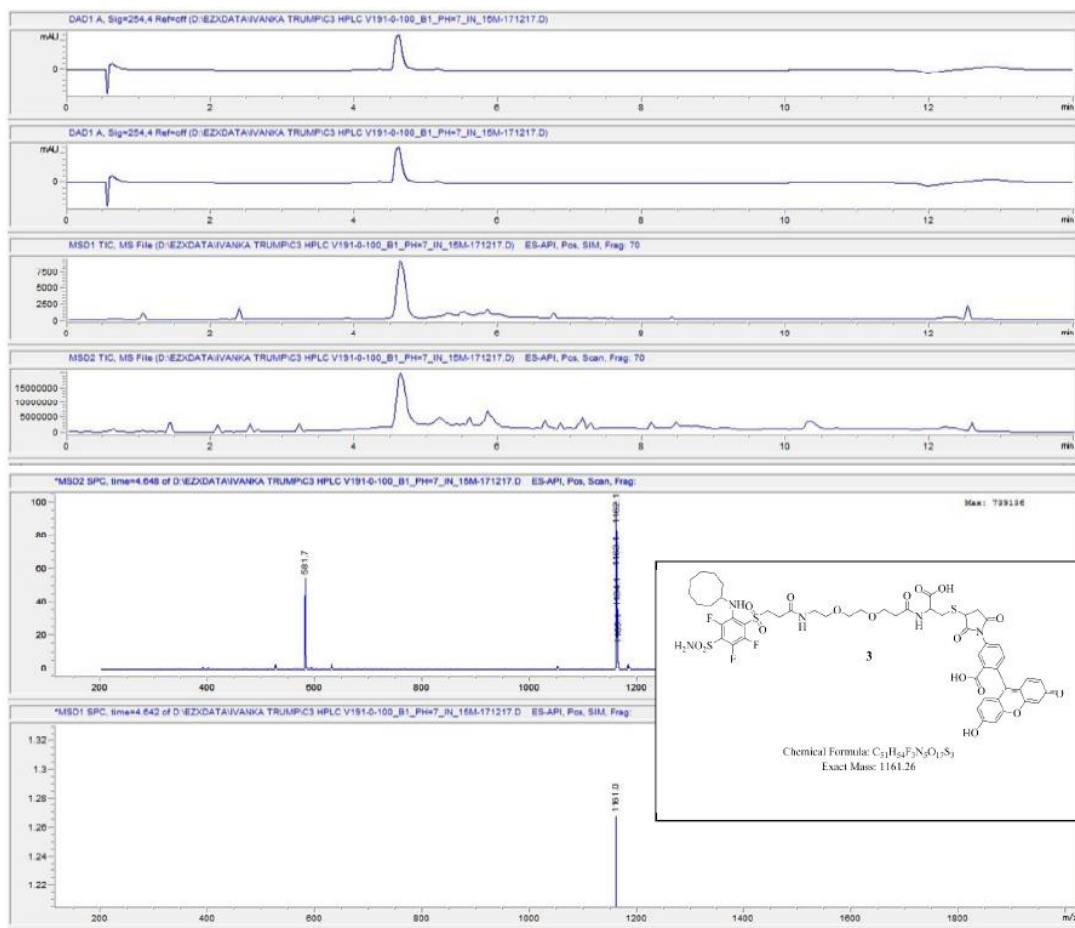


Figure S10. LC-MS characterization of compound 3.

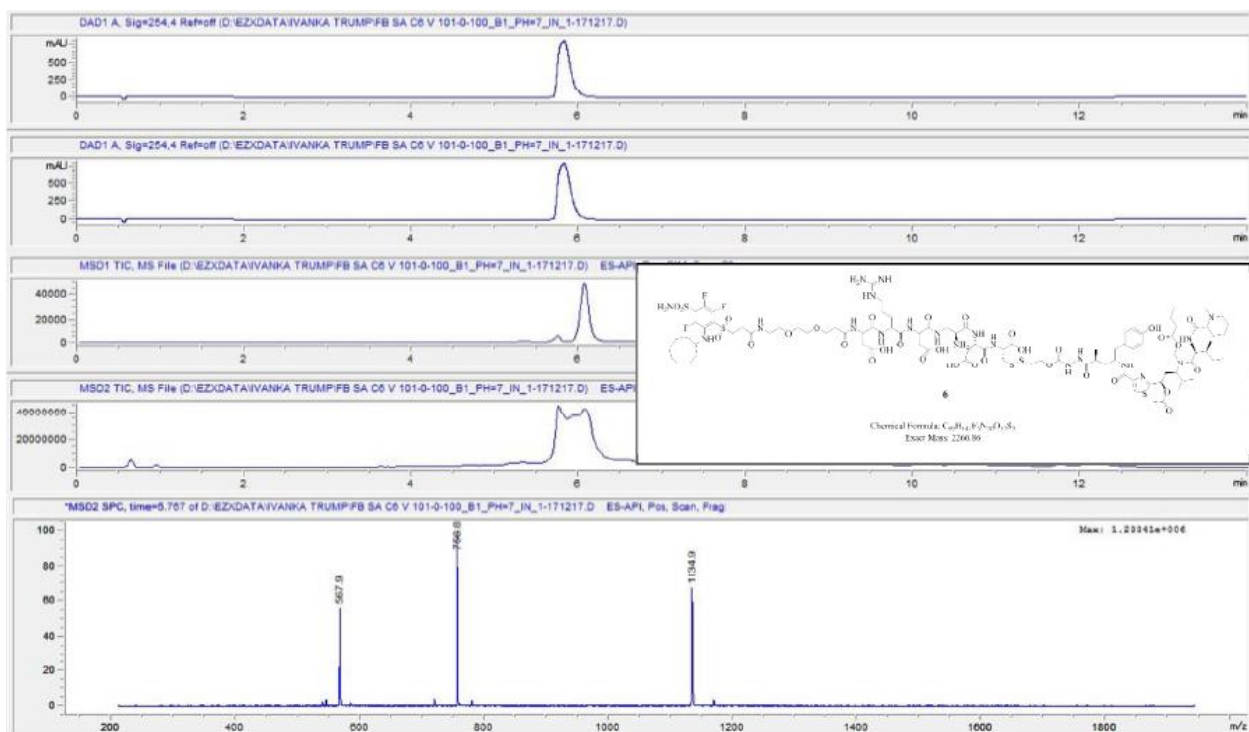


Figure S11. LC-MS characterization of compound 6.

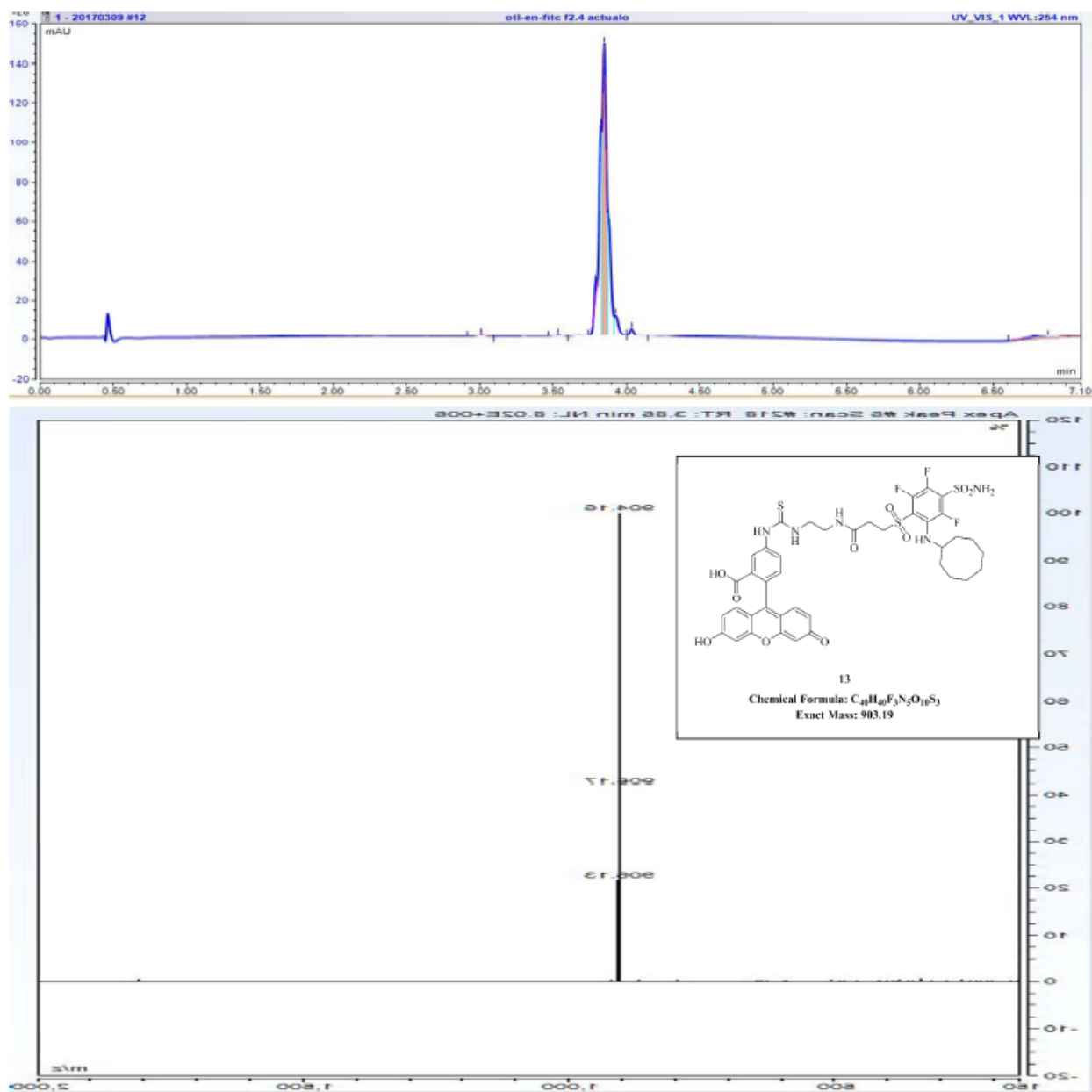


Figure S13. LC-MS characterization of compound 13.

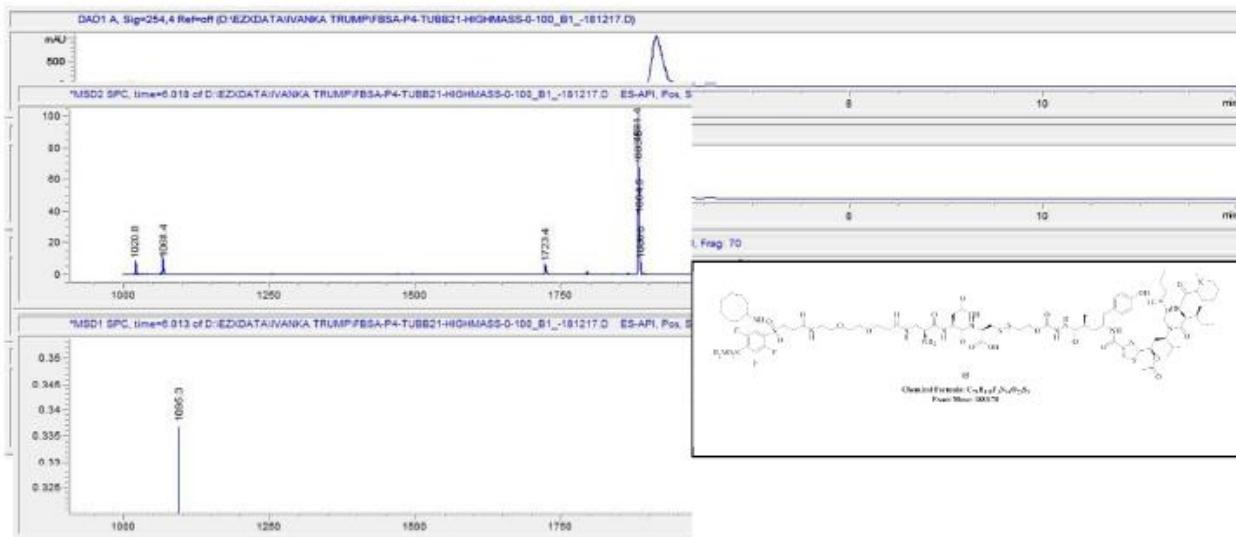


Figure S14. LC-MS characterization of compound 15.

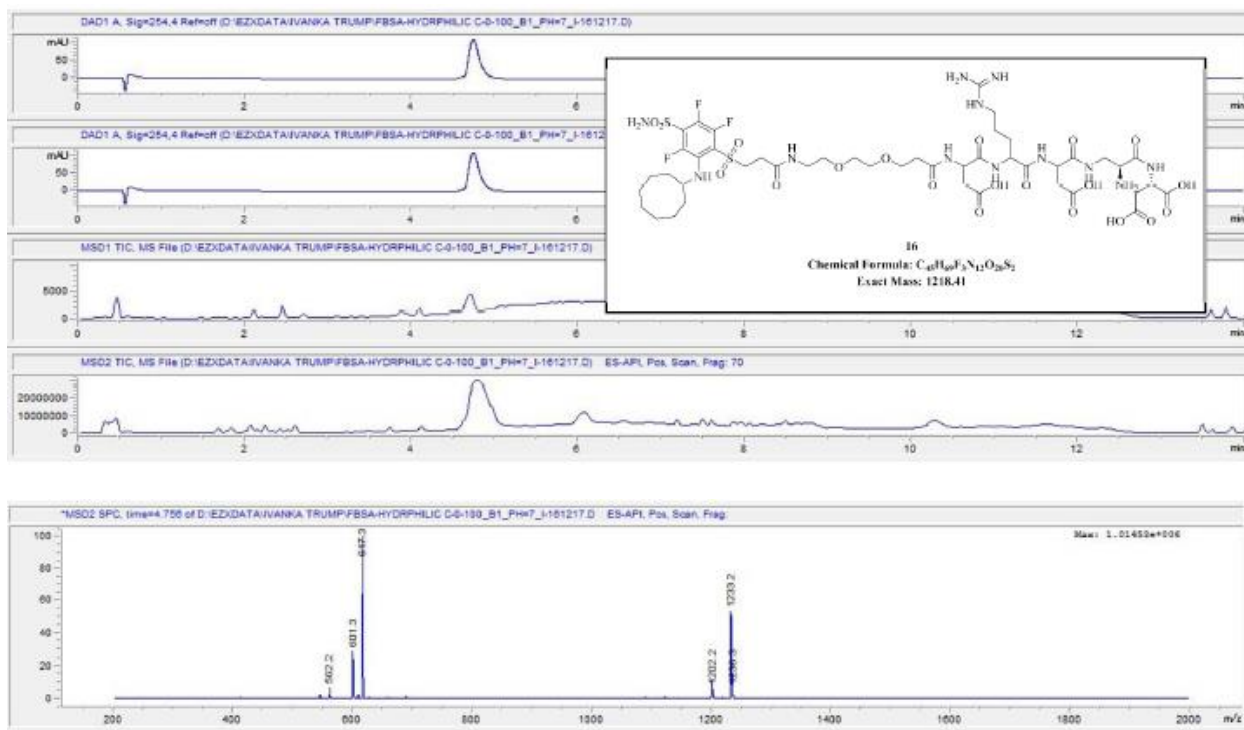


Figure S15. LC-MS characterization of compound 16.

1.8 Appendix B Carbonic Anhydrase IX Book Chapter Review

Use of Carbonic Anhydrase IX Inhibitors for Selective Delivery of Attached Drugs to Solid Tumors. Reprinted/adapted by permission from [Springer Nature]: [Springer) [Carbonic Anhydrase as a Drug Target] by [Daumantas Matulis] [2019] (2019)

Spencer Gardeen and Philip S. Low

Abstract

Central to the goal of precision medicine lies the ability to target an effective drug specifically to diseased cells, thereby avoiding the uptake and collateral toxicity that arises when good drugs accumulate in healthy cells. While antibody-drug conjugates (ADCs) have pioneered many efforts in this field, small molecule drug conjugates (SMDCs) with high specificities for diseased cell types are now displaying equal if not greater potential because of their improved abilities to penetrate solid tissues. For both technologies, however, success has invariably depended on an ability to identify a receptor that is overexpressed on the desired pathologic cell (e.g., cancer cell, virus-infected cell, inflammatory cell, etc.), but absent or weakly expressed on all other healthy cells. While few cell surface receptors can satisfy these criteria, one that has attracted considerable recent attention has been carbonic anhydrase IX (CA IX), a cell surface enzyme that is expressed in virtually all hypoxic tissues, but minimally expressed, if at all, in healthy tissues. Because most solid tumors are hypoxic, CA IX-targeted SMDCs are now being explored as broad-spectrum agents for the diagnosis and therapy of CA IX-expressing malignancies. The following chapter highlights some of the groundbreaking research in this area and provides key insights into how the design of a CA IX-targeted SMDC can impact efficacy.

Introduction

In the era of precision medicine, ligand-targeted drugs that can deliver an attached therapeutic payload selectively to diseased cells are receiving increased attention, because they frequently increase drug uptake by pathologic cells while suppressing its accumulation in healthy cells [1–3]. While antibody-drug conjugates that exploit an antibody's affinity for a disease-specific receptor have been explored for some applications, their inability to efficiently penetrate solid tumors and other dense tissues have limited their envisioned uses [4]. In contrast, small molecule drug conjugates that rely on low molecular weight targeting ligands to deliver attached imaging or therapeutic agents to diseased cells have attracted increasing interest, primarily because of their improved abilities to penetrate pathologic tissues and their rapid clearance from receptor-negative healthy tissues [5, 6]. Moreover, after binding to disease-specific receptors on target cells, many of these small molecule drug conjugates enter the target cells by receptor-mediated

endocytosis [7], thereby trapping the drug conjugate within the target cell and reducing its chance of diffusing into adjacent healthy cells. While many low molecular weight ligand-drug conjugates have entered clinical trials, the most successful ligand-targeted drugs to date have been targeted to either folate receptors [3] or prostate-specific membrane antigen [8]. Folate receptor alpha (FR α), for example, is overexpressed on approximately 40% of human cancers [9], including cancers of the ovary, lung, endometrium, kidney, colon, bladder, and breast [9]. Folate receptor beta (FR β), in contrast, is upregulated on myelogenous leukemia cells (i.e., AML and CML) and also on activated but not resting macrophages [10,11]. Due to its over-expression on activated macrophages, FR β is abundantly observed in virtually all inflamed tissues, including lesions associated with rheumatoid arthritis, inflammatory bowel diseases, multiple sclerosis, idiopathic pulmonary fibrosis, psoriasis, osteoarthritis, sarcoidosis, scleroderma, and Sjogren's disease [12–17]. Prostate-specific membrane antigen, on the other hand, is overexpressed on almost all prostate cancer cells [18], and more recently, has been found to be upregulated on the neovasculature of many solid tumors [19–22]. While folate receptor and prostate-specific membrane antigen targeting ligands enable delivery of attached therapeutic and imaging agents to over half of all human cancers, there are still a large number of lethal malignancies for which no targeting ligands currently exist. In an effort to identify targeting ligands for those malignancies not addressed by folate receptor or prostate-specific membrane antigen-targeted drugs, we have searched for other cell surface receptors that might be upregulated in multiple human cancers but largely absent from normal tissues [23–27]. After examination of the literature, we concluded that carbonic anhydrase IX (CA IX), a membrane-spanning CA isoform that catalyzes the interconversion of $\text{H}_2\text{CO}_3 \leftrightarrow \text{H}_2\text{O} + \text{CO}_2$, might constitute an attractive target for further evaluation [28]. Thus, CA IX is a membrane-spanning carbonic anhydrase whose active site is exposed on the extra-cellular surface of a cell and whose expression is normally negligible except under

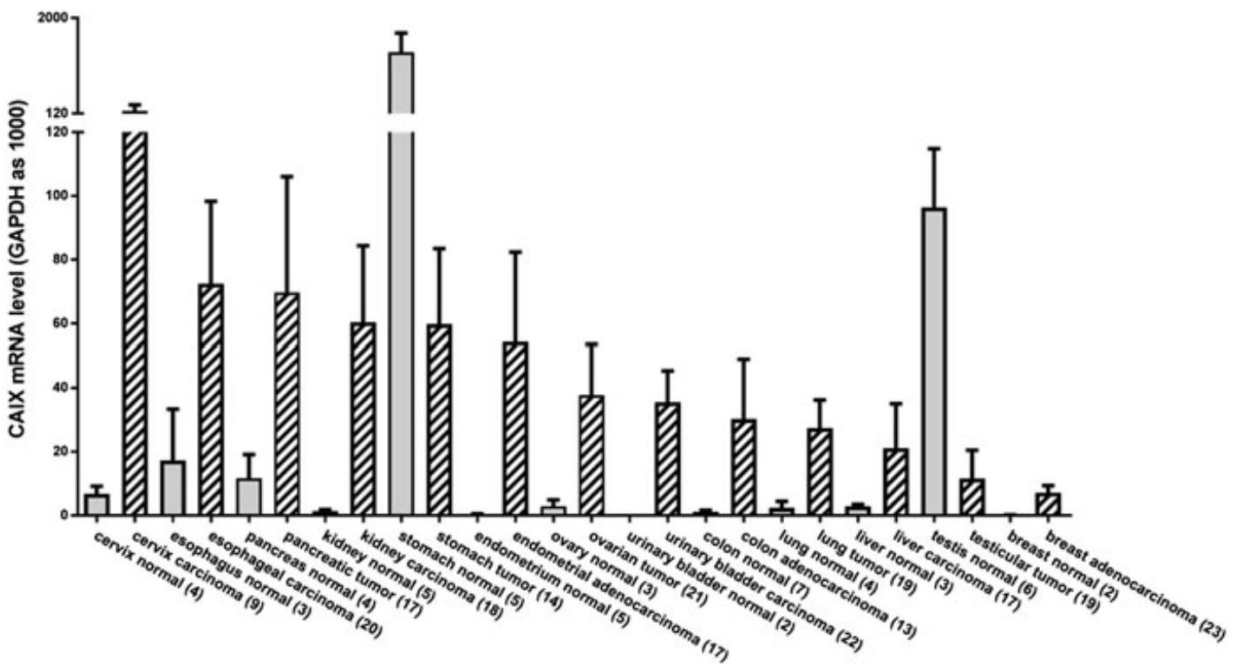


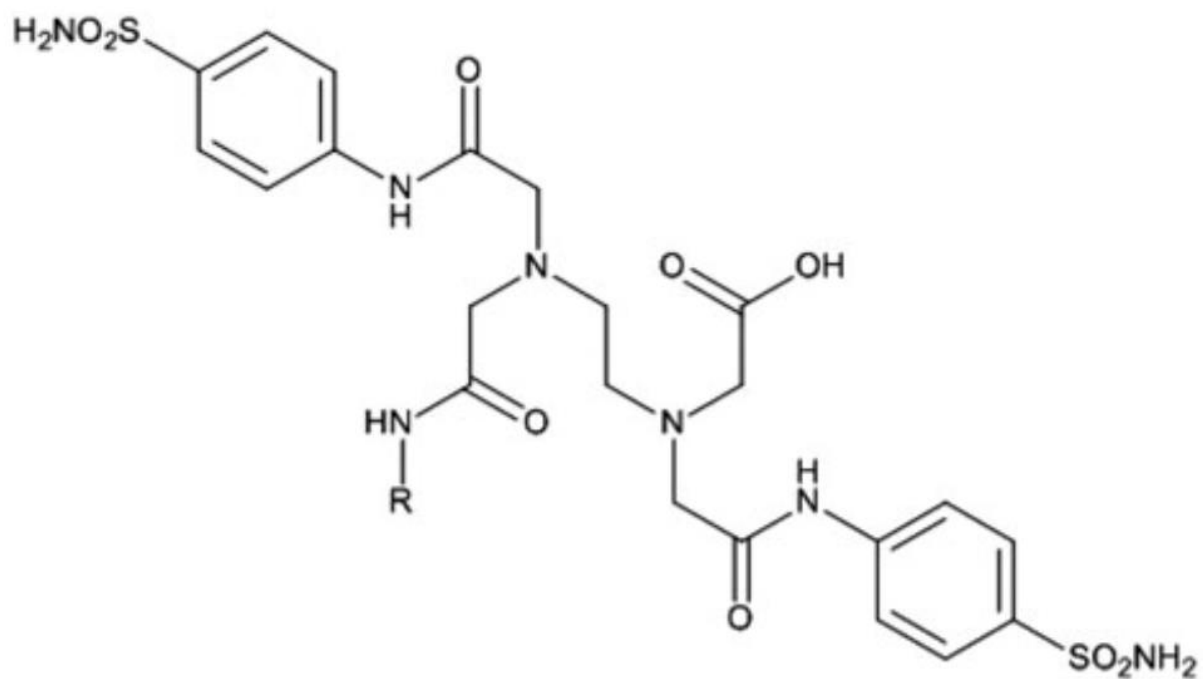
Fig 19.1 Expression of CA IX relative to GAPDH in various human cancers and adjacent normal tissues. GAPDH gene expression in each tissue sample was set arbitrarily at 1000 and the cDNA level of CA IX gene expression was calculated from the threshold cycle (C_t) difference ($C_t(\text{CA IX}) - C_t(\text{GAPDH})$). The numbers of each tissue type examined are provided in parentheses and values are expressed as mean \pm SEM. Reprinted with permission from Bioconjugate Chemistry

[30]

hypoxic conditions where it is strongly induced [29]. Because most solid tumors are highly hypoxic, CA IX appears to be upregulated in most malignant masses, but largely absent from the corresponding normal tissues [23–27]. Quantitative rtPCR of multiple tissue samples from many human cancers has indeed confirmed this hypothesis. Thus, as shown in Fig.19.1, expression of CA IX in most malignant lesions exceeds its expression in the corresponding normal tissues by anywhere from 5 to 100fold. In fact, only stomach and testes exhibit greater expression in normal than cancer tissues. Based on this tumor specificity, we and others have elected to design, synthesize, and test a variety of CA IX targeted drugs for their tumor-selective uptake. The brief review below summarizes many of the results of these efforts.

CA IX Targeting with a Benzenesulfonamide Ligand. One of the more common groups of ligands used for targeting drugs to CA IX contains benzenesulfonamide as the central scaffold in the CA IX binding moiety. In this ligand, as in other CA IX ligands described in this and other articles in this book, the sulfonamide moiety binds to a catalytic zinc atom in the active site, whereas the other substituents on the ligand are designed to enhance affinity and confer specificity for the desired carbonic anhydrase isozyme. In the case of CA IX, the catalytic pocket is 20Å deep [1], dictating that a linker must be inserted between the targeting ligand and the desired payload in order to allow the sulfonamide moiety to engage the zinc at the bottom of the catalytic pocket. Moreover, because the catalytic pocket is narrow in places, if the linker is not optimally designed, its conjugation to the targeting ligand can reduce the ligand's affinity for CA IX. For example, whereas the bis-benzenesulfonamide inhibitor originally developed by Rami et al. displayed single digit nanomolar affinity for CA IX [31], an infrared dye and ^{99m}Tc conjugate of the same ligand were found to bind CA IX-expressing cancer cells with dissociation constants of 45 and 54 nM, respectively. This comparison indicates that care must be taken in the design of the linker to assure that neither the linker nor the attached payload interfere with binding to the enzyme [32,33]. In general, the benzenesulfonamide ligands have been primarily exploited to deliver either SPECT (¹⁸⁸Re, ^{99m}Tc) or PET (⁶⁸Ga, ¹⁸F) imaging agents to solid tumors [34–40]. While many of the benzenesulfonamide-based imaging agents retain excellent affinity for CA IX [34, 35, 40], there has been a general lack of specificity for tumor over normal tissue [34, 39], resulting in unfavorable biodistribution patterns that have led to complicated whole body images. Except for a trimeric ⁶⁸Ga conjugate produced by Lau et al., most compounds have displayed tumor-to-blood ratios less than 1 with considerable uptake in healthy organs such as liver, kidney, and intestines

[38]. Given the much higher expression of CA IX in malignant than healthy tissues (Fig.19.1), the question must be asked whether benzenesulfonamide-derived ligands might exhibit off-target affinities for other metal-containing enzymes or whether the imaging payload might significantly alter the biodistribution of the intact conjugate. Regarding the latter possibility, we have noticed that a strongly anionic aromatic payload exhibits much lower healthy tissue accumulation than the same benzenesulfonamide ligand linked via an identical PEG12spacer to a peptidic payload [41]. Thus, an EDTA-bridged bis-benzenesulfonamide connected via PEG12to the indocyanine dye, S0456, shows little nonmalignant tissue retention in tumor-bearing mice except in the kidneys, whereas the same EDTA-bridged bis-benzenesulfonamide-PEG12construct linked to a tetrapeptide payload displays considerable uptake in many normal tissues[41, 42]. While the cause of this difference in tissue retention has not been investigated, we hypothesize that the unwanted normal tissue retention exhibited by the peptidic conjugate might derive from widely expressed peptide scavenger receptors that are present in many healthy tissues [43]. In addition to the above imaging applications, the latter EDTA-bridged bis-benzenesulfonamide ligand has also been exploited for delivery of a therapeutic warhead for treatment of CA IX-expressing tumors [44]. Thus, Lv et al. have shown that an EDTA-bridged bis-benzenesulfonamide conjugate of tubulysin B hydrazide (Fig.19.2) can prevent tumor growth in mice bearing human cancer xenografts [44]. Although the tumors were not completely eradicated, the ability of the conjugate to block tumor expansion without causing observable toxicity argued that the conjugate deserved further investigation [44]. This absence of detectable toxicity to healthy organs also suggested that the off-target uptake seen with several benzenesulfonamide-targeted imaging agents was probably replicated when the ligand was covalently linked to tubulysin B hydrazide, i.e., again suggesting that the payload can influence biodistribution of the intact conjugate.



R = PEG₁₂-EC20-Tubulysin b Hydrazide

Fig. 19.2 General structure of bis-benzenesulfonamide targeting ligand

CA IX Targeting with Acetazolamide or 6-Aminosaccharin A second major class of CA IX targeted conjugates has exploited the use of the CA IX inhibitor, acetazolamide, to deliver attached payloads. Although acetazolamide-derived ligands generally have higher affinities for carbonic anhydrase than the benzenesulfonamides [41, 45], their specificity for CA IX over other carbonic anhydrases is much worse. As a consequence, the acetazolamide-targeted conjugates must be designed to be completely membrane impermeable so that they only enter cells when associated with a cell surface exposed carbonic anhydrase. Because both major extracellularly exposed carbonic anhydrases (CA IX and CA XII) are upregulated primarily in malignant tissues, use of a pan-carbonic anhydrase targeting ligand to selectively image or treat cancer tissues might be acceptable if the only path for entry of the targeted payload into cells was via internalization of the extracellularly exposed carbonic anhydrase. Utilizing this principle, Krall et al. synthesized and tested several acetazolamide drug conjugates containing a peptide-based linker attached to the drug payload via a self-immolative disulfide bridge [46,47]. As shown in Fig.19.3, the authors were able to achieve a stable disease state with limited dosing of a targeted cytotoxic drug (DM1) in mice bearing SKRC52 renal cell carcinoma xenografts [46], suggesting that the conjugate was therapeutically active. It should be noted, however, that an acetazolamide conjugate of a different cytotoxic agent, duocarmycin, only yielded delayed tumor growth with unacceptable toxicity [46]. As seen in other small molecule drug conjugates [48], these results emphasize the critical importance stable, and have proper release kinetics to effectively deliver therapeutic levels of drug to the intended target. For more details on payload selection, please consult the following detailed reviews [32,33]. of payload selection when designing SMDCs. Payloads must be potent, metabolically

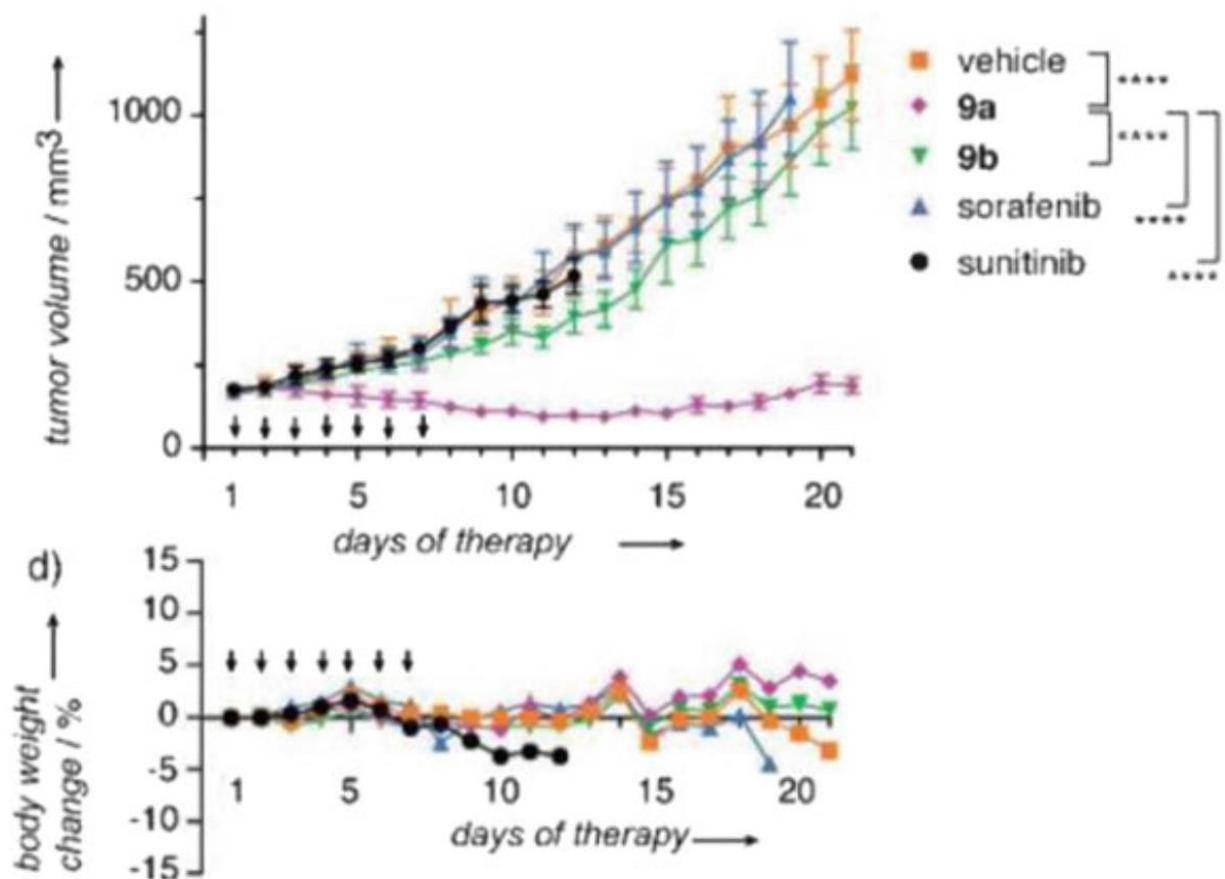


Fig. 19.3 In vivo efficacy of acetazolamide-targeted drug conjugates. Mice bearing SKRC52 xenografts were treated with 70 nmols acetazolamide-targeted (9a) untargeted (9b) DM1 and appropriate controls for 7 days, then monitored for 3 weeks. Arrows indicate days of dosing. Reprinted with permission from Angewandte Chemie [46]

Success in using acetazolamide to deliver cytotoxic drugs to CA IX-expressing cancers prompted Krall et al. to publish a subsequent paper in which they attached a peptide-based ^{99m}Tc chelating agent previously employed in EC20 [49] to create a SPECT radio imaging agent for localization of CA IX positive tumors [45]. Although tumor:blood ratios were acceptable, tumor to other tissue ratios revealed poor tumor specificity (Fig.19.4)[45]. Given the apparent tumor specificity of the acetazolamide-targeted DM1 conjugate, we suspect that the strongly peptidic nature of this imaging agent may have diverted much of the conjugate to peptide scavenger receptors in the healthy tissues. Acetazolamide has also been exploited to deliver attached near infrared fluorescent dyes to tumor tissues for intended use in fluorescence-guided surgery of cancer. As shown in Fig.19.5, Bao et al. [50] were able to construct an acetazolamide-VivoTag 680 conjugate that displayed significant uptake in only the tumor and kidney, with little dye retention in most other tissues. Moreover, with a slight variation in linker length and the use of a phenyl-oxo-bridged S0456 NIR dye, Mahalingam et al. observed a similarly improved biodistribution pattern, except the uptake in the kidneys was still further reduced (Fig.19.6)[2]. These data support the previously stated hypothesis that linker chemistry and payload composition can influence the biodistribution of a ligand-targeted drug conjugate.

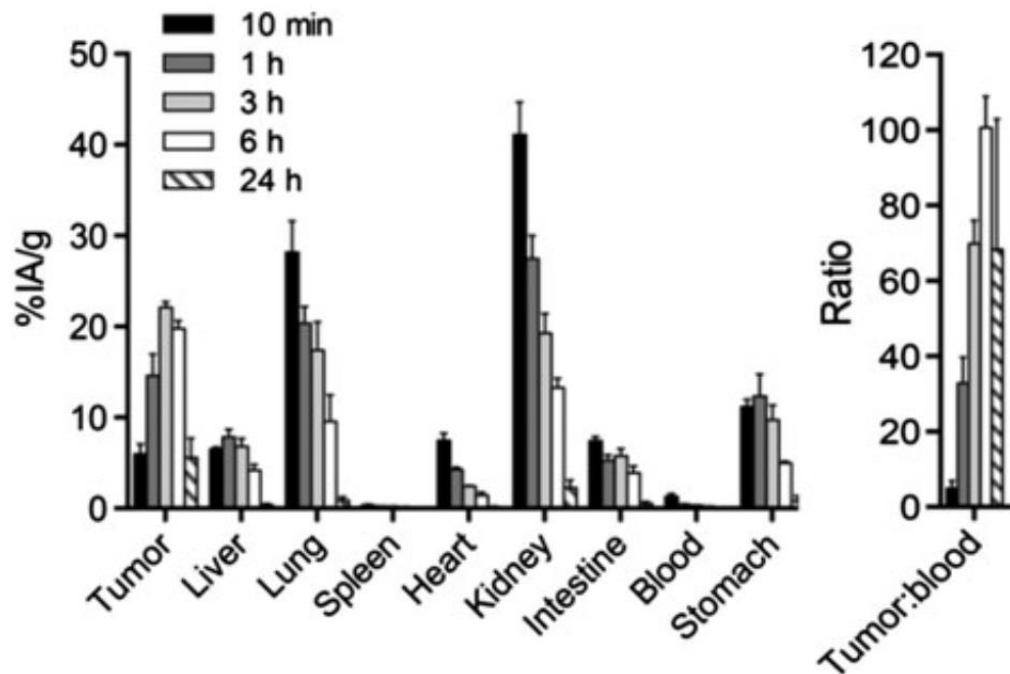
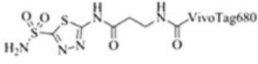


Fig. 19.4 Biodistribution of acetazolamide-99mTc in mouse with SKRC-52 tumor. Mice bearing SKRC52 xenografts were injected with 0.17 MBq of chelated 99mTc targeted with acetazolamide and subsequently sacrificed at the indicated time points to carry out biodistribution. Reprinted with permission from Journal of Nuclear Medicine [45] (2 figures)

While variations in linker length/composition as well as dye choice can influence the eventual biodistribution, enhancing tumor uptake and improving tumor-to-healthy tissue ratios can also be achieved by increasing the affinity of the targeting ligand for its CA IX receptor. This principle demonstrated by Wichert et al. in a DNA encoded library of more than 100,000 compounds was used to identify moieties that might increase the binding affinity of acetazolamide. Thus, when a higher affinity CA IX targeting ligand was used to deliver a near infrared fluorescent dye, increased tumor accumulation, prolonged tumor retention, and greater tumor-to-background ratios were observed (Fig.19.7)[51]. These data were interpreted to demonstrate that higher ligand affinity can also improve the performance of a ligand-drug conjugate [2]. Finally, in other studies it has been noted that the rate of tumor accumulation and healthy tissue clearance can also be impacted by the different components of the targeted drug [52]. Taken together, the above data argue that all components of a ligand-targeted drug conjugate (i.e., ligand, linker, and payload) must be independently optimized to achieve the most favorable pharmacokinetics, pharmacodynamics, and biodistribution of the final conjugate.

CA IX Targeting with 3-((2-(Cyclooctylamino)-3,5,6-Trifluoro-4-Sulfamoylphenyl)Sulfonyl)Propanoic Acid

The final class of CA IX-targeted conjugates (see Fig.19.8, below) employs a high affinity, high specificity substituted benzenesulfonamide CA IX inhibitor originally developed by Matulis and colleagues for delivery of attached imaging and therapeutic agents [53]. As shown in Fig.19.8, the CA IX targeting moiety distinguishes itself from those described above in that the benzenesulfonamide is reprivatized with a cyclooctylamine-ring that presumably fills a hydrophobic pocket in the binding site of CA IX not occupied by other inhibitors and thereby increases the scaffold's affinity for CA IX by at least 1000-fold [53].

	HS680	Control Agent
Structure		
MW	1372 g/mol	1341 g/mol
Absorbance	670 nm	670 nm
Emission	686 nm	685 nm

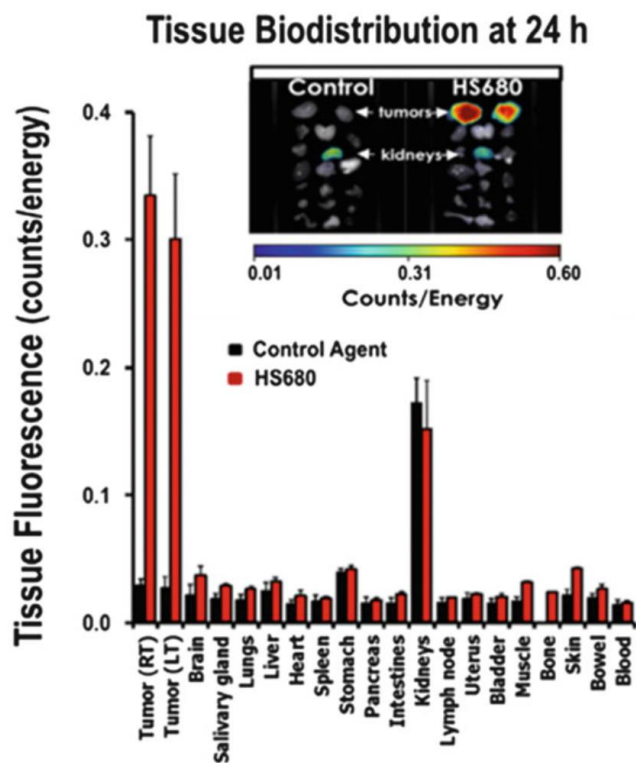
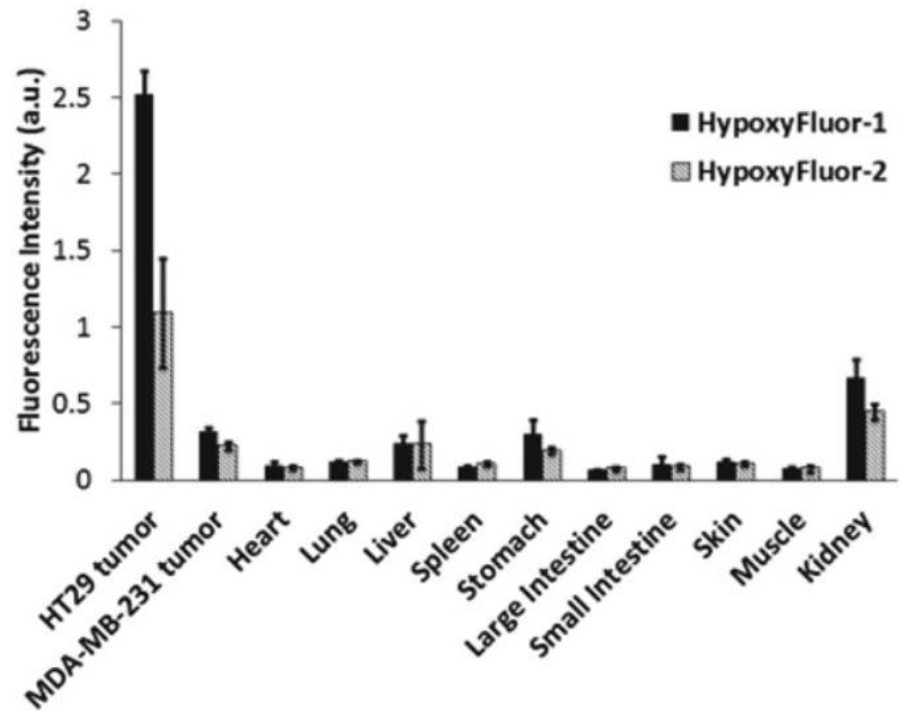
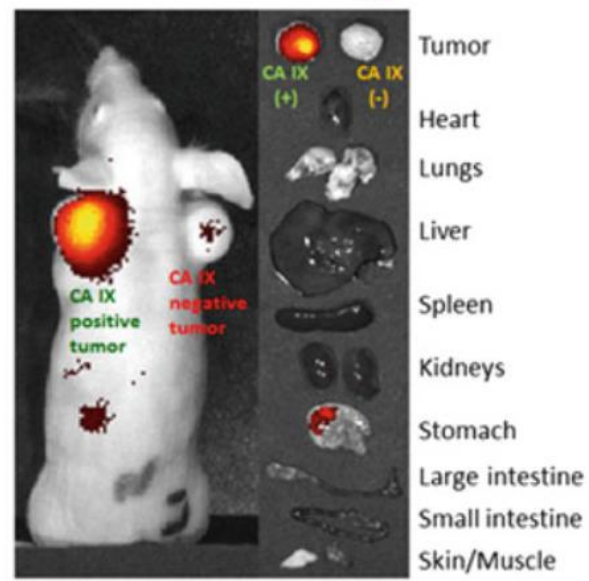
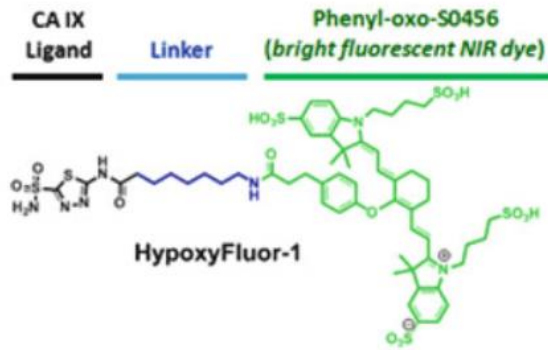


Fig. 19.5 Biodistribution of acetazolamide targeted and untargeted near infrared dye. Mice bearing HeLa tumor xenografts were injected with 2 nmols of acetazolamide targeted or untargeted NIR dye and sacrificed after 24 h for subsequent biodistribution analysis. Reprinted with permission from PLOS ONE [50].

Use of the improved CA IX ligand for delivery of an attached cytotoxic drug (tubulysin B hydrazide) was found to generate a highly potent antitumor agent that was able to block the growth of HT 29 colorectal cancer xenografts in athymic nude mice [1]. Thus, as shown in Fig.19.9, $\approx 150\text{mm}^3$ tumors largely disappeared from mice treated 2 \times per week with $1.25\mu\text{moles/kg}$ without causing any unwanted weight loss (a measure of systemic toxicity) from the mice [1]. Because free tubulysin B is so toxic to healthy tissues that it kills mice before it induces any suppression of tumor growth, these data indicate that the cyclooctylamine-modified CA IX ligand has excellent tumor specificity with minimal uptake in normal tissues. When compared to the bis-benzenesulfonamide tubulysin B studies carried out by Lv et al., the FBSA ligand was shown to be more efficacious at approximately half the amount of administered compound [1, 44]. This highlights the enormous benefits of using a selective sub-nanomolar binding targeting ligand. Generally, higher affinity targeting ligands require less administered compound, which reduces side effects associated with hepatically cleared conjugate, thereby rendering effective chemotherapy treatment with minimal to no side effects.

Fig. 19.6 Structure, imaging, and biodistribution of acetazolamide-targeted phenyl-oxo-S0456. The mouse in the image shown above bears both HT-29 (CA IX-positive) and MDA-MB0231 (CA IX-negative) tumor xenografts. The mouse was imaged 4 h after being injected with 10nmols of conjugate. The biodistribution above was done under similar conditions with either an acetazolamide (HypoxyFluor-1) or 6-aminosaccharin (HypoxyFluor-2) CA IX inhibitor and sacrificed at 24 h. Reprinted with permission from Bioconjugate Chemistry [2]



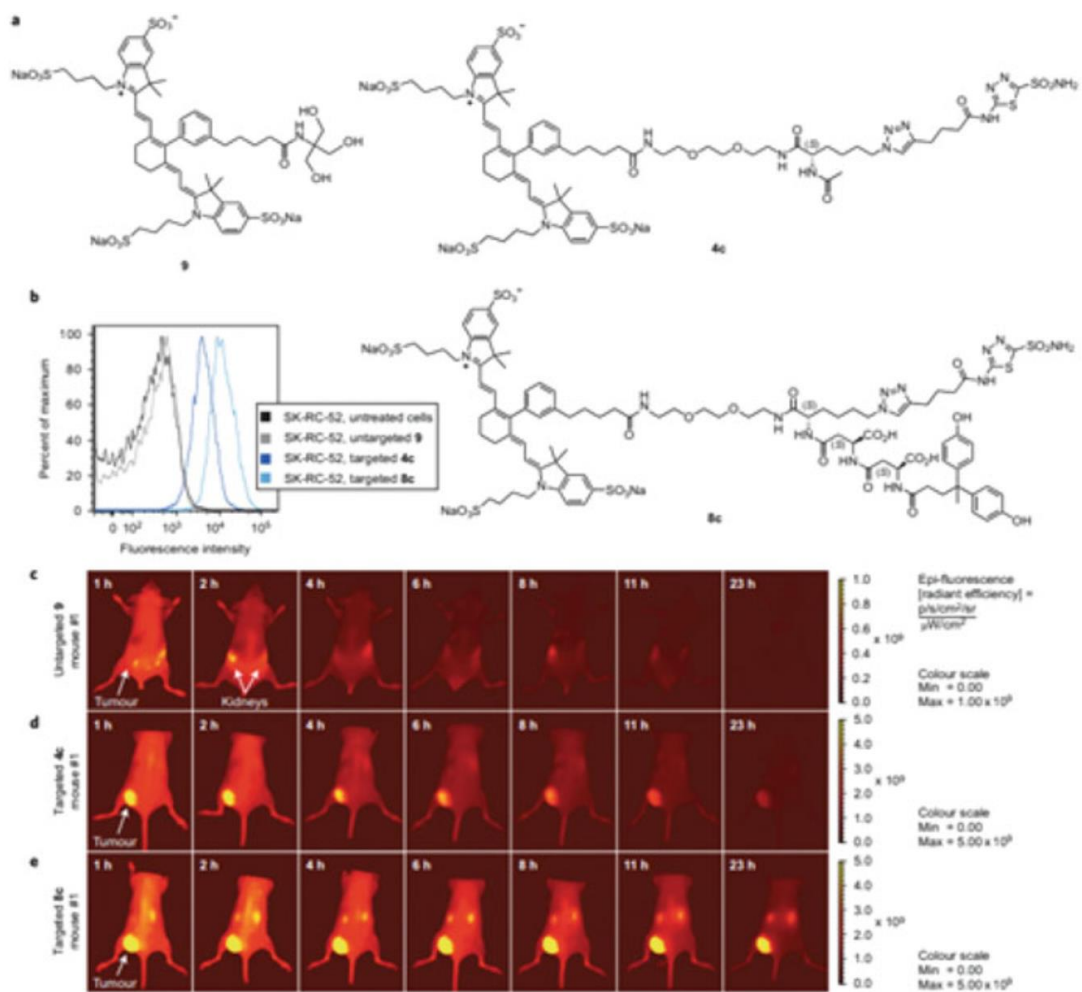


Fig. 19.7 Chemical structure and in vivo biodistribution of modified acetazolamide-targeted NIR conjugates. Mice bearing SKRC-52 tumor xenografts were injected with 3 nmol of the various compounds shown above and imaged periodically. Reprinted with permission from Nature Chemistry [51].



Fig. 19.8 Overall structure of FBSA targeted tubulysin B conjugate. Reprinted with permission from Molecular Pharmaceutics [1]

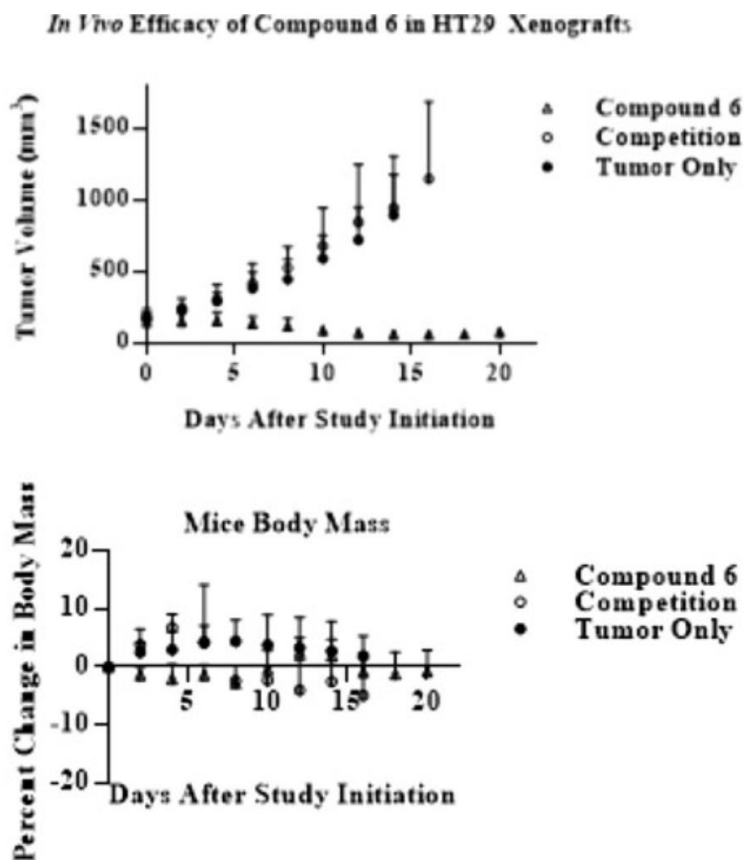


Fig. 19.9 In vivo testing of FBSA targeted tubulysin B conjugate. Mice bearing HT-29 colorectal tumor xenografts were treated twice per week with 1.25 μ moles/kg of compound shown in Fig.19.8 and monitored for tumor size and body weight. Reprinted with permission from Molecular Pharmaceutics [1]

References

1. Marks, I.S., et al.: Development of a small molecule tubulysin B conjugate for treatment of carbonic anhydrase IX receptor expressing cancers. *Mol. Pharm.*15, 2289–2296 (2018)
2. Roy, J., Kaake, M., Srinivasarao, M., Low, P.S.: Targeted tubulysin B hydrazide conjugate for the treatment of luteinizing hormone-releasing hormone receptor-positive cancers. *Bioconjug.Chem.*29, 2208–2214 (2018)
3. Shum, C.F., et al.: Novel use of folate-targeted intraoperative fluorescence, OTL38, in Robot-assisted laparoscopic partial nephrectomy: report of the first three cases. *J. Endourol. Case Rep.*2, 189–197 (2016)
4. Thurber, G.M., Schmidt, M.M., Wittrup, K.D.: Antibody tumor penetration: transport opposed by systemic and antigen-mediated clearance. *Adv. Drug Deliv. Rev.*60, 1421–1434 (2008)
5. Vlashi, E., Kelderhouse, L.E., Sturgis, J.E., Low, P.S.: Effect of folate-targeted nanoparticle size on their rates of penetration into solid tumors. *ACS Nano*7, 8573–8582 (2013)
6. Mahalingam, S.M., et al.: Evaluation of novel tumor-targeted near-infrared probe for fluorescence-guided surgery of cancer. *J. Med. Chem.*61(21), 9637–9646 (2018)
7. Paulos, C.M.: Ligand binding and kinetics of folate receptor recycling in vivo: impact on receptor-mediated drug delivery. *Mol. Pharmacol.*66, 1406–1414 (2004)
8. Paganelli, G., De Giorgi, U.: [177 Lu]-PSMA-617 for targeted prostate cancer treatment: a magic bullet? *Lancet Oncol.*19, 725–726 (2018)
9. Parker, N., et al.: Folate receptor expression in carcinomas and normal tissues determined by a quantitative radioligand binding assay. *Anal. Biochem.*338, 284–293 (2005)
10. Ross, J.F., et al.: Folate receptor type β is a neutrophilic lineage marker and is differentially expressed in myeloid leukemia. *Cancer*85, 348–357 (1999)
11. Shen, J., et al.: Folate receptor- β constitutes a marker for human proinflammatory monocytes. *J. Leukoc. Biol.*96, 563–570 (2014)
12. Nakashima-Matsushita, N., et al.: Selective expression of folate receptor β and its possible role in methotrexate transport in synovial macrophages from patients with rheumatoid arthritis. *Arthritis Rheum.*42, 1609–1616 (1999)
13. Low, P.: Folate receptor-targeted drugs for cancer and inflammatory diseases. *Adv. Drug Deliv. Rev.*56, 1055–1058 (2004)
14. Schupp, J.C., et al.: Macrophage activation in acute exacerbation of idiopathic pulmonary fibrosis. *PLoS One*10(ed Ryffel, B.), e0116775 (2015)

15. Han, W., et al.: Molecular imaging of folate receptor β -positive macrophages during acute lung inflammation. *Am. J. Respir. Cell Mol. Biol.*53, 50–59 (2015)
16. Chia, J.J., Lu, T.T.: Update on macrophages and innate immunity in scleroderma. *Curr. Opin.Rheumatol.*27, 530–536 (2015)
17. Zhou, D., et al.: Critical involvement of macrophage infiltration in the development of Sjögren’s syndrome-associated dry eye. *Am. J. Pathol.*181, 753–760 (2012)
18. Wright, G.L., Haley, C., Beckett, M.L., Schellhammer, P.F.: Expression of prostate-specific membrane antigen in normal, benign, and malignant prostate tissues. *Urol. Oncol. Semin. Orig.Investig.*1, 18–28 (1995)
19. Heitkötter, B., et al.: Neovascular PSMA expression is a common feature in malignant neoplasms of the thyroid. *Oncotarget*9(11), 9867–9874 (2018)
20. Schmidt, L.H., et al.: Prostate specific membrane antigen (PSMA) expression in non-small cell lung cancer. *PLoS One*12(ed Ahmad, A.), e0186280 (2017)
21. Stock, K., et al.: Neovascular prostate-specific membrane antigen expression is associated with improved overall survival under palliative chemotherapy in patients with pancreatic ductal adenocarcinoma. *Biomed. Res. Int.*2017, 1–8 (2017)
22. Silver, D.A., Pellicer, I., Fair, W.R., Heston, W.D., Cordon-Cardo, C.: Prostate-specific membrane antigen expression in normal and malignant human tissues. *Clin. Cancer Res. Off. J. Am. Assoc. Cancer Res.*3, 81–85 (1997)
23. Smyth, L.G., et al.: Carbonic anhydrase IX expression in prostate cancer. *Prostate Cancer Prostatic Dis.*13, 178–181 (2010)
24. Genega, E.M., et al.: Carbonic anhydrase IX expression in renal neoplasms: correlation with tumor type and grade. *Am. J. Clin. Pathol.*134, 873–879 (2010)
25. Ilie, M., et al.: High levels of carbonic anhydrase IX in tumour tissue and plasma are biomarkers of poor prognostic in patients with non-small cell lung cancer. *Br. J. Cancer*102, 1627–1635(2010)
26. Loncaster, J.A., et al.: Carbonic anhydrase (CA IX) expression, a potential new intrinsic marker of hypoxia: correlations with tumor oxygen measurements and prognosis in locally advanced carcinoma of the cervix. *Cancer Res.*61, 6394–6399 (2001)
27. Ivanov, S., et al.: Expression of hypoxia-inducible cell-surface transmembrane carbonic anhydrases in human cancer. *Am. J. Pathol.*158, 905–919 (2001)
28. Mboge, M., Mahon, B., McKenna, R., Frost, S.: Carbonic anhydrases: role in pH control and cancer. *Metabolites*8, 19 (2018)

29. Chrastina, A.: High cell density-mediated pericellular hypoxia is a crucial factor inducing expression of the intrinsic hypoxia marker CA IX in Vitro in HeLa cells. *Neoplasma* 50, 251–256 (2003)
30. Mahalingam, S.M., Chu, H., Liu, X., Leamon, C.P., Low, P.S.: Carbonic anhydrase IX-targeted near-infrared dye for fluorescence imaging of hypoxic tumors. *Bioconjug. Chem.* 29, 3320–3331 (2018)
31. Rami, M., et al.: Carbonic anhydrase inhibitors: design of membrane-impermeant copper(II) complexes of DTPA-, DOTA-, and TETA-tailed sulfonamides targeting the tumor-associated transmembrane isoform IX. *ChemMedChem* 3, 1780–1788 (2008)
32. Srinivasarao, M., Low, P.S.: Ligand-targeted drug delivery. *Chem. Rev.* 117, 12133–12164 (2017)
33. Srinivasarao, M., Galliford, C.V., Low, P.S.: Principles in the design of ligand-targeted cancer therapeutics and imaging agents. *Nat. Rev. Drug Discov.* 14, 203–219 (2015)
34. Lau, J., et al.: Synthesis and evaluation of ¹⁸F-labeled tertiary benzenesulfonamides for imaging carbonic anhydrase IX expression in tumours with positron emission tomography. *Bioorg. Med. Chem. Lett.* 24, 3064–3068 (2014)
35. Asakawa, C., et al.: Radiosynthesis of three [¹¹C]ureido-substituted benzenesulfonamides as PET probes for carbonic anhydrase IX in tumors. *Bioorg. Med. Chem. Lett.* 21, 7017–7020 (2011)
36. Lau, J., et al.: PET imaging of carbonic anhydrase IX expression of HT-29 tumor xenograft mice with ⁶⁸Ga-labeled benzenesulfonamides. *Mol. Pharm.* 13, 1137–1146 (2016)
37. Lau, J., et al.: Trimeric radiofluorinated sulfonamide derivatives to achieve in vivo selectivity for carbonic anhydrase IX-targeted PET imaging. *J. Nucl. Med.* 56, 1434–1440 (2015)
38. Lu, G., et al.: Synthesis and SAR of novel Re/^{99m}Tc-labeled benzenesulfonamide carbonic anhydrase IX inhibitors for molecular imaging of tumor hypoxia. *J. Med. Chem.* 56, 510–520 (2013)
39. Akurathi, V., et al.: Synthesis and biological evaluation of a ^{99m}Tc-labelled sulfonamide conjugate for in vivo visualization of carbonic anhydrase IX expression in tumor hypoxia. *Nucl. Med. Biol.* 37, 557–564 (2010)
40. Can, D., et al.: [(Cp-R)M(CO)₃] (M=Re or ^{99m}Tc) arylsulfonamide, arylsulfamide, and arylsulfamate conjugates for selective targeting of human carbonic anhydrase IX. *Angew. Chem. Int. Ed.* 51, 3354–3357 (2012)
41. Lv, P.C., Putt, K.S., Low, P.S.: Evaluation of nonpeptidic ligand conjugates for SPECT imaging of hypoxic and carbonic anhydrase IX-expressing cancers. *Bioconjug. Chem.* 27, 1762–1769 (2016)

42. Lv, P.C., Roy, J., Putt, K.S., Low, P. S.: Evaluation of a carbonic anhydrase IX-targeted near-infrared dye for fluorescence-guided surgery of hypoxic tumors. *Mol. Pharm.*13, 1618–1625(2016)
43. Terada, T., Inui, K.i.: In:Current Topics in Membranes, pp. 257–274. Elsevier, Amsterdam(2012)
44. Lv, P.C., Roy, J., Putt, K.S., Low, P.S.: Evaluation of nonpeptidic ligand conjugates for the treatment of hypoxic and carbonic anhydrase IX-expressing cancers. *Mol. Cancer Ther.*16,453–460 (2017)
45. Krall, N., Pretto, F., Mattarella, M., Muller, C., Neri, D.: A ^{99m}Tc-labeled ligand of carbonic anhydrase IX selectively targets renal cell carcinoma in vivo. *J. Nucl. Med.*57, 943–949 (2016)
46. Krall, N., et al.: A small-molecule drug conjugate for the treatment of carbonic anhydrase IX expressing tumors. *Angew. Chem. Int. Ed.*53, 4231–4235 (2014)
47. Krall, N., Pretto, F., Neri, D.: A bivalent small molecule-drug conjugate directed against carbonic anhydrase IX can elicit complete tumour regression in mice. *Chem. Sci.*5, 3640(2014)
48. Reddy, J.A., et al.: Pre-clinical evaluation of EC1456, a folate-tubulysin anti-cancer therapeutic. *Sci.Rep.*8(1), 8943 (2018)
49. Fisher, R.E., et al.: Exploratory study of ^{99m}Tc-EC20 imaging for identifying patients with folate receptor-positive solid tumors. *J. Nucl. Med.*49, 899–906 (2008)
50. Bao, B., et al.: In vivo imaging and quantification of carbonic anhydrase IX expression as an endogenous biomarker of tumor hypoxia. *PLoS One*7, e50860 (2012)
51. Wichert, M., et al.: Dual-display of small molecules enables the discovery of ligand pairs and facilitates affinity maturation. *Nat. Chem.*7, 241–249 (2015)
52. Leamon, C.P., et al.: Reducing undesirable hepatic clearance of a tumor-targeted vinca alkaloid via novel saccharopeptidic modifications. *J. Pharmacol. Exp. Ther.*336, 336–343 (2011)
53. Dudutiene, V., et al.: Discovery and characterization of novel selective inhibitors of carbonic anhydrase IX. *J. Med. Chem.*57, 9435–9446 (2014)
54. Majmundar, A.J., Wong, W.J., Simon, M.C.: Hypoxia-inducible factors and the response to hypoxic stress. *Mol. Cell*40, 294–309 (2010)
55. Morandi, A., Taddei, M.L., Chiarugi, P., Giannoni, E.: Targeting the metabolic reprogramming that controls epithelial-to-mesenchymal transition in aggressive tumors. *Front. Oncol.*7,40(2017).

CHAPTER 2. SYNTHESIS AND VALIDATION OF A FOLATE TARGETED ACROLEIN SCAVENGER

2.1 Abstract

Acrolein is a highly electrophilic metabolic byproduct of lipid peroxidation produced through the generation of reactive oxygen species. Due to its abundance and detriment in spinal cord injury, we sought to design and test drug conjugates that could target known acrolein scavengers to sites of inflammation within damaged spinal cord tissue using a highly reproducible drop weight injury rat model. Overall, we were able to validate the efficacy of a folate targeted hydralazine in scavenging acrolein in damaged spinal tissue. Off-site toxicity was also eliminated as demonstrated by blood pressure data collected after injection of the conjugate or free hydralazine.

2.2 Introduction

Spinal cord injuries (SCI) have severe and long lasting cognitive and physiological complications that can result in permanent damage to central nervous system (CNS) tissues, which in turn can lead to loss of movement and cognitive abilities.^{1,2} To date there has been an abundance of research conducted to elucidate variables that contribute to CNS damage pathologies.³ Of these, the accumulation of acrolein in damaged cord tissues has been identified as one of the main contributing factors that impairs recovery from CNS injury.⁴⁻⁷ The production of acrolein in the damaged cord is a direct result of auto-generated reactive oxygen species (ROS) interacting with the fatty acid rich myelin sheath present on nerves, resulting in lipid peroxidation and subsequent acrolein formation.^{8,9} Acrolein is extremely electrophilic three carbon α/β unsaturated aldehyde that participate in the crosslinking of various biomolecules including DNA, proteins and lipids which ultimately contributes to cellular apoptosis or necrosis.^{6,10} In order to circumvent the detrimental downstream effects of acrolein, several studies have investigated the use of acrolein scavenging drugs containing a varying number of nucleophilic functional groups that react with acrolein to neutralize its crosslinking potential.^{4-7,11} The use of such acrolein scavengers has shown great promise in rat SCI models and has demonstrated therapeutic value by resorting the use of paralyzed limbs and reducing the amount of cell death that takes place at the

injury site.⁶ In particular, the acrolein scavenger hydralazine^{6,11}, an FDA approved blood pressure lowering medication, has shown promise in sequestering SCI acrolein *in vivo*. Unfortunately, SCI patients generally have low blood pressure (BP) due to their injury and systemic dosing of hydralazine can lead to detrimental or even fatal BP levels

While the ability to form acrolein is ubiquitous among mitochondrial containing cells, those involved in the immune response have been shown to generate higher levels of ROS.¹² In particular, macrophages can express the myeloperoxidase protein¹³, which has been shown to enhance the production of acrolein. In the classical innate immune response, monocytes in the blood stream will extravasate into damaged tissue and from there differentiate into macrophages that help clear cellular debris, engulf pathogens and ultimately orchestrate the healing process.¹⁴ To a certain extent this spatial localization and accumulation has also been shown to happen with microglia or tissue resident brain macrophages.¹⁵ When traditional monocytes/macrophages first enter the damaged tissue, they adopt a proinflammatory state classified simply as M1. It has also been well documented that these M1 macrophages also express folate receptor beta (FR β) and subsequent studies have shown that these proinflammatory macrophages can be selectively targeted using folate linked imaging agents.^{16, 17}

Therefore, we hypothesized that the macrophages/microglia typically found in damaged tissue/spinal cord would not only express FR β , but that we could utilize folate targeting technology to selectively deliver the acrolein scavenger hydralazine. This could not only concentrate the acrolein scavengers in the damaged tissue but also specifically in the main cell types that are thought to be responsible for acrolein formation. In addition, we also hypothesized that by conjugating hydralazine to folate via a hydrophilic linker, we could prevent binding of the drug to its native receptor and thereby reduce or eliminate the undesired blood pressure lowering activity typically observed with the free drug. By selective delivery and toxicity mediation we desired to develop a first of its class drug that could provide efficacy for the treatment of patients with SCI, while exhibiting no undesired side effects.

2.3 Materials and Methods

2.3.1 Animals and Diet:

Young male Sprague Dawley rats were used in accordance to approved Purdue Animal Care and Use Committee protocols. Rats were first placed on a special low folate diet for 2 - 3 weeks before use, to lower serum folate concentrations to physiologically human relevant levels. This is done to avoid unwanted competition with our folate-drugs, since standard rat chow contains an unnecessarily high level of folate. At the time of experimental use, rats had grown to approximately 200 – 240 grams.

2.3.2 Injury

Rats were given standard, clinically relevant spinal cord injuries as previously described. Briefly, rats were anesthetized using an intraperitoneal injection of a ketamine-xylazine cocktail. A T10 laminectomy was done followed by a moderate level injury with a NYU weight drop impactor. Approximately 30 minutes – 1 hour post injury, rats were given NSAID Ketoprofen (10mg/kg subcutaneously) and grouped to receive either hydralazine (5mg/kg intravenous), F-HDZ (5mg/kg intravenous), or injury only (sham injection). Sham rats received laminectomy with no injury to the spinal cord, or sham injection. Healthy control rat? Ketoprofen was administered following surgery and for 2 dpi. Hydralazine, F-HDZ, or sham injections were administered after surgery and once each day until sacrifice on day 8.

2.3.3 Blood pressure

Rats were acclimated to blood pressure setup and room during the two-week period prior to experiments. Rats blood pressure measurements were recorded by a single, blind investigator, using Kent Scientific CODA tail cuff system. Rats were acclimated until consistent baseline levels could be recorded. After injury, rats received IV injections of drug each day as described. Approximately 30 min – 1 hour after injection, on both 4 dpi and 7 dpi, blood pressure measurements were taken. System would record 5 – 10 measurements every session for each rat, which were then averaged by the investigator. All diastolic and systolic measurements were normalized to each individual rat's baseline (preinjury) recordings before final statistics.

2.3.4 Perfusion:

On day 8, after receiving a final drug injection in the morning, rats were sacrificed later in the afternoon. Intracardial perfusion was done using Krebs solution after heavy ketamine/xylazine anesthesia. Rat spinal cords were dissected and immediately placed in 4% formalin/PBS solution for 2 days, followed by 30% sucrose/PBS solution for 3 days. Cords were then frozen in OTC cubes using an isopentane/dry ice slurry, and cryo-sliced in transverse sections at 25 μ m thickness. Sections were then stored in 0.01% Sodium Azide and PBS at 4C until biochemical analysis.

2.3.5 Immunohistochemistry

T10 spinal sections were immunostained overnight with anti-acrolein-lysine (StressMarq) followed by biotinylated secondary antibodies (Vector Laboratories), incubated in ABC avidin/biotin complex solution (Thermo Scientific™, #32020) and developed using the DAB Peroxidase (HRP) Substrate Kit, 3,3'-diaminobenzidine (Pierce™ DAB Substrate Kit). Images were taken using a standard light microscope (Olympus). Quantification was done using standard techniques for measuring DAB intensity on ImageJ software.

2.3.6 Fluorescent and NIR Microscopy

Near Infra-Red dye conjugated to Folate (F-NIR) was administered to a group of spinal injured rats by tail IV on 7 dpi. Another group of injured rats instead received injections of unconjugated dye (NIR Only). Rats were sacrificed on 8 dpi and T10 spinal tissue collected and processed for histology as described. For fluorescence signal, sections were immunostained overnight with anti-IBA1 (Abcam), followed by incubation in TexasRed secondary (JacksonImmuno). Sections were then mounted on glass slides and cover slipped using ProLong Gold Antifade Mountant. Images were taken using a microscope with TexasRed filters and a special NIR filter (Nikon, NIR dye shows blue). Alternatively, sections from F-NIR or NIR Only injected rats were directly mounted (no co-staining) from storage and cover slipped. Sections were then scanned using Sapphire Western Blot Scanner with NIR capabilities (NIR dye shows Green). Green fluorescent intensity was quantified using standard techniques and ImageJ.

2.3.7 Statistics

All data are presented as mean \pm standard error of the mean (SEM). One way ANOVA with Tukey or Fisher post hoc and Student's t test were used for statistical assessment where necessary (JMP 13 Software). The statistical significance threshold was set at $p < 0.05$.

2.3.8 Synthesis of Folate Hydralazine

Synthesis of Folate-Dap-(D)Glu-Dap-Cys (Compound 1)

500mg of (0.918mmol/g loading) 2-Cl-Trt resin was first loaded with 807mg (3eq) Fmoc-Cys-OH and 798uL (10eq) diisopropylethylamine (DIPEA) in 15mL anhydrous dichloromethane for 2 hours, then capped by the addition of 10% by volume methanol for 20min. Then using standard solid phase peptide synthesis protocols DMF/DCM/DMF, Fmoc deprotection of 20% piperidine in DMF, and 564.3mg (3eq) HATU coupling with 861uL DIPEA amino acids 633mg (3eq) Fmoc-DAP(Boc)-OH and 632mg (3eq) Fmoce-(D)Glu(OtBu)-OH were coupled to the solid phase resin. Then, folate was coupled to the resin via generation of folate-NHS by adding folic acid 1.311g (6eq), 613mg (6eq) DCC, and NHS 342mg (6eq) in DMSO (15mL) overnight. The resulting solution was vacuum filtered, and the subsequent solution was bubbled under argon gas in a peptide synthesis vessel for 3 hours. The final product was cleaved from the resin using 10mL of 95:2.5:2.5 TFA/TIPS/water with 15mg of TCEP-HCl for 2 hours. The resulting solution was filtered, precipitated, and washed with diethyl ether (246.6mg yield). LCMS (M+1): 846.3

Synthesis of 6-chloro-1H-benzo[d][1,2,3]triazol-1-yl (2-(pyridin-2-yl)disulfaneyl)ethyl carbonate (Compound 2)

2.3mL of methoxycarbonyl sulfonyl chloride was dissolved in 10mL acetonitrile (ACN) and cooled to 0C, followed by the addition of 2-mercaptoethanol in 10mL of ACN this was placed on ice for 30 minutes. After stirring at room temperature for two hours 2-mercaptopyridine was added in 10mL of CAN as a suspension and was refluxed for 4 hours. The reaction was then cooled on ice for 1 hr before filtering and washing with ACN (3.903g crude yield). This precipitate was then dissolved in 15mL DCM containing 2.9mL trimethylamine. This solution was then added dropwise to a solution of 1.8476g of triphosgene in 15mL DCM at 0C, then allowed to come to room temperature. After stirring for 1 hr at RT a second solution of 3.493g HOBt-Cl in 15mL DCM and 2.9ml trimethylamine was added at 0C dropwise and allowed to stir overnight. The

resulting solution was washed with brine, dried over magnesium sulfate, filtered, and evaporated (8.6807g yield). LCMS (M+1): 383.0, ¹H NMR (500 MHz, DMSO) δ 10.06 (s, 1H), 8.49 – 8.36 (m, 1H), 8.20 – 8.11 (m, 0H), 8.01 (d, J = 8.8 Hz, 1H), 7.86 – 7.73 (m, 2H), 7.40 (d, J = 9.0 Hz, 1H), 7.22 (tq, J = 13.4, 5.6 Hz, 1H), 4.98 (s, 0H), 3.60 (t, J = 6.4 Hz, 1H), 3.04 (dt, J = 11.8, 5.8 Hz, 4H), 2.90 (t, J = 6.4 Hz, 1H), 1.17 (t, J = 7.3 Hz, 6H).

Synthesis of 2-(pyridin-2-yl)disulfaneyl)ethyl 2-(phthalazin-1-yl)hydrazine-1-carboxylate (Compound 3)

In 500 μ L of DMSO 25mg of hydralazine-HCl was combined with 66.3 μ L of DIPEA and 48.7mg of compound 2. This was allowed to stir overnight at room temperature. The resulting solution was diluted with brine and DI water, extracted with ethyl acetate and purified by flash chromatography using 0-100% hexane/ethyl acetate over 25 minutes on a Teledyne automated combiflash (10mg yield). LCMS (M+1): 374.1

Synthesis of F-HDZ

10mg of Compound 3 was dissolved in 300 μ L THF and added to a vigorously stirring solution of 27.2mg compound 1 in a pH 6-6.5 ammonium acetate buffer. This solution was allowed to stir overnight and purified by RP-HPLC 20mM ammonium acetate pH7/Acetonitrile. The final product was confirmed via LCMS. LCMS (M+1): 1108.2

2.4 Results

2.4.1 Validation of Folate Targeting in Spinal Cord Injury *In Vivo*

To assess the prevalence of folate receptors that are present in the damaged spinal cord tissue, we first utilized F-NIR (A-C) and NIR dye (D) alone by injecting approximately 40 nmols via a tail vein injection into rats in the presence or absence of a spinal cord injury. As seen in Fig 2.1 most of the fluorescence is concentrated in the damaged cord epicenter (B), while only minimal uptake is seen in the sham and rostral samples. It is important to note that there was no uptake of the dye only sample. Additionally, the F-NIR uptake within the same cord (A and B) was further quantified using mean fluorescence intensity and represented in bar graph form in (E) showing a statistically significant difference between injured and uninjured cord.

To further validate targeting of the F-NIR to the injured cord, confocal microscopy was implemented to ascertain the cell types within the damaged cord that could be responsible for drug

uptake. As seen in Fig 2.2, results mimic those observed in Fig 2.1 with only injured spinal cord (C) showing any significant uptake of the F-NIR conjugate while the control and sham cords showed minimal uptake. Most importantly in Fig 2.2C F-NIR shows strong correlation with staining for the ionized calcium binding adapter molecule 1 (IBA1), a documented microglia/macrophage surface marker.

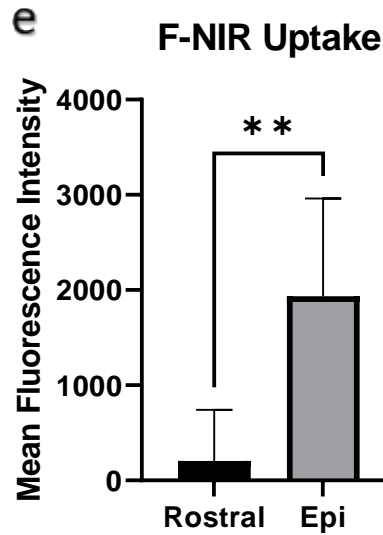
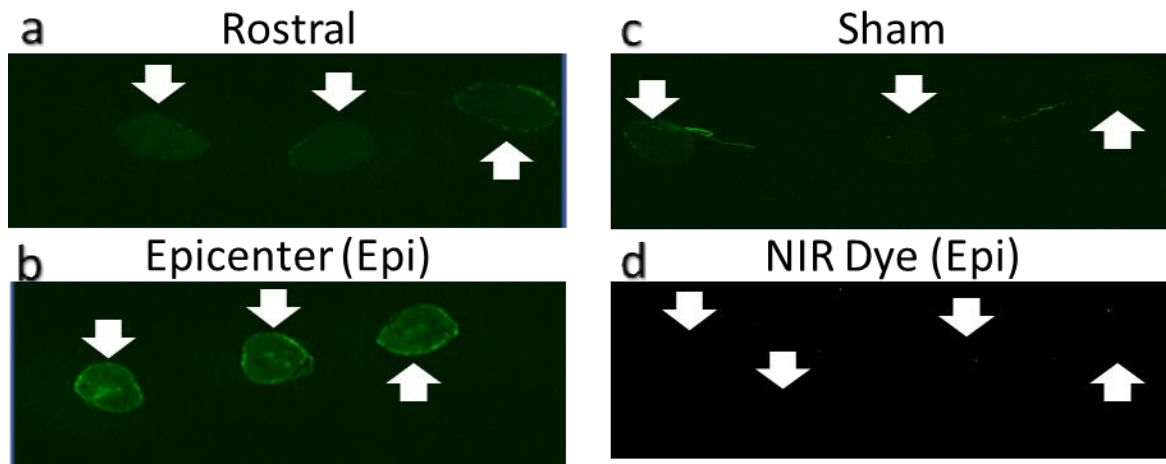
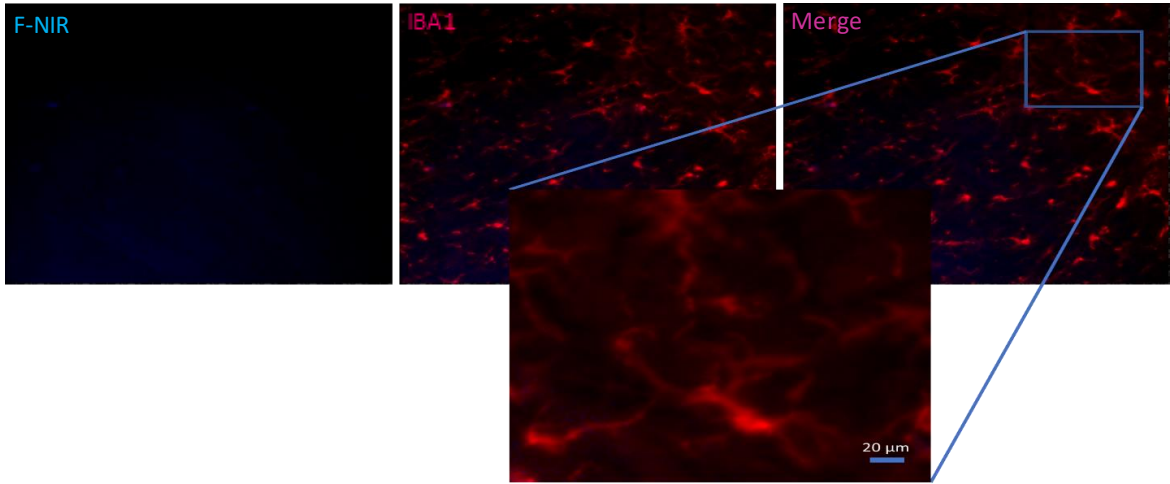


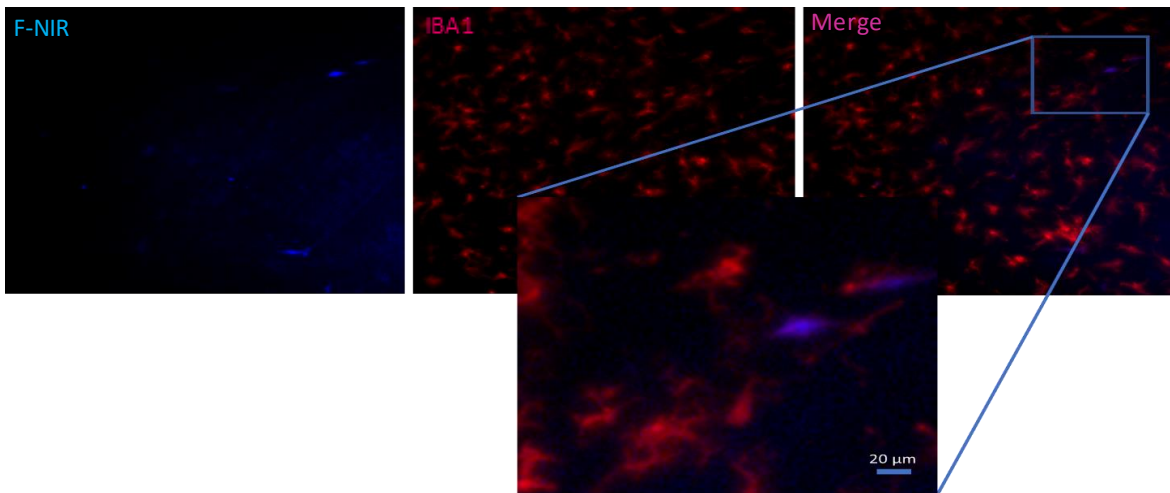
Figure 2.1. Uptake and Quantification of Folate Near-Infrared Dye in Spinal Cord Injury. All animals received 40nmols of compound injected i.v. and after 24 hours were euthanized via perfusion. All arrows pointing to sliced sections of cord tissue. (A)Rostral cord sections (B) Epicenter/damaged cord (C) Surgery performed on rat, but no weight dropped on the spinal cord. (D) NIR dye with no folate targeting ligand of the epicenter. (E) MFI quantification of images A and B. Statistical significance represents a p-value < 0.01.

Figure 2.2 Confocal Microscopy Localization of F-NIR and Microglia/Macrophages in Injured Rat Spinal Cord. All animals received 40nmols of compound injected i.v. and after 24 hours were euthanized via perfusion. All arrows pointing to sliced sections of cord tissue (A) Sham (B) Rostral (C) Injury

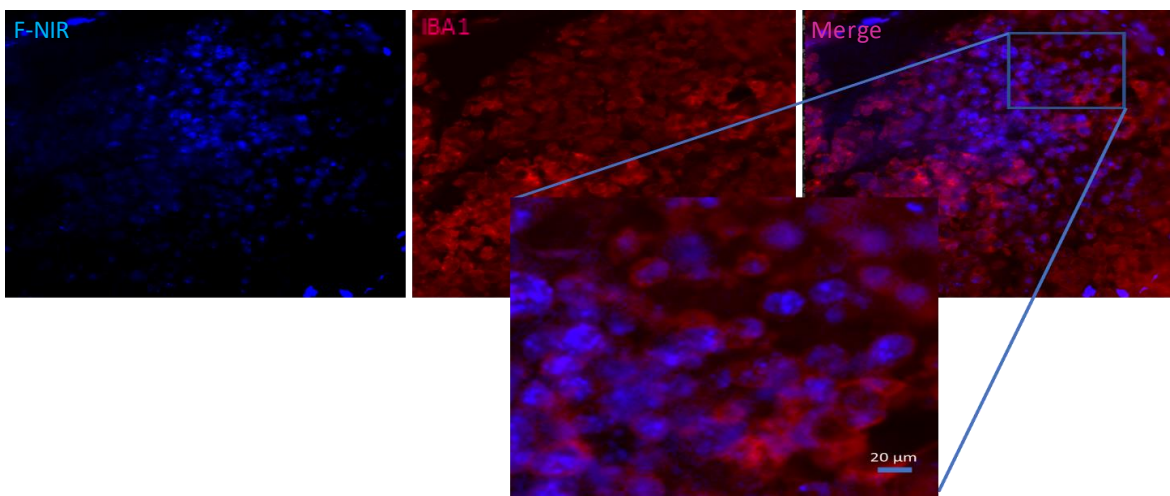
A



B



C



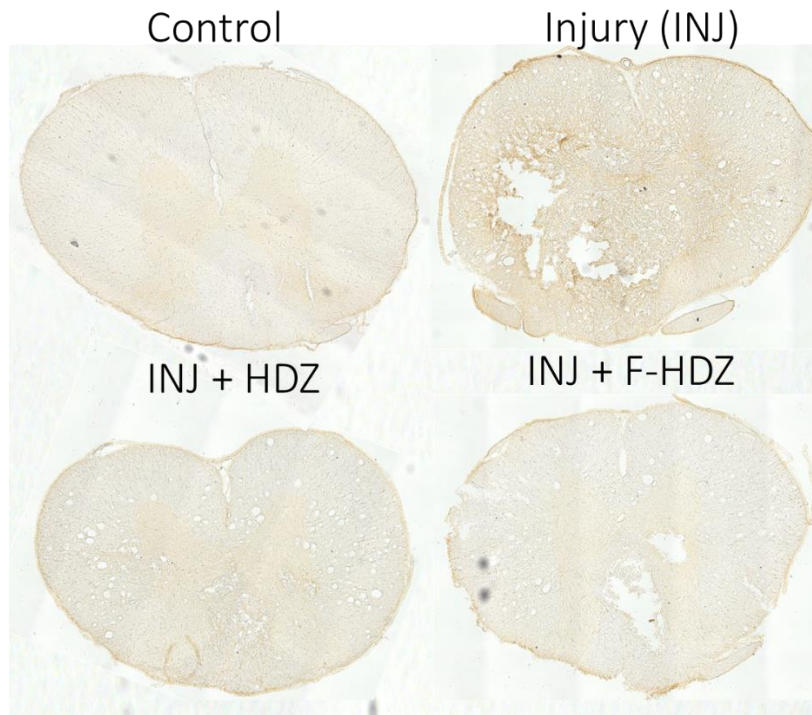
2.4.2 Folate-Hydralazine Acrolein Scavenging Efficacy and Ablation of Toxicity

To test the hypothesis that a folate targeted acrolein scavenger can adequately reduce or eliminate acrolein while not producing any negative side effects. A folate-hydralazine (F-HDZ) was synthesized as outlined in the materials and methods (see appendix A for structure) and tested *in vivo* using a drop weight spinal cord injury rat model. Rats were either injured, sham, or uninjured (control) and either received F-HDZ or just hydralazine (HDZ) via a tail vein injection daily for 8 days post injury. Sections of the respective cords seen in Fig 2.3A show the relative amount of immunohistochemical stain for acrolein. Acrolein is abundant in the injured cord while significantly less can be observed in the other three samples. Acrolein staining in (A) was quantified by mean pixel intensity of the acrolein stain on and represented in bar graph 2.3B. This graph shows statistically lower levels of acrolein for rats treated with the F-HDZ relative to the injury only group while the free drug failed to achieve a statistically significant difference. In addition, further validation of F-HDZ was observed with no significant difference between the F-HDZ and the control group, implying these two groups have relatively the same amount of acrolein.

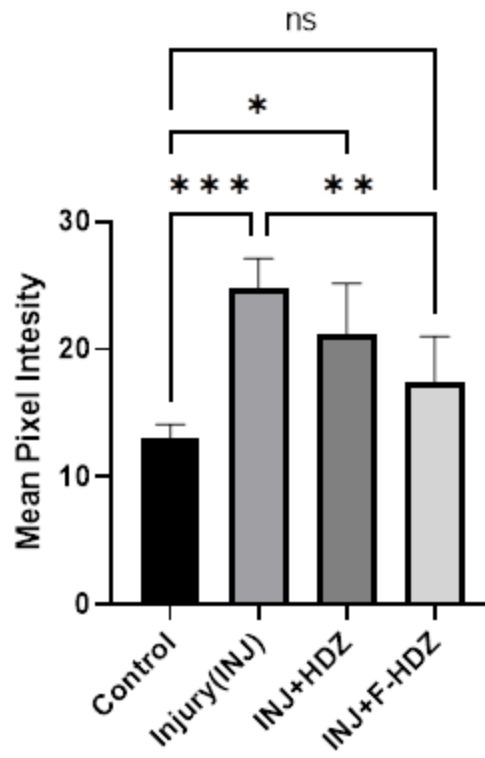
Furthermore, to test potential toxicity, F-HDZ was tested directly against the free HDZ drug by measuring systolic and diastolic blood pressure at day 4 and day 7 in spinal cord injury rats. As seen in Fig .4A/B, on both days 4 and 7 there are significantly lower blood pressures in rats that were given no intervention or given the free hydralazine relative to the control group. Conversely, at each time points the F-HDZ group retained blood pressures that showed no significant difference from the uninjured control group, highlighting the conjugates ability to maintain efficacy while eliminating hydralazine's normal side effect of lowering blood pressure.

Figure 2.3 Acrolein Staining and Quantification in Injured Rat Spinal Cords (A) Representative cord slices of immunohistochemical staining for acrolein for the respective experimental groups. (B) Quantification of representative images showing mean pixel intensity of acrolein staining. NS = not significant, * = p-value < 0.05, ** = p-value < 0.01, *** = p-value < 0.005.

A



B



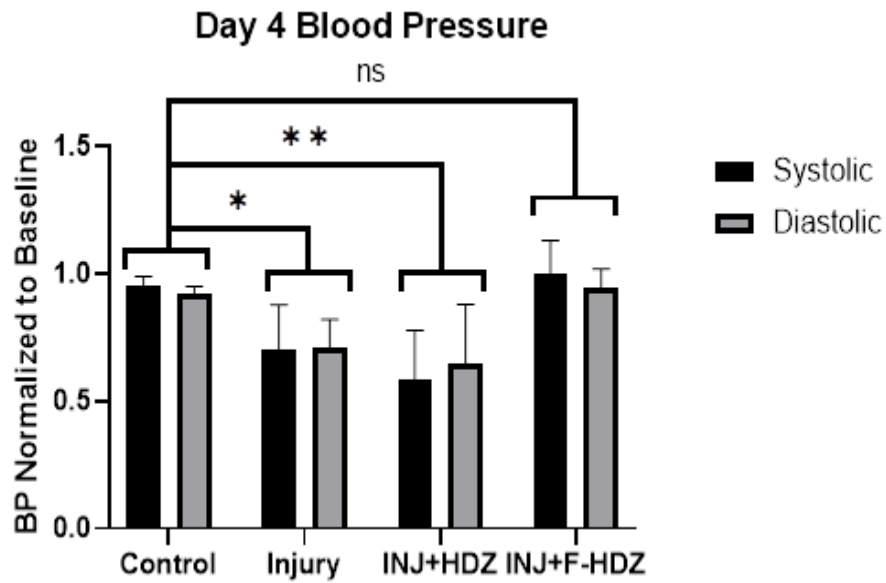
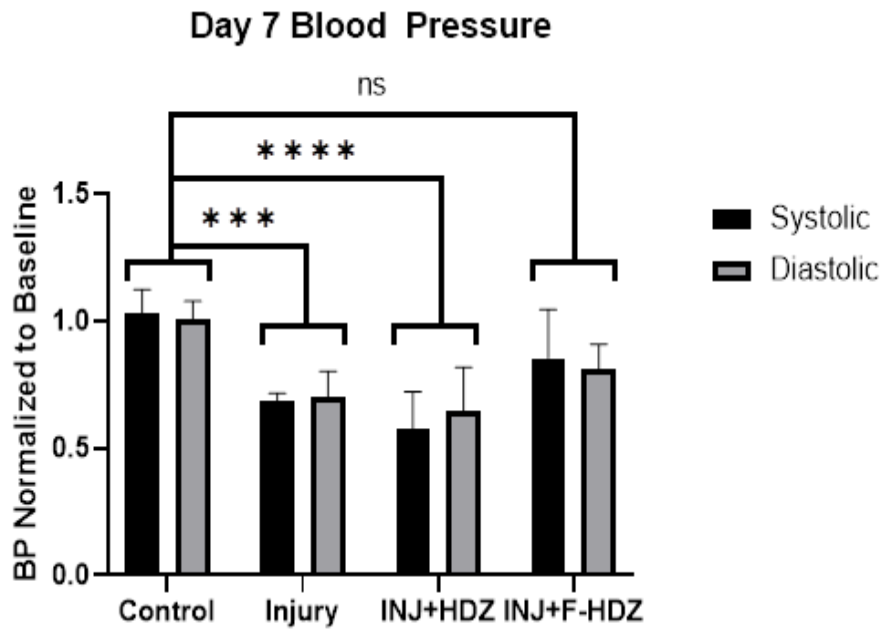
A**B**

Figure 2.4 Rat Spinal Cord Injury Blood Pressure Readings (A) Systolic and diastolic readings for rats day 4 (B) Systolic and diastolic readings for rats day 7. NS = not significant, * = p-value < 0.05, ** = p-value < 0.01, *** = p-value < 0.005, **** = p-value < 0.001.

2.5 Discussion

With no FDA approved treatments for spinal cord injury, it is imperative that research be carried out to help the approximately 18,000 new SCI patients that are diagnosed every year. Due to its prevalence in spinal cord injury, acrolein is an attractive pharmacological target and literature has shown that the sequestering or scavenging of acrolein can result in positive benefits. Specifically, hydralazine, an FDA approved blood pressure lowering medication has shown positive value in not only scavenging acrolein but also showing clinically relevant positive outcome in rats with SCI's. Unfortunately, hydralazine cannot be given to spinal cord patients since it could lower their blood pressure to a critical level that may result in further complications or death.

To circumvent this pitfall, we decided to synthesize a drug conjugate of hydralazine due to the overwhelming literature that has provided evidence that conjugation of drugs to targeting ligands has the ability to lessen or eliminate undesired toxicities. Our choice of targeting ligand, folate, was selected due to the prevalence of folate receptor beta positive macrophages that have been found at sites of inflammation in a variety of inflammatory diseases and infected wounds. As seen in Fig 2.1 and 2.2, the first step in this endeavor was to validate that targeting of injured spinal tissue was possible. Uptake was seen in the chord both on the macroscopic (Fig 2.1) and microscopic (Fig 2.2) levels. In Fig 2.1 it was observed that even within the same cord that were was selective uptake of the F-NIR reporter as shown by the strong fluorescent signal in the epicenter of the injury while the rostral or part of the cord further down the spinal column shows very little uptake. This internal control provides powerful evidence that folate conjugates can be selectively retained in the traumatized tissue. Furthermore, colocalization of the F-NIR dye depicted in the confocal images of Fig 2.2 with the microglia/macrophage marker IBA1 demonstrates that a large portion of the macrophage population in the injured spinal cord is taking up the targeted dye. Since microglia are generators of reactive oxygen species, it seemed logical to synthesize a folate targeted hydralazine conjugate.

To test the efficacy of the F-HDZ conjugate, we utilized the same drop weight SCI model as was done in the imaging experiments but equally dosed the injured rats either free hydralazine or F-HDZ daily via an i.v. injection daily for eight day. As seen in Fig 2.3A/B there was significantly less acrolein in the F-HDZ group than the injury only rats. Additionally, no significant difference was found between the uninjured control and F-HDZ group, showing that the folate targeted

acrolein scavenger was able to efficiently clear the majority of acrolein to achieve basal physiological levels. Interestingly the conjugate was able to outperform the free drug at scavenging acrolein. This may be due to the intentional design of incorporating two primary amines into the linker of the conjugate to help further sequester more acrolein. More experiments should be conducted in the future to modulate the number of primary amine in the linker, more drug payloads and folate with/without hydralazine but with primary amines in the linker. These must be done to further ascertain the contributions of these various groups to the overall scavenging potential.

Along with confirming efficacy of the F-HDZ molecule, the general blood pressure lowering toxicity usually exhibited by free hydralazine was shown to be eliminated upon conjugation to folate (Fig 2.4). This is most likely due covalent bond formed between the hydrazine of hydralazine and the carbonyl of the carbamate. It is assumed that this conjugation restricted binding of the molecule to its normal drug target.

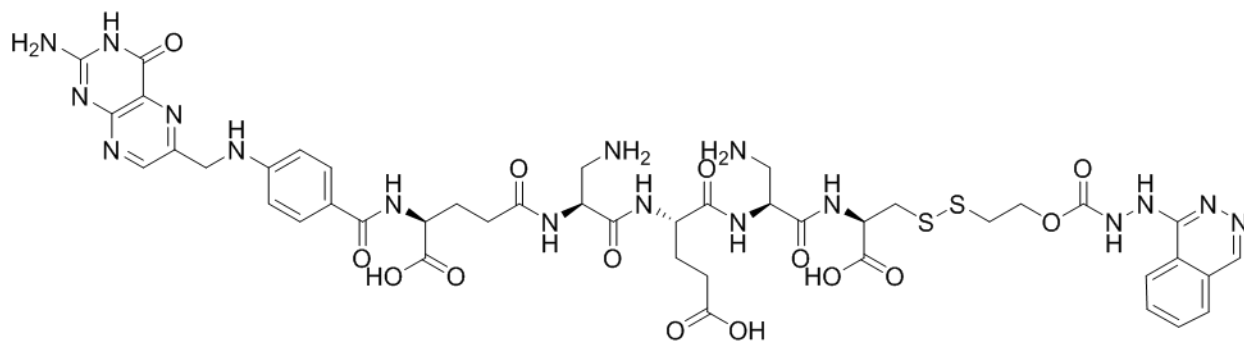
2.6 Conclusion

By performing initial studies on a new drug that can potentially be used to treat spinal cord injury, these results highlight the potential future applicability of folate targeted acrolein scavengers. Showing that the conjugate was able to scavenge acrolein while not exhibiting any blood pressure lowering phenotypes was not only novel but could provide future patients the hope of a better life.

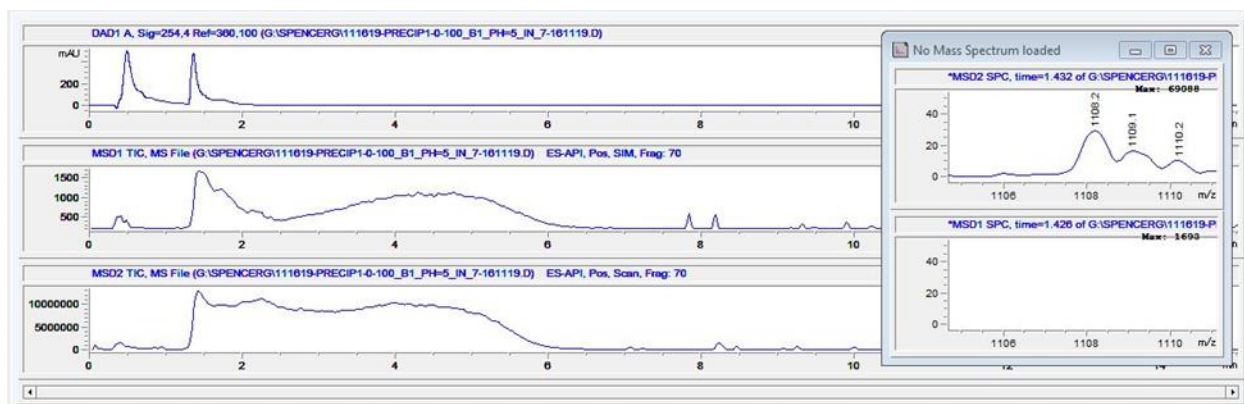
2.7 References

1. Hagen, E. M. Acute complications of spinal cord injuries. *World J Orthop* **2015**, *6*, (1), 17-23.
2. Qian, J.; Herrera, J. J.; Narayana, P. A. Neuronal and axonal degeneration in experimental spinal cord injury: in vivo proton magnetic resonance spectroscopy and histology. *J Neurotrauma* **2010**, *27*, (3), 599-610.
3. Walter, J.; Zweckberger, K. [Traumatic Injuries of the Central Nervous System]. *Anesthesiol Intensivmed Notfallmed Schmerzther* **2018**, *53*, (10), 668-681.
4. Gianaris, A.; Liu, N.-K.; Wang, X.-F.; Oakes, E.; Brenia, J.; Gianaris, T.; Ruan, Y.; Deng, L.-X.; Goetz, M.; Vega-Alvarez, S.; Lu, Q.-B.; Shi, R.; Xu, X.-M. Unilateral microinjection of acrolein into thoracic spinal cord produces acute and chronic injury and functional deficits. *Neuroscience* **2016**, *326*, 84-94.

5. Park, J.; Zheng, L.; Acosta, G.; Vega-Alvarez, S.; Chen, Z.; Muratori, B.; Cao, P.; Shi, R. Acrolein contributes to TRPA1 up-regulation in peripheral and central sensory hypersensitivity following spinal cord injury. *Journal of neurochemistry* **2015**, *135*, (5), 987-997.
6. Park, J.; Zheng, L.; Marquis, A.; Walls, M.; Duerstock, B.; Pond, A.; Vega-Alvarez, S.; Wang, H.; Ouyang, Z.; Shi, R. Neuroprotective role of hydralazine in rat spinal cord injury -attenuation of acrolein-mediated damage. *Journal of neurochemistry* **2014**, *129*, (2), 339-349.
7. Tian, R.; Shi, R. Dimercaprol is an acrolein scavenger that mitigates acrolein-mediated PC-12 cells toxicity and reduces acrolein in rat following spinal cord injury. *Journal of neurochemistry* **2017**, *141*, (5), 708-720.
8. Moghe, A.; Ghare, S.; Lamoreau, B.; Mohammad, M.; Barve, S.; McClain, C.; Joshi-Barve, S. Molecular mechanisms of acrolein toxicity: relevance to human disease. *Toxicol Sci* **2015**, *143*, (2), 242-255.
9. Li, L.; Jiang, L.; Geng, C.; Cao, J.; Zhong, L. The role of oxidative stress in acrolein-induced DNA damage in HepG2 cells. *Free Radical Research* **2008**, *42*, (4), 354-361.
10. Stevens, J. F.; Maier, C. S. Acrolein: sources, metabolism, and biomolecular interactions relevant to human health and disease. *Mol Nutr Food Res* **2008**, *52*, (1), 7-25.
11. Zhu, Q.; Sun, Z.; Jiang, Y.; Chen, F.; Wang, M. Acrolein scavengers: reactivity, mechanism and impact on health. *Mol Nutr Food Res* **2011**, *55*, (9), 1375-90.
12. Sun, L.; Wang, X.; Saredy, J.; Yuan, Z.; Yang, X.; Wang, H. Innate-adaptive immunity interplay and redox regulation in immune response. *Redox Biol* **2020**, *37*, 101759-101759.
13. Rodrigues, M. R.; Rodriguez, D.; Russo, M.; Campa, A. Macrophage activation includes high intracellular myeloperoxidase activity. *Biochem Biophys Res Commun* **2002**, *292*, (4), 869-73.
14. Kim, S. Y.; Nair, M. G. Macrophages in wound healing: activation and plasticity. *Immunol Cell Biol* **2019**, *97*, (3), 258-267.
15. Greenhalgh, A. D.; Zarruk, J. G.; Healy, L. M.; Baskar Jesudasan, S. J.; Jhelum, P.; Salmon, C. K.; Formanek, A.; Russo, M. V.; Antel, J. P.; McGavern, D. B.; McColl, B. W.; David, S. Peripherally derived macrophages modulate microglial function to reduce inflammation after CNS injury. *PLoS Biol* **2018**, *16*, (10), e2005264-e2005264.
16. Varghese, B.; Vlashi, E.; Xia, W.; Ayala Lopez, W.; Paulos, C. M.; Reddy, J.; Xu, L.-C.; Low, P. S. Folate Receptor- β in Activated Macrophages: Ligand Binding and Receptor Recycling Kinetics. *Molecular Pharmaceutics* **2014**, *11*, (10), 3609-3616.
17. Chandrupatla, D. M. S. H.; Molthoff, C. F. M.; Lammertsma, A. A.; van der Laken, C. J.; Jansen, G. The folate receptor β as a macrophage-mediated imaging and therapeutic target in rheumatoid arthritis. *Drug Delivery and Translational Research* **2019**, *9*, (1), 366-378.



Exact Mass: 1107.34



CHAPTER 3. SYNTHESIS AND DEMONSTRATION OF FOLATE STEROID CONJUGATES

3.1 Abstract

Inflammation lies at the heart of many diseases and disorders that affect hundreds of millions of people worldwide. While several options are available to patients such as nonsteroidal anti-inflammatory drugs (NSAIDs), anti-TNF α antibodies, and steroids. These options either lack sustained efficacy or undesired side effects. To develop a class of drugs that could provide both sustained efficacy without undesired side effects, we set out to synthesize a series of folate targeted dexamethasone conjugates that vary in their stability and ability to release free dexamethasone in areas of inflammation.

3.2 Introduction

Just over half of all Americans are affected by one or more chronic inflammatory diseases such as rheumatoid arthritis, diabetes, psoriatic arthritis, irritable bowel disease, Crohn's disease chronic obstructive pulmonary disease (COPD), etc.¹ By 2026 it is thought that the total cost of these diseases will be approximately \$6 trillion, making the overall market value of drugs for the treatment of these diseases astronomical.² Current treatment options include lifestyle changes, non-steroidal anti-inflammatories, monoclonal antibodies and steroids.³ While steroids are considered a gold standard in controlling inflammation, they also have a broad range of undesirable side effects including insulin resistance, decreased bone density, steroid dependency and a weakened immune system.^{4, 5}

In order to overcome these negative side effects, a great deal of research has been conducted to formulate the steroids into antibody drug conjugates, polymer micelles, liposomes and creams for topical use.⁶⁻⁹ While many of these approaches provide a mechanism by which they can deliver steroids to their desired tissues, each formulation/conjugate has its own pitfalls that prevent translation to a clinical setting. Antibody drug conjugates (ADCs) usually show very good specificity and tend to have long blood circulation time but unfortunately these tend to suffer from premature breakdown in the blood stream.¹⁰ Additionally, ADC excretion tends to proceed via the liver and ultimately feces.¹¹ In the case of steroid conjugates this poses a problem. If ADC steroid

conjugates were to be administered antibody metabolism in the liver would likely lead to the release of free drug, resulting in potential insulin resistance.¹² While most liposomal and nanoparticle formulations have the advantage of delivering large quantities of drug to poorly vascularized or damaged vasculature, this phenomenon is known as the EPR effect or enhanced permeability and retention effect.¹³ Indeed, this observation is often found in mouse models but rarely translates to humans.¹⁴ Therefore, due to its efficacy, specificity and cost effectiveness¹⁵, a small molecule drug conjugate remains the best option to utilize potent immunosuppressing steroids. To date there has yet to be published research describing a small molecule drug conjugate that can specifically deliver steroids to sites of inflammation.

When a tissue experiences high levels of inflammation this leads to the recruitment of monocytes originally derived in the bone marrow.¹⁶ Once the monocytes in the blood stream and encounter proinflammatory cytokines, they then begin to enter the tissue and differentiate into proinflammatory macrophages designated with the M1 classification.^{17, 18} These M1 macrophages will then typically produce additional proinflammatory cytokines, phagocytose cellular debris and produce reactive oxygen species.¹⁸ Then under normal circumstances these macrophages would polarize to anti-inflammatory M2 macrophages that typically aid in helping control inflammation in tissue repair but in the case of chronic inflammatory diseases the macrophages fail to polarize to the M2 phenotype to a certain extent, this results in a vicious cycle of recurring monocyte infiltration resulting in swollen, red, and painful tissue.¹⁹

To help treat chronic inflammation one promising route relies involves the forced polarization of these M1 macrophages to their M2 state^{19, 20} and this has been previously demonstrated by utilizing folate as a targeting ligand, to deliver anti-inflammatory drugs specifically to the proinflammatory macrophages.²¹⁻²⁶ Due to the powerful anti-inflammatory properties of steroid, this makes them an ideal candidate to polarize the M1 macrophages to M2 within inflamed tissues but to date there have been no reports of such molecules.²⁷ Herein you will find the synthesis of several folate-steroid small molecule drug conjugates that show promise in selectively delivering and reducing chronic inflammation.

3.3 Materials and Methods

3.3.1 Synthesis of Folate Steroid Conjugates

Synthesis of Pyr-SS-Carbonate-Dex

100mg of dexamethasone and 95.2mg of compound 2 (from chapter 2 materials and methods) was dissolved in 3mL of DMF, to which 133uL (3eq) DIPEA was added and allowed to stir overnight. The reaction mixture was then purified by flash chromatography 0-20% DCM/MEOH (34mg yield). ¹H NMR (500 MHz, DMSO) δ 8.47 (s, 3H), 7.95 (s, 2H), 7.80 (s, 4H), 7.62 (s, 2H), 7.27 (s, 3H), 5.20 (s, 1H), 5.08 (s, 1H), 4.79 (s, 1H), 4.32 (s, 2H), 4.20 (s, 2H), 4.15 (s, 2H), 3.85 (s, 2H), 3.62 (s, 3H), 3.22 (s, 5H), 3.14 (s, 6H), 2.88 (s, 9H), 2.73 (s, 8H), 2.32 (s, 3H), 2.15 (s, 3H), 1.76 (s, 2H), 1.48 (s, 4H), 1.34 (s, 3H), 1.22 (s, 3H), 1.16 (s, 4H), 1.07 (s, 4H), 0.89 (s, 4H), 0.79 (s, 4H). ¹³C NMR (126 MHz, DMSO) δ 185.74, 162.82, 153.24, 150.15, 138.65, 138.30, 121.80, 119.87, 103.19, 90.96, 70.82, 65.67, 59.60, 48.52, 40.53, 40.36, 40.19, 40.02, 39.86, 39.64, 36.30, 31.28, 22.87, 15.60.

Synthesis of Fol-HydroLink-Cys

Using Fmoc-Cys(Trt)-OH loaded 2-cl trt resin along with standard HBTU/PyBop solid phase peptide synthesis protocols, 3X DMF washes, Fmoc deprotection using 20% piperidine in DMF, Fmoc-PEG2-OH, Fmoc-DAP(Boc)-OH and Fmoc-(D)Glu(OtBu)-OH amino acids were used to synthesize the Fol-PEG2-DAP-(D)Glu-DAP-(D)Glu-DAP-(D)Glu-DAP-Cys-OH (Fol-PEG2-HydroLink) utilizing Fmoc-Glu-OtBu and N10-TFA-Pteronic acid. The N10 TFA protection was removed using 50/50 ammonium hydroxide/DMF. The final product was cleaved from the resin using 10mL of 95:2.5:2.5 TFA/TIPS/water with 15mg of TCEP-HCl for 2 hours. The resulting solution was filtered, precipitated, and washed with diethyl ether.

Synthesis of Fol-HydroLink-Cys-Carbonate-Dex

5mg of Fol-HydroLink-Cys was dissolved in 100uL of 20mM ammonium acetate buffer pH 6.5. To this solution 2.3mg of Pyr-SS-Carbonate-Dex dissolved in 100uL of THF was added quickly using a vigorous stir. The reaction was allowed to stir for 12 hours at room temperature, then purified by RPHPLC utilizing 20mM ammonium acetate buffer/acetonitrile and verified by LC-MS. LC-MS (M+1): 1770.7

Synthesis of 2-(pyridin-2-yl)disulfaneyl)ethan-1-amine acid chloride salt

25.6mmols of methoxycarbonyl sulfonyl chloride in 10mL of acetonitrile was cooled to 0C, followed by the addition of 25.6mmols of 2-aminoethanol hydrochloride. Then 23mmols of

2-mercaptopyridine in 15mL of methanol was added and the mixture was refluxed for 2hrs. The vessel was then cooled to 0C for one hour and the resulting precipitate was collected by filtration. (2.5660g yield)

Synthesis of Pyr-SS-Carbamate-Dex

392mg Dexamethasone and 230mg p-Nitrophenylchloroformate were loaded into a capped vial containing a magnetic stir bar. The solids were dissolved in 10mL chloroform followed by the addition of 1mL pyridine, the reaction was run at room temperature and monitored by LC-MS. Then, 320mg of 2-(pyridin-2-yl-disulfaneyl)ethan-1-amine acid chloride salt was mixed in a separate container with 2.5mL chloroform with 752uL of diisopropylethylamine (DIPEA) and continued to be monitored by LC-MS. Upon completion, the reaction was purified by flash chromatography utilizing a 0-20% dichloromethane/methanol gradient. The product was verified by LC-MS. (460.0mg yield). LC-MS (M+1): 383.0, ¹H NMR (500 MHz, DMSO) δ 8.56 (d, J = 6.4 Hz, 2H), 8.45 (d, J = 6.9 Hz, 2H), 7.79 (dp, J = 14.8, 7.3 Hz, 6H), 7.56 – 7.51 (m, 2H), 7.36 (d, J = 7.1 Hz, 3H), 7.31 – 7.21 (m, 5H), 6.20 (t, J = 8.2 Hz, 2H), 5.98 (d, J = 6.1 Hz, 2H), 5.38 (d, J = 6.3 Hz, 2H), 5.07 (d, J = 6.5 Hz, 2H), 4.91 (dd, J = 17.8, 6.4 Hz, 2H), 4.72 – 4.64 (m, 2H), 4.12 (s, 1H), 3.29 – 3.21 (m, 7H), 2.87 (dq, J = 13.4, 6.7 Hz, 7H), 2.64 – 2.55 (m, 3H), 2.47 (s, 4H), 2.36 (s, 1H), 2.33 – 2.26 (m, 4H), 2.11 (s, 2H), 1.77 – 1.72 (m, 2H), 1.61 (d, J = 9.5 Hz, 2H), 1.54 (d, J = 15.7 Hz, 3H), 1.46 (d, J = 6.2 Hz, 7H), 1.38 – 1.29 (m, 3H), 1.04 (s, 2H), 0.88 – 0.83 (m, 7H), 0.75 (d, J = 7.2 Hz, 7H). ¹³C NMR (126 MHz, DMSO) δ 206.46, 185.76, 167.58, 159.55, 156.06, 153.25, 150.08, 138.33, 136.60, 129.46, 124.56, 124.38, 121.70, 119.74, 102.46, 101.06, 90.88, 71.11, 70.83, 68.15, 48.50, 48.30, 43.73, 40.48, 40.31, 40.14, 39.97, 39.81, 39.64, 39.47, 38.96, 38.09, 36.12, 35.63, 34.11, 33.96, 32.37, 30.73, 27.75, 23.46, 16.72, 15.63.

Fol-PEG2-HydroLink-DimethylCys

506.3mg of ~0.918mmol/g 2-cl-trt resin was loaded for 2 hours with 285.3mg Fmoc-Pen(trt)-OH and 404uL DIPEA, then capped by the addition of 10% by volume methanol for 20min. This resin was washed with DCM/DMF/DCM and loaded onto an Aapptec peptide synthesizer that utilizes standard HBTU/Pybop coupling, 3X DMF washes, and 20% piperidine Fmoc deprotection. Using these protocols Fmoc-DAP-(D)Glu-DAP-(D)Glu-DAP-(D)Glu-DAP-DimethylCys-OH was synthesized. Using the same protocols but using 529.9mg (3eq) HATU, 808uL (3eq) DIPEA with 557mg (3eq) Fmoc-PEG2-OH, Fmoc-Glu-OtBu or 569.2mg (3eq) N10-TFA-Pteric acid. The N10 TFA protection was removed using 50/50 ammonium

hydroxide/DMF. The final product was cleaved from the resin using 10mL of 95:2.5:2.5 TFA/TIPS/water with 15mg of TCEP-HCl for 2 hours. The resulting solution was filtered, precipitated, and washed with diethyl ether (334.1 mg yield). LC-MS (M-1): 1461.5

Fol-PEG2-Hydrolink-DimethylCys-Carba-Dex

30mg of Fol-PEG2-Hydrolink-DimethylCys was dissolved in 100uL of 20mM ammonium acetate buffer pH 6.5. To this solution 2.3mg of Pyr-SS-Carbonate-Dex dissolved in 100uL of THF was added quickly using a vigorous stir. The reaction was allowed to stir for 12 hours at room temperature, then purified by RPHPLC utilizing 20mM ammonium acetate buffer/acetonitrile and verified by LC-MS. LC-MS (half-mass of M+1 observed): 971.0

Synthesis of Dexamethasone-21 Phosphate

1g of dexamethasone was added to a 50mL round bottom flask followed by 5mL of anhydrous THF. Then, the reaction was cooled to -40C with a dry ice/acetonitrile cold bath. 1.06mL of diphosphoryl chloride was added and the reaction was stirred at -40C for 1 hour. The reaction was quenched with water, titrated to ~pH 8 with saturated sodium bicarbonate, then the pH was brought to ~2 with 1M hydrochloric acid. The resulting precipitate was extracted with ethyl acetate, washed with acidified brine, dried over sodium sulfate then de vacuo and used in the next step without further purification. (1.0231g yield). LC-MS (M+1): 473.3

Synthesis of Fmoc-Phosphate

1g of (9H-fluoren-9-yl)methyl (2-hydroxyethyl)carbamate was added to a 50mL round bottom flask followed by 6.8mL of anhydrous THF. Then, the reaction was cooled to -40C with a dry ice/acetonitrile cold bath. 1.2mL of diphosphoryl chloride was added and the reaction was stirred at -40C for 1 hour. The reaction was quenched with water, titrated to ~pH 8 with saturated sodium bicarbonate, then the pH was brought to ~2 with 1M hydrochloric acid. The resulting precipitate was extracted with ethyl acetate, washed with acidified brine, dried over sodium sulfate then de vacuo and used in the next step without further purification. (1.2870g yield). LC-MS (M-1): 362.0

Synthesis of Fmoc-Pyro-Dex

109mg of Fmoc-Phosphate was dissolved in 1mL of DMF, followed by the addition of 0.042mL Trimethylamine and 118mg of carbonyl diimidazole (CDI) for approximately 30 minutes. Then 132mg of dexamethasone-21 phosphate was added, followed by 150mg of anhydrous zinc (II)

chloride. The reaction was monitored by LC-MS and upon completion, acetonitrile and 20mM ammonium acetate buffer pH 7 were added and was lyophilized. This resulting residue was then dissolved in DMSO and purified by RPHPLC. (98.6mg yield). LC-MS (M+1): 857.5, ¹H NMR (500 MHz, DMSO) δ 8.20 (s, 1H), 7.86 (d, J = 7.5 Hz, 4H), 7.73 (t, J = 6.4 Hz, 4H), 7.39 (t, J = 7.4 Hz, 5H), 7.32 (t, J = 7.7 Hz, 5H), 7.27 (d, J = 10.1 Hz, 2H), 6.17 (d, J = 10.0 Hz, 2H), 6.04 (s, 1H), 5.98 (s, 2H), 5.23 (s, 1H), 4.63 (dd, J = 17.9, 9.5 Hz, 2H), 4.58 – 4.50 (m, 2H), 4.26 – 4.09 (m, 8H), 3.78 (q, J = 6.3 Hz, 4H), 3.17 (d, J = 6.2 Hz, 4H), 2.96 – 2.85 (m, 2H), 2.64 – 2.54 (m, 2H), 2.32 – 2.24 (m, 3H), 2.11 – 2.00 (m, 4H), 1.95 – 1.87 (m, 4H), 1.73 (d, J = 11.7 Hz, 2H), 1.57 (q, J = 11.6 Hz, 2H), 1.47 (s, 5H), 1.33 (qd, J = 12.9, 5.1 Hz, 2H), 1.03 (s, 1H), 0.87 (s, 5H), 0.75 (d, J = 7.1 Hz, 5H). ¹³C NMR (126 MHz, DMSO) δ 185.84, 156.77, 144.47, 141.11, 128.04, 127.65, 126.06, 124.59, 120.48, 102.39, 90.94, 66.09, 63.68, 48.45, 47.73, 47.12, 43.80, 40.48, 40.40, 40.31, 40.23, 40.14, 39.98, 39.81, 39.64, 39.48, 35.33, 34.67, 34.23, 30.77, 27.73, 21.59, 16.94, 15.87.

Synthesis of Fmoc-PEG12-Pyro-Dex

30.5mg of Fmoc-Pyro-Dex was first dissolved in 10mL of 6% diethylamine (DEA) in DCM, Fmoc deprotection was monitored by LC-MS. The DEA/DCM mixture was then removed under vacuum. A solution of 31.3mg Fmoc-PEG12-acid was activated with 14.1mg HATU, 14.1mg Cl-HOBt, 900uL DMF and 40.9uL NMM. This mixture was then added to the Fmoc deprotected Pyro-Dex residue and upon reaction completion monitored by LC-MS, purified by RPHPLC 20mM ammonium acetate buffer pH 7/acetonitrile and verified by LC-MS. LC-MS (M+1): 1417.5

Synthesis of Folate-NHS

100mg of folic acid was dissolved in 10mL of DMSO followed by the addition of 31.3mg NHS and 46.7mg N,N'-Dicyclohexylcarbodiimide. The mixture was allowed to stir overnight at room temperature. The product was then precipitated in ethyl acetate, filtered by vacuum filtration, and washed three times with diethyl ether. The resulting solid was used without further purification. (103.4mg yield)

Synthesis of Folate-PEG12-Pyro-Dex

Fmoc-PEG12-Pyro-Dex was then deprotected with DEA/DCM, then dried under vacuum and 2.2mg of the resulting deprotected compound was mixed with 2mg of Folate-NHS in 250uL

of DMSO and 1 μ L of DIPEA. The reaction was monitored by LC-MS and upon completion was purified by RPHPLC and verified by LC-MS. (1.93mg yield). LC-MS (M+1): 1618.5

3.3.2 Mechanistic Studies Using Peritonitis

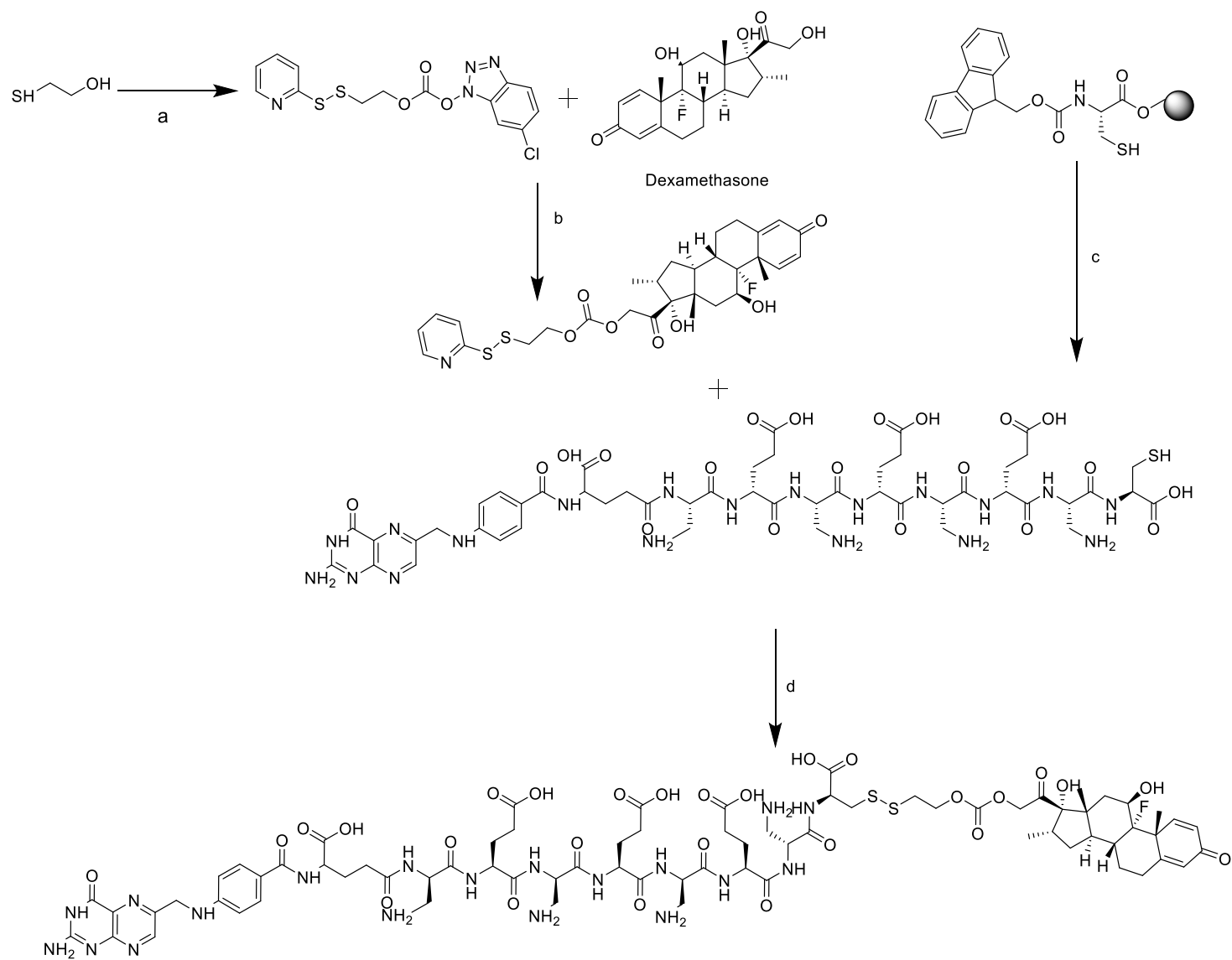
Induced peritonitis with 1.5mL 3% thioglycolate injected I.P. into either BALB/C or Swiss Webster mice maintained on a folate free diet for at least three weeks and treated with 10nmol Folate-peg2-hydroxymethyl-dimethylcysteine-carbamate-dex injected I.V. 48hrs after induction. After an additional 48hrs the mice were euthanized, and peritoneal lavage was performed using 2% fetal bovine serum (FBS) in phosphate buffered saline (PBS). Cells were passed through a 70 μ m cell filter to remove debris then counted using a hemocytometer. Approximately 1 million cells pre-incubated in anti-CD16/32 (to block endogenous Fc receptor binding) for one hour on ice in 100 μ L of 2% FBS in PBS. Then the cells incubated with at least one of the following fluorescently labeled antibodies for cell surface markers: PE-F4/80 or PE/Cy7-F4/80 (mouse macrophage), FITC-CD4 (T helper cell), APC-CD8 (cytotoxic T cell), and PerCP/Cy5.5-Ly6G (neutrophil) according to the manufacturers recommended procedure on ice for 1 hour. Cells were washed twice with 1mL of ice cold 2% FBS in PBS then suspended in 2% FBS in PBS. Controls included unstained cells as the negative control as well as the use of 1 drop of compensation beads per dye-antibody (1 μ L) for a positive control incubated for 1 hour on ice and washed twice with 1mL 2% FBS in PBS. All samples were centrifuged at 400xg for 10min between washes, transfers and after incubation to remove supernatant.

Samples and appropriate controls were analyzed on an Attune NxT Acoustic Focusing Cytometer collecting between 10,000 and 30,000 events per sample utilizing laser lines BL1-A, BL2-A, BL3-A, and YL4-A for FITC-CD4, PE-F4/80, PerCP/Cy5.5-Ly6G and APC-CD8 or PE/Cy7-F4/80, respectively. Flow cytometry data analysis involved first observing the cells run in the experiment using forward and side-scattering light (FSC and SSC, respectively). All observed cells were gated (R1) and analyzed for relative abundance of F4/80 (mouse macrophage), CD4 (T helper cell), CD8 (cytotoxic T cell), and Ly6G (neutrophil) cells within the population. Values from quadrant gating based on negative controls were then represented in bar graph form.

3.4 Result

Initial development of a folate steroid conjugate started with functionalization of the potent FDA approved steroid dexamethasone.²⁸ Nucleophilicity of the single primary hydroxyl group on dexamethasone was utilized to react with the activated pyridyl disulfide carbonate molecule seen in Scheme 3.1 to form Pyr-SS-Carbonate-Dex. Next, a hydrophilic linker of alternating DAP and D-Glu amino acids (HydroLink™) were synthesized on a cysteine loaded 2-chlorotrityl resin via an Aapptec automated peptide synthesizer using HBTU/PyBop coupling along with standard solid phase peptide synthetic (SPPS) protocols. Then using HATU coupling folate was added to the resin via use of TFA protected pteric acid (normal pteric acid has limited solubility in SPPS compatible solvents), then deprotected by 50/50 ammonium hydroxide in DMF. After isolation, this compound was reacted with Pyr-SS-Carbonate-Dex by disulfide bond exchange to afford the final product that was purified by reverse phase HPLC and verified by LC-MS.

Scheme 3.1 Synthesis of Folate-Hydrolink-Cys-Carbonate-Dex. (a) Methoxycarbonylsulfonyl Chloride, 2-mercaptopyridine ACN, (b) DMF, DIPEA (c) Cysteine 2-cholotrityl resin, HBTU/PyBop solid phase peptide synthesis (d) 50/50 THF/20mM ammonium acetate buffer ~pH 6-6.5



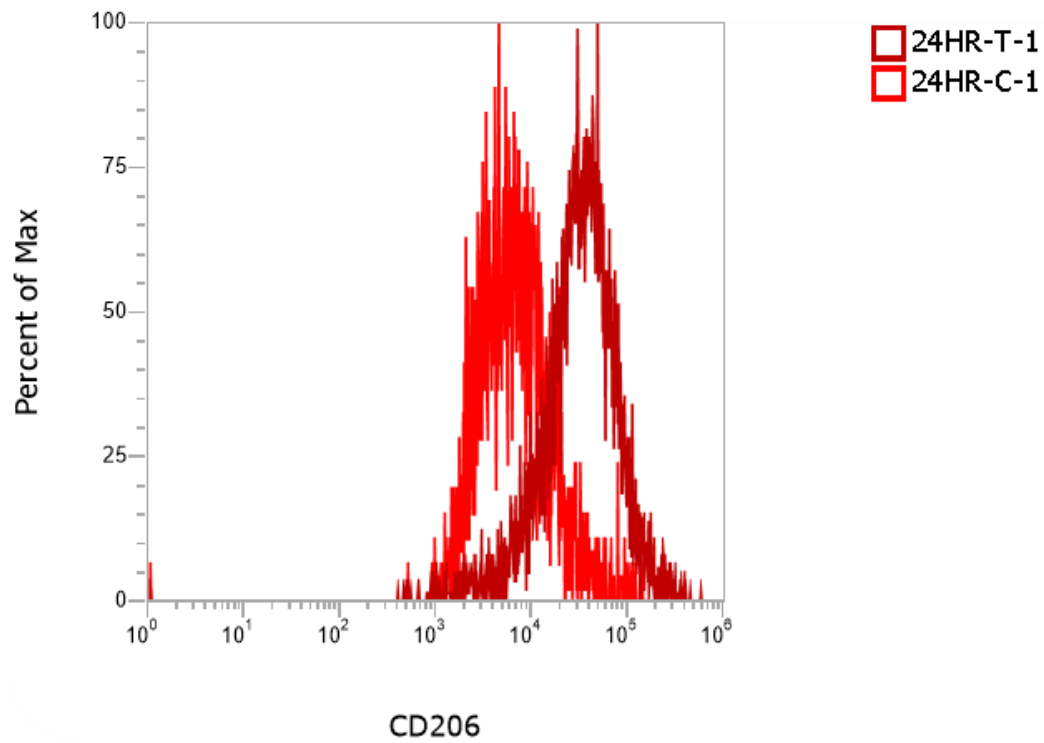


Figure 3.1 M2 Polarization of Macrophages Exposed to Folate-HydroLink-Cys-Carba-Dex. 24HR-T-1; Cells incubated for 24hrs with Folate-HydroLink-Cys-Carba-Dex. 24-HR-C-1; Cells incubated for 24hrs with Folate-HydroLink-Cys-Carba-Dex and 100X concentration of folate-glucosamine as competition ligand.

To test the efficacy of Folate-HydroLink-Cys-Carbonate-Dex, the compound was incubated with murine peritoneal macrophages that were elicited with 3% thioglycolate. These macrophages were plated with the compound or the compound with the addition of 100 times the concentration of competition molecule folate-glucosamine for 24hrs. These cells were then washed, incubated with labeled antibodies to identify macrophages and the cell surface M2 marker CD206. As seen in Fig 3.1 macrophages incubated with compound expressed a much higher relative amount of CD206, showing that they had converted to a more M2 anti-inflammatory state. By contrast the competition group has a much lower expression of CD206 providing evidence that the upregulation of CD206 in the other group was due to receptor mediated uptake of the drug conjugate.

Seen in Scheme 3.2 and 3.3, two additional folate dexamethasone conjugates were synthesized to create alternate linkages to the steroid that could have better stability and/or provide an alternative release mechanism to afford the free drug once it reached the inflammatory macrophages. In Scheme 3.2, synthesis of the carbamate linked dexamethasone was very similar to that of the carbonate linked drug found in Scheme 3.1, with the major difference being dexamethasone was initially reacted with p-nitrophenyl chloroformate followed by the addition of 2-(pyridin-2-yl)disulfaneyl)ethan-1-amine acid chloride salt and DIPEA in a one-pot reaction to afford the dexamethasone carbamate linked pyridyl disulfide compound. Synthesis of Fol-PEG12-Pyro-Dex in Scheme 3.3 borrowed chemistries initially developed by scientists at Merck.⁵ This process involved treating dexamethasone and Fmoc protected 2-aminoethanol with diphosphoryl chloride at -40C in an acetonitrile/dry ice cold bath followed by hydrolysis via the addition of water, then using HCl and saturated bicarbonate to adjust the pH to ~8 then to 1 to first hydrolyze the pyrophosphate to a monophosphate, then to form the phosphoric acid for subsequent extraction. The next reaction involves the use of zinc catalyzed carbodiimidazole (CDI) reaction to couple the Fmoc-Phosphate to the dexamethasone-phosphate in order to form a new pyrophosphate. The subsequent reactions involve a series of first removing Fmoc via diethylamine in dichloromethane, then performing amide bond coupling reactions to add Fmoc-PEG12 and folate to afford the final product that was purified by reverse phase HPLC and verified by LC-MS.

Scheme 3.2 Synthesis of Folate-PEG2-HydroLink-DimethylCys-Carba-Dex. (a) Methoxycarbonylsulfonyl Chloride, 2-mercaptopyridine ACN, (b) Chloroform, pyridine, DIPEA (c) 50/50 THF/20mM ammonium acetate buffer ~pH 6-6.5

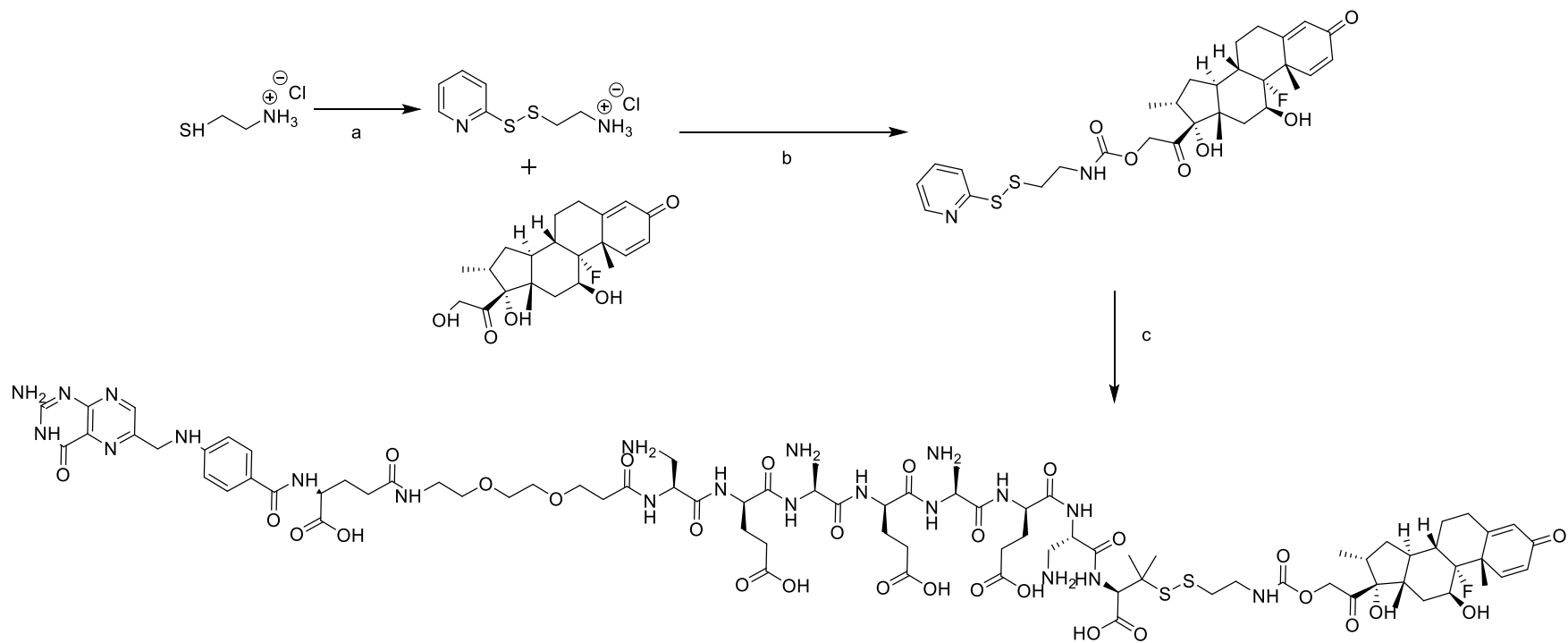


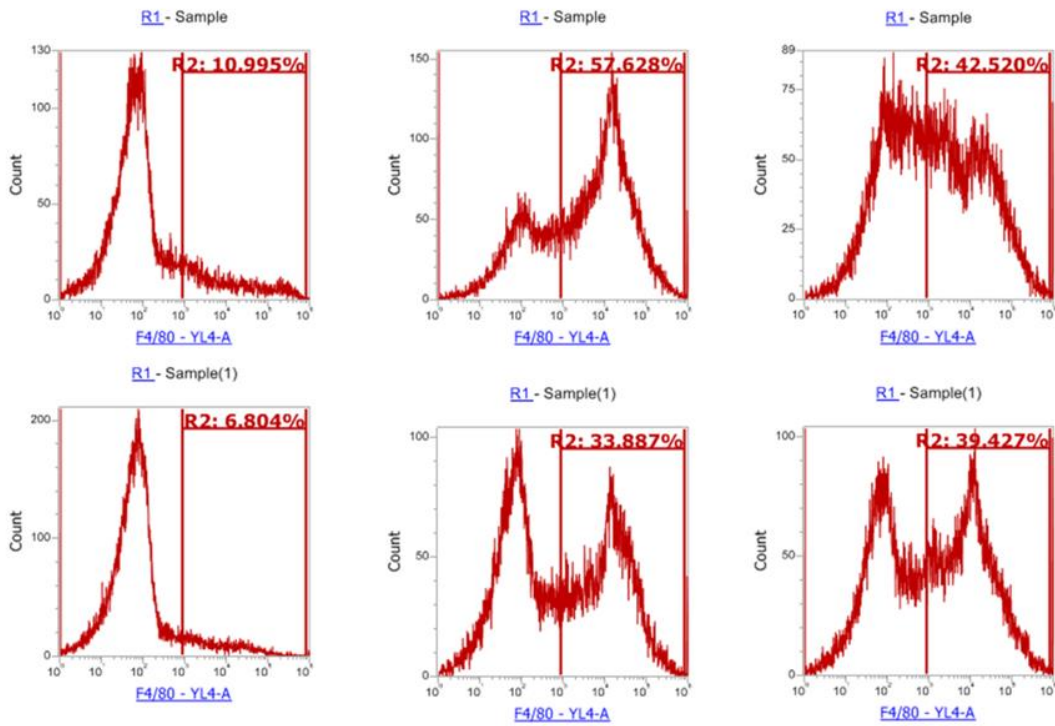
Figure 3.2 Blocking Recruitment of Macrophages with Folate-PEG2-HydroLink-DimethylCys-Carba-Dex. Peritoneal macrophages were generated by IP injection of 3% thioglycolate into the peritoneal cavity of mice. 2 days later mice were treated with a single 10nmol injection of Folate-PEG2-HydroLink-DimethylCys-Carba-Dex. 2 days after treatment macrophages were isolated by peritoneal lavage, labeled with fluorescently conjugated antibody markers, and analyzed by flow cytometry. Experiment was performed in duplicate.

Fol-PEG2-Hydro-DimethylCys-Carba-Dex

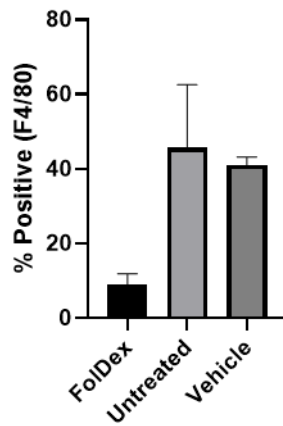
Treated

Untreated

Vehicle



Fol-PEG2-Hydro-DimethylCys-Carba-Dex



Scheme 3.3 Synthesis of Folate-PEG12-Pyro-Dex. (a) THF, Diphosphoryl chloride, -40C, workup (b) DMF, CDI, zinc (II) chloride (c) 1. Diethylamine/DCM 2. HATU, DIPEA, DMF, Fmoc-PEG12-acid (d) 1. Diethylamine/DCM 2. HATU, DIPEA, DMSO, Folate-NHS

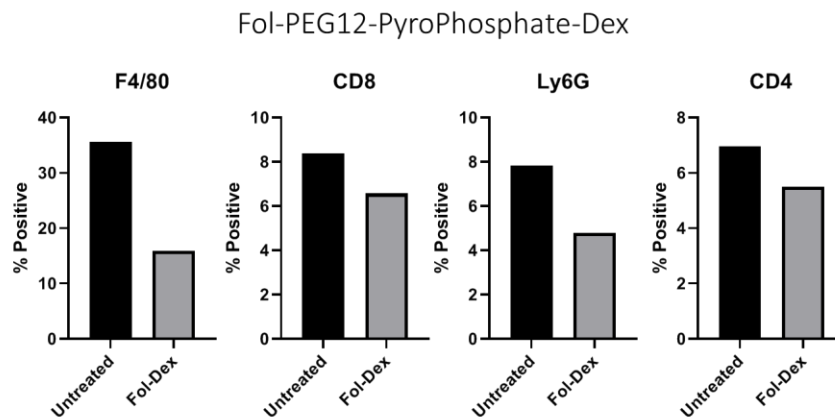
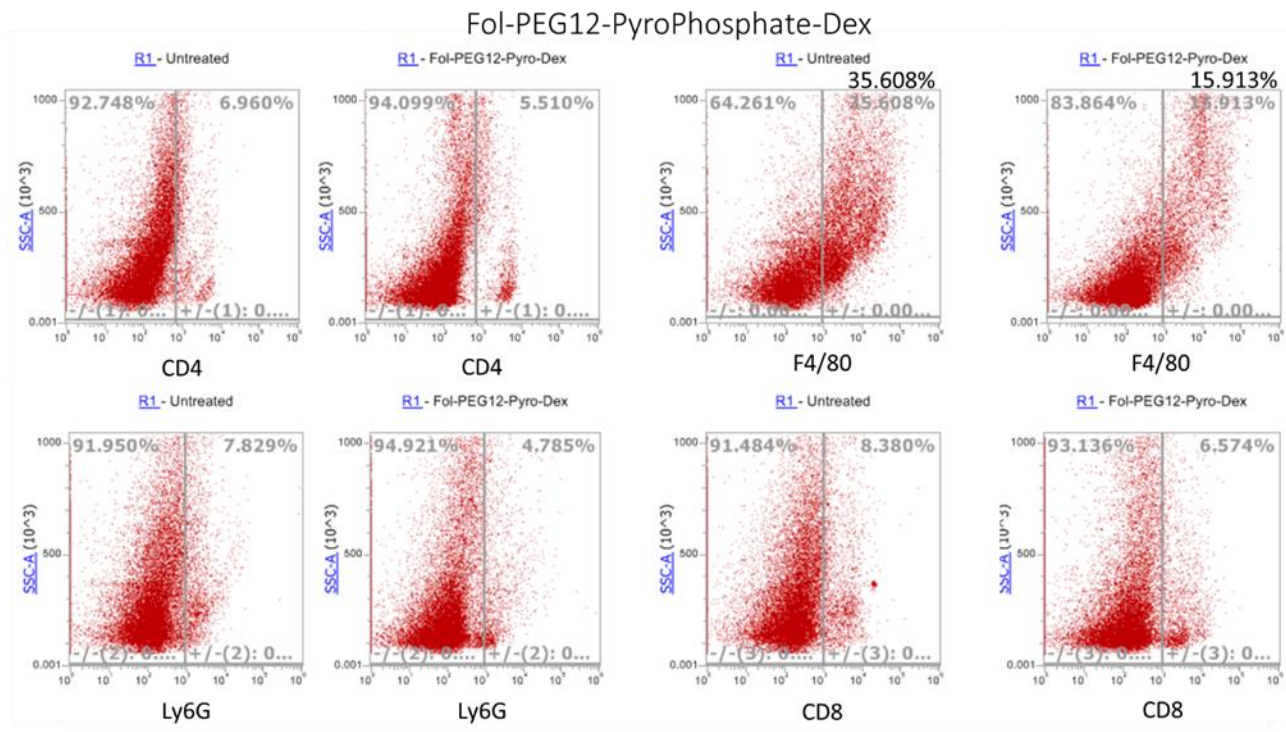


Figure 3.3 Blocking Recruitment of Immune Cells with Folate-PEG12-Pyro-Dex. Peritoneal macrophages were generated by IP injection of 3% thioglycolate into the peritoneal cavity of a mouse. 2 days later mice were treated with a single 10nmol injection of Folate-PEG12-Pyro-Dex. 2 days after treatment macrophages were isolated by peritoneal lavage, labeled with fluorescently conjugated antibody markers, and analyzed by flow cytometry. Pilot experiment was performed with a single mouse.

Figures 3.2 and 3.3 depict pilot experiments that may hint at the effectiveness of the folate-dexamethasone conjugates. In these studies mice were given an intraperitoneal injection of 3% thioglycolate to elicit an immune response of primarily monocyte derived macrophages. Two days after thioglycolate injection the mice were treated with their respective compounds via a 10nmol tail vein injection. Subsequent flow cytometry analysis revealed a drastic decrease in F4/80 positive cells (macrophages) for Figure 3.2. This effect was also seen in Figure 3.3, but additionally other immune cells monitored also showed reduced accumulation in the peritoneal cavity, suggesting both compounds have viable immunosuppressing capabilities.

3.5 Discussion

Designs for all folate targeted steroids presented herein rely on functionalizing the only primary hydroxyl group that is located at the 21-position of dexamethasone. Due to its nucleophilicity and absence of steric hindrance relative to the other hydroxyls in dexamethasone. Additionally, initial derivatization of dexamethasone at the 21-position using the methods herein, with the exception of the dexamethasone-carbonate linkage has previously been validated by others. Utilizing this selectivity, the first generation of folate targeted steroids seen in Fig 3.1 was synthesized by reacting dexamethasone with the activated carbonate of 6-chloro-1H-benzo[d][1,2,3]triazol-1-yl (2-(pyridin-2-yl)disulfaneyl)ethyl carbonate. This molecule was then subsequently reacted with the free thiol of a folate-hydrophilic linker (HydroLink) via a disulfide bond exchange to produce Fol-HydroLink-Carbonate-Dex. This compound showed correct mass by LC-MS validation and excellent solubility in phosphate buffered saline pH 7.2.

To test the efficacy of this compound, proinflammatory peritoneal macrophages were generated by injecting 3% thioglycolate into the peritoneal cavity of mice. Once isolated, these cells were either subjected to 24hrs of 20nM Fol-HydroLink-Carbonate-Dex or Fol-HydroLink-Carbonate-Dex plus 100X folate-glucosamine to act as a competitive inhibitor. As seen in Fig 3.2, flow cytometry analysis revealed that the targeted group was able to effectively upregulate the CD206 M2 marker in the macrophages and thereby effectively polarize the cells to a more M2 phenotype. This change was not observed in the competition group, providing evidence that the change was due to the folate receptor uptake of the drug and not due to non specific decomposition and release of free dexamethasone. Unfortunately, when this molecule was translated to in vivo

experiments competition groups performed the same as the targeted, implying that the molecule was breaking down in biological systems (data not shown). Utilizing a pilot stability study using human blood (data not shown), the drug was found to decompose on a relatively quick time scale and after much literature searching it was discovered that carbonates can be recognized and hydrolyzed by esterases that are typically found in blood. Since non-specific release of the free drug is what results in undesired side effects, we opted to explore other self-immolative release mechanism that would be more stable. Alternatively, the carbonate linked drug may serve as a viable “extended release” or “long-lasting” alternative to the free drug. Typically, free dexamethasone has a biological half-life of 36-72hrs, but only remains in the blood stream for approximately 30min. Perhaps conjugation of dexamethasone via a carbonate bond to a long polyethylene glycol linker could produce a nanoparticle/micelle that could slowly undergo hydrolysis to provide constant sustained release.

We then set out to develop folate targeted dexamethasone conjugates that could provide more stable self-immolative release mechanisms to properly and specifically release the steroid in the desired tissue and not break down in the blood. To accomplish this, folate-dexamethasone conjugates that use either a disulfide-carbamate release (Fig 3.3) or a pyrophosphate bond (Fig3.5). Testing of the carbamate linkage in human blood revealed a half-life of approximately 3 days (data not shown) and was able to effectively block macrophage recruitment as seen in Fig 3.4. This was also seen with the pyrophosphate linked molecule, this also potentially revealed the ability of these molecules to block the recruitment of other immunological cell types including CD4/CD8 T-cells as well as Ly6G positive neutrophils. Further studies that need to be undertaken to further this project include extensively characterizing the phenotype of macrophages either murine or human to further establish and supports claims around macrophage polarization. Further stability tests and with pharmacokinetic profiles should be carried out to further validate these molecules before testing in chronic inflammatory models such as multiple sclerosis, rheumatoid arthritis, and diabetes.

3.6 Conclusion

The development of folate targeted steroids offers a great opportunity to develop medicines that can act as extremely potent anti-inflammatory while also negating the side effects that are

typically associated with these drugs. The key development steps will involve validating key drug release mechanism that will be stable in the blood and other bodily fluids but will also release the steroid in the appropriate time frame when delivered to the inflamed tissue. Designs shown above have the potential to satisfy these requirements and hopefully bring relief to future patients suffering from inflammatory diseases.

3.7 References

1. Pahwa, R.; Goyal, A.; Bansal, P.; Jialal, I., Chronic Inflammation. In *StatPearls*, StatPearls Publishing

Copyright © 2021, StatPearls Publishing LLC.: Treasure Island (FL), 2021.

2. Wylezinski, L. S.; Gray, J. D.; Polk, J. B.; Harmata, A. J.; Spurlock, C. F., 3rd. Illuminating an Invisible Epidemic: A Systemic Review of the Clinical and Economic Benefits of Early Diagnosis and Treatment in Inflammatory Disease and Related Syndromes. *J Clin Med* **2019**, *8*, (4), 493.
3. Custodero, C.; Mankowski, R. T.; Lee, S. A.; Chen, Z.; Wu, S.; Manini, T. M.; Hincapie Echeverri, J.; Sabbà, C.; Beavers, D. P.; Cauley, J. A.; Espeland, M. A.; Fielding, R. A.; Kritchevsky, S. B.; Liu, C. K.; McDermott, M. M.; Miller, M. E.; Tracy, R. P.; Newman, A. B.; Ambrosius, W. T.; Pahor, M.; Anton, S. D. Evidence-based nutritional and pharmacological interventions targeting chronic low-grade inflammation in middle-age and older adults: A systematic review and meta-analysis. *Ageing Res Rev* **2018**, *46*, 42-59.
4. Grennan, D.; Wang, S. Steroid Side Effects. *Jama* **2019**, *322*, (3), 282.
5. King, T.; Faiman, B. Steroid-Associated Side Effects: A Symptom Management Update on Multiple Myeloma Treatment. *Clin J Oncol Nurs* **2017**, *21*, (2), 240-249.
6. Jain, S. K.; Jain, A.; Gulbake, A.; Shilpi, S.; Khare, P. Steroid-coupled liposomes for targeted delivery to tumor. *Ther Deliv* **2010**, *1*, (2), 345-57.
7. Khan, I.; Yousaf, S.; Subramanian, S.; Alhnan, M. A.; Ahmed, W.; Elhissi, A. Proliposome Powders for the Generation of Liposomes: the Influence of Carbohydrate Carrier and Separation Conditions on Crystallinity and Entrapment of a Model Antiasthma Steroid. *AAPS PharmSciTech* **2018**, *19*, (1), 262-274.

8. Kern, J. C.; Cancilla, M.; Dooney, D.; Kwasnjuk, K.; Zhang, R.; Beaumont, M.; Figueroa, I.; Hsieh, S.; Liang, L.; Tomazela, D.; Zhang, J.; Brandish, P. E.; Palmieri, A.; Stivers, P.; Cheng, M.; Feng, G.; Geda, P.; Shah, S.; Beck, A.; Bresson, D.; Firdos, J.; Gately, D.; Knudsen, N.; Manibusan, A.; Schultz, P. G.; Sun, Y.; Garbaccio, R. M. Discovery of Pyrophosphate Diesters as Tunable, Soluble, and Bioorthogonal Linkers for Site-Specific Antibody–Drug Conjugates. *Journal of the American Chemical Society* **2016**, *138*, (4), 1430-1445.
9. Jia, Z.; Wang, X.; Wei, X.; Zhao, G.; Foster, K. W.; Qiu, F.; Gao, Y.; Yuan, F.; Yu, F.; Thiele, G. M.; Bronich, T. K.; O'Dell, J. R.; Wang, D. Micelle-Forming Dexamethasone Prodrug Attenuates Nephritis in Lupus-Prone Mice without Apparent Glucocorticoid Side Effects. *ACS nano* **2018**, *12*, (8), 7663-7681.
10. Durbin, K. R.; Nottoli, M. S.; Catron, N. D.; Richwine, N.; Jenkins, G. J. High-Throughput, Multispecies, Parallelized Plasma Stability Assay for the Determination and Characterization of Antibody–Drug Conjugate Aggregation and Drug Release. *ACS Omega* **2017**, *2*, (8), 4207-4215.
11. Lucas, A. T.; Price, L. S. L.; Schorzman, A. N.; Storrie, M.; Piscitelli, J. A.; Razo, J.; Zamboni, W. C. Factors Affecting the Pharmacology of Antibody-Drug Conjugates. *Antibodies (Basel)* **2018**, *7*, (1), 10.
12. Nicod, N.; Giusti, V.; Besse, C.; Tappy, L. Metabolic Adaptations to Dexamethasone-Induced Insulin Resistance in Healthy Volunteers. *Obesity Research* **2003**, *11*, (5), 625-631.
13. Shi, Y.; van der Meel, R.; Chen, X.; Lammers, T. The EPR effect and beyond: Strategies to improve tumor targeting and cancer nanomedicine treatment efficacy. *Theranostics* **2020**, *10*, (17), 7921-7924.
14. Rosenblum, D.; Joshi, N.; Tao, W.; Karp, J. M.; Peer, D. Progress and challenges towards targeted delivery of cancer therapeutics. *Nature Communications* **2018**, *9*, (1), 1410.
15. Makurvet, F. D. Biologics vs. small molecules: Drug costs and patient access. *Medicine in Drug Discovery* **2021**, *9*, 100075.
16. van Furth, R.; Beekhuizen, H., Monocytes. In *Encyclopedia of Immunology (Second Edition)*, Delves, P. J., Ed. Elsevier: Oxford, 1998; pp 1750-1754.
17. Yunna, C.; Mengru, H.; Lei, W.; Weidong, C. Macrophage M1/M2 polarization. *Eur J Pharmacol* **2020**, *877*, 173090.
18. Ginhoux, F.; Jung, S. Monocytes and macrophages: developmental pathways and tissue homeostasis. *Nature Reviews Immunology* **2014**, *14*, (6), 392-404.
19. Parisi, L.; Gini, E.; Baci, D.; Tremolati, M.; Fanuli, M.; Bassani, B.; Farronato, G.; Bruno, A.; Mortara, L. Macrophage Polarization in Chronic Inflammatory Diseases: Killers or Builders? *Journal of Immunology Research* **2018**, *2018*, 8917804.

20. Funes, S. C.; Rios, M.; Escobar-Vera, J.; Kalergis, A. M. Implications of macrophage polarization in autoimmunity. *Immunology* **2018**, *154*, (2), 186-195.
21. Lu, Y.; Parker, N.; Kleindl, P. J.; Cross, V. A.; Wollak, K.; Westrick, E.; Stinnette, T. W.; Gehrke, M. A.; Wang, K.; Santhapuram, H. K.; You, F.; Hahn, S. J.; Vaughn, J. F.; Klein, P. J.; Vlahov, I. R.; Low, P. S.; Leamon, C. P. Antiinflammatory Activity of a Novel Folic Acid Targeted Conjugate of the mTOR Inhibitor Everolimus. *Mol Med* **2015**, *21*, (1), 584-96.
22. Chandrupatla, D. M. S. H.; Molthoff, C. F. M.; Lammertsma, A. A.; van der Laken, C. J.; Jansen, G. The folate receptor β as a macrophage-mediated imaging and therapeutic target in rheumatoid arthritis. *Drug Delivery and Translational Research* **2019**, *9*, (1), 366-378.
23. Yi, Y.-S. Folate Receptor-Targeted Diagnostics and Therapeutics for Inflammatory Diseases. *Immune Netw* **2016**, *16*, (6), 337-343.
24. Poh, S.; Putt, K. S.; Low, P. S. Folate-Targeted Dendrimers Selectively Accumulate at Sites of Inflammation in Mouse Models of Ulcerative Colitis and Atherosclerosis. *Biomacromolecules* **2017**, *18*, (10), 3082-3088.
25. Hu, Y.; Wang, B.; Shen, J.; Low, S. A.; Putt, K. S.; Niessen, H. W. M.; Matteson, E. L.; Murphy, L.; Ruppert, C.; Jansen, G.; Oliver, S. J.; Feng, Y.; Dimitrov, D. S.; Nickerson-Nutter, C.; Low, P. S. Depletion of activated macrophages with a folate receptor-beta-specific antibody improves symptoms in mouse models of rheumatoid arthritis. *Arthritis Research & Therapy* **2019**, *21*, (1), 143.
26. Boss, S. D.; Ametamey, S. M. Development of Folate Receptor-Targeted PET Radiopharmaceuticals for Tumor Imaging-A Bench-to-Bedside Journey. *Cancers (Basel)* **2020**, *12*, (6), 1508.
27. Desgeorges, T.; Caratti, G.; Mounier, R.; Tuckermann, J.; Chazaud, B. Glucocorticoids Shape Macrophage Phenotype for Tissue Repair. *Frontiers in Immunology* **2019**, *10*, (1591).
28. Cronin, J.; Kennedy, U.; McCoy, S.; an Fhailí, S. N.; Crispino-O'Connell, G.; Hayden, J.; Wakai, A.; Walsh, S.; O'Sullivan, R. Single dose oral dexamethasone versus multi-dose prednisolone in the treatment of acute exacerbations of asthma in children who attend the emergency department: study protocol for a randomized controlled trial. *Trials* **2012**, *13*, (1), 141.

3.8 Appendix A

